EFFECTS OF PHASE DIFFERENCE BETWEEN AXIAL AND CONTACT LOADS ON FRETTING FATIGUE BEHAVIOR OF TITANIUM ALLOY

THESIS

Mohammad Almajali, Ltc, Royal Jordanian Air Force

AFIT/GAE/ENY/06- S02

DEPARTMENT OF THE AIR FORCE
AIR UNIVERSITY

AIR FORCE INSTITUTE OF TECHNOLOGY

Wright-Patterson Air Force Base, Ohio

The views expressed in this thesis are those of the author and do not reflect the official policy or position of the United States Air Force, Department of Defense, or the United States Government.

AFIT/GAE/ENY/06 - S02

EFFECTS OF PHASE DIFFERENCE BETWEEN AXIAL AND CONTACT LOADS ON FRETTING FATIGUE BEHAVIOR OF TITANIUM ALLOY

THESIS

Presented to the Faculty

Department of Aeronautics and Astronautics

Graduate School of Engineering and Management

Air Force Institute of Technology

Air University

Air Education and Training Command

In Partial Fulfillment of the Requirements for the

Degree of Master of Science in Aeronautical Engineering

Mohammad Almajali

Ltc, Royal Jordanian Air Force

September 2006

AFIT/GAE/ENY/06- S02

EFFECTS OF PHASE DIFFERENCE BETWEEN AXIAL AND CONTACT LOADS ON FRETTING FATIGUE BEHAVIOR OF TITANIUM ALLOY

Mohammad Almajali

Ltc, Royal Jordanian Air Force

Approved:

_____/signed/_____ __
Shankar Mall (Chairman) date

_____/signed/_____ __
Vinod K. Jain (Member) date

_____/signed/_____ __
Michael L. Heil (Member) date

Abstract

Fretting fatigue is the surface damage that occurs at the interface between two components that are undergoing a small amplitude oscillatory movements. It results in a reduction of the material life as compared to the plain fatigue. Most of the previous works were accomplished under a constant applied normal load and a little effort was done under a variable contact load, while none of these studies has considered the phase difference between the axial load and the contact load. The primary goal of this study is to investigate the effect of phase difference between axial and contact loads on fretting fatigue behavior of Ti-6Al-4V alloy. The frequency of both axial and contact loads was the same. i.e. 10 Hz. Under variable contact load condition; only the axial stress range and the phase angle were varied. Cracks were always found to initiate at the contact surface and near the trailing edge in all tests. The software program, ABAQUAS, was used in Finite Element Analysis FEA to determine the contact region state variables such as stress, strain, and displacement. The fatigue parameters; such as the stress range, effective stress, and modified shear stress range (MSSR) were analyzed to predict the fatigue life. The fatigue life with in-phase variable contact load was almost same as that of constant contact load. The out of phase condition increased the fatigue life from 20% to 30% in the low cycle regime and up to 150% in the high cycle regime relative to its counterpart from in-phase loading. The MSSR parameter, a critical plane based fretting fatigue parameter, was very effective in predicting the fatigue life, crack initiation location, and the crack initiation orientation.

Acknowledgments

I would like to thank and appreciate my thesis advisor Dr. Mall for his guidance and teaching throughout this work. It was honor for me to work under his supervision. I also want to thank Mrs. Annette Robb and the international office in AFIT for their effort by making the life in States easier to me and my family.

In addition, I would like to express my thank to my wife for her support and patience during my attending the Master of Science at AFIT.

Finally, I would like to express my gratitude to Royal Jordanian Air Force that believed in me and gave me this opportunity and honor to complete my Master of Science degree in Aeronautical Engineering in AFIT, USA.

Mohammad Almajali

Table of Contents

Page

Page

Page

List of Figures

Figure Page

Page

Page

Page

List of Tables

Table Page

List of Symbols

a	contact half-width
A	a specimen's cross section area
b	a specimen's half thickness
c	stick zone boundary
c'	fatigue ductility exponents
E	modulus of elasticity
f	coefficient of friction
h	depth of penetration
k	the curvature
L	specimen length
N_f	numbers of cycles to fatigue
N_i	numbers of cycles to crack initiation
p	pressure distribution in the contact zone
P	normal load
P_0	maximum contact pressure or Hertzian Peak Pressure
q	surface shear stress distribution
Q	tangential loads
R_σ	stress ratio of axial stress
R_ε	strain ratio
R_τ	shear stress ratio
S_{xx} or σ_{xx}	normal stress along x-direction

S_{xy} or σ_{xy}	shear stress on x-y plane
S_{yy} or σ_{yy}	normal stress along y-direction
u	displacement
V	axial load
w	specimen width
w(x)	weight function
Y_0	the depth within a specimen where residual stress is zero
ε_a	total strain amplitude
ε_f'	fatigue ductility coefficient
ε_{max}	maximum strain
ε_{min}	minimum strain
ε_{xx}	strain induced by the axial stress
ν	Poisson's ratio
θ	direction of stress in a material, observed angle of orientation
ϕ	phase angle
$\Delta\sigma$	axial stress range
$\Delta\varepsilon$	plastic strain amplitude
$\Delta\tau$	shear stress range
σ	normal stresses at a given point with a specific orientation
σ_{axial}	applied axial stress
σ_{eff}	effective axial stress
σ_f'	fatigue strength coefficient

$(\sigma_{xx})_{axial}$	x-direction normal stress contributed from axial load
$(\sigma_{xx})_{contact}$	x-direction normal stress contributed from contact load
$(\sigma_{xx})_{tangential}$	x-direction normal stress contributed from tangential load
S_y	yield strength
τ	shear stress at a given point with a specific orientation

EFFECTS OF PHASE DIFFERENCE BETWEEN AXIAL LOAD AND CONTACT LOAD ON FRETTING FATIGUE BEHAVIOR OF TITANIUM ALLOY

1. Introduction

The introduction chapter will discuss the material failure criterion, the definition of the fretting fatigue phenomenon, the methodology that was used to model the fretting fatigue, and the objectives and purposes of this study which involves the investigation into the effects of the phase difference between the variable applied contact load and the axial load, and the combination of the fretting fatigue and plain fatigue on the fretting fatigue behavior of titanium Ti-6A1-4V alloy.

1.1. Material Failure

When engineers first start to design a product, one of their first concerns is to determine the harshest conditions that the product will experience in service. The product is then designed to minimize the hazards associated with the worst case scenario which requires a complete understanding of the product; its loading, and its service environment. It has been known that the failure occurs when a device or structure is no longer able to function as intended, and the failure can be costly and tragic. Once the actual service environment is determined, the weakness which caused the failure can be corrected and future failures might be avoided.

The most common forms of material failures are fracture, corrosion, wear, and deformation. When a component has been subjected to a load and this component is separated into two or more pieces due to an extending crack, this failure is known as a fracture, and if this load has been applied as a cyclic load, the fracture in this case is known as fatigue. In addition; if there is a contact between two surfaces, where small oscillatory sliding displacements occur while one or both of the contacting surfaces could be subjected to fluctuating stresses, then this type of fracture is known as fretting fatigue. This study is focused in this direction.

1.2. Fretting Fatigue

Fretting fatigue is the state when a cyclic stress is applied to a component in contact with another one. It causes a small amplitude oscillatory movements and a tangential force resisting these movements, and this produces surface damage resulting in a state of stress and strain which decreases the fatigue resistance of the material and produces the crack initiation. If the contacting components are made from castings of not good quality and they have a pre-exist number of defects, there will be no time of crack initiation phase and the entire life is expended in a propagation phase. However if they have been made to be used in a high technology applications, such as in aircraft structure or engine, there are therefore no pre-existing defects and the crack initiation should be monitored by determining the stress within the components, and the origin, the form, and the location of the initial defects.

The crack is generated at the edge of the contact where the tensile load is highest, it is initiated by Mode II crack loading, and it extends in the direction of maximum shear (±45 degree), then at some critical crack length the crack turns at an orientation giving the maximum Mode I stress intensity, which is normal to the surface, and finally the crack will propagate quickly until failure. The results of fretting fatigue are the reduction of the material life time as will as the increase of maintenance cost, therefore the aircraft companies in the civil arena and in military around the world are interesting in the investigation of the fretting fatigue phenomenon.

1.3. Purposes and Objectives

Titanium alloy is used in many components which are subjected to fretting fatigue phenomenon; such as the disk slot and blade attachment in the turbine section of a gas turbine engine as shown in Figure 1.1, so several studies, as will be seen in the next chapter, have been accomplished to provide a better understanding of the crack initiation mechanism. These will help to develop techniques to decrease the maintenance cost and increase operating hours for newly designed components. These previous studies were done in different loading environments to investigate the effect of different contributing factors and variables, such as friction, contact geometry, shot-peening process, elevated temperature, environment corrosion, and the load frequency. Most of these studies have been investigated under a constant applied contact load condition, while a little effort has been carried out with the variable contact load. Further, none of these studies has

investigated the effect of the phase difference between the axial and the contact loads which will be the main focus in this study.

There are two goals of this study; the first one is to determine the fretting fatigue behavior under the cyclic contact load. This study mainly focused on the effect of phase difference between the axial load and the applied contact load on titanium Ti-6A1-4V alloy. The frequency of both the axial and the applied contact loads was the same i.e.10 Hz, and the mean stress of the axial load was varied while the mean stress of the applied contact load was kept constant with maximum magnitude of 4448 N and minimum magnitude of 2224 N. The second goal of this study is to investigate how the material behaves under a combination of the fretting fatigue and plain fatigue loading conditions. The results of this research will be compared with the previous researches, as discussed in chapter II, to see how are the fatigue life, crack initiation location, and crack initiation orientation affected under these conditions.

1.4. Methodology

As seen in Figure 1.1, it is very difficult to model the geometry of the disk slot and blade attachment in the turbine section where the contact mechanism should be studied. In addition; it will be very expensive and it will consume a lot of time and effort to study the fretting fatigue behavior by using this configuration. So this geometry can be idealized as well as simplified by a cylinder-on-flat contact model as shown in details in Figure 1.2. The simplified model will be the experimental setup in this study in order to investigate the effect of phase difference between the axial and contact loads on fretting

fatigue behavior and the difference between the fretting and the plain fatigue under different load conditions. The desired magnitude of the applied contact and axial loads along with their frequencies and their state with any phase difference can be applied by a bi-axial servo-hydraulic machine, as will be shown in chapter III. This machine can also record the other data of the experiments.

The Scanning Electron Microscopy (SEM) was performed to examine the fracture surface, contact half-width, crack initiation location, crack initiation orientation, and other details of damage mechanisms. Finite element analysis was conducted to compute local fretting variables such as; stress, strain, and displacement. The stress, stress distribution, contact half-width, and other variables were also analyzed under variable contact loads at different load steps. In addition, several fretting fatigue parameters, such as the stress range, effective stress, and modified shear stress range were evaluated for their effectiveness on fretting fatigue predictions in terms of fatigue life, crack initiation location, and crack initiation orientation.

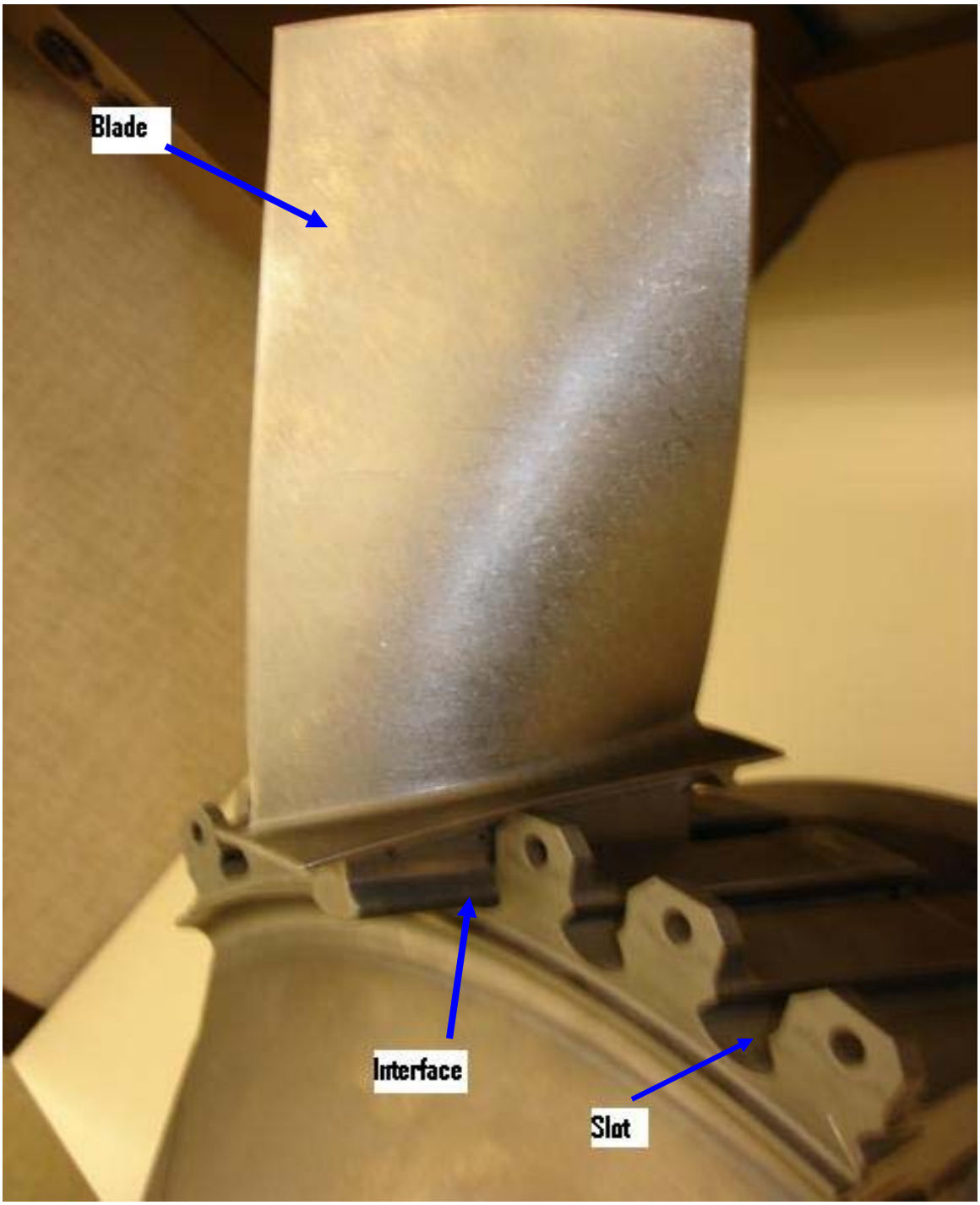

Figure 1.1 Dovetail joint in turbine engine disk

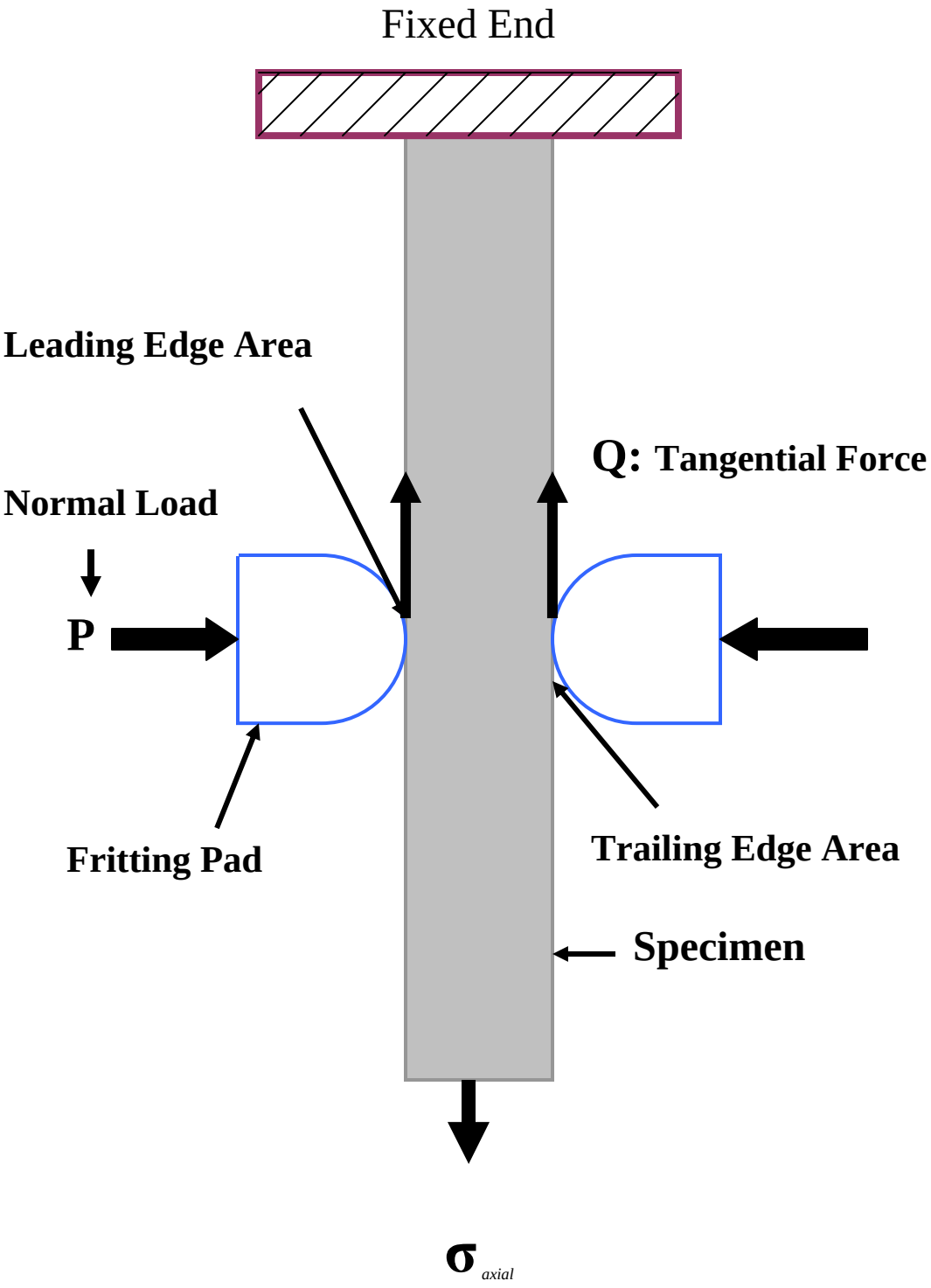

Figure 1.2 Schematic diagram of fretting fatigue model

2. Background

This chapter introduces the discussion of contact mechanics as a review of Hills and Nowell's work [1] who analyzed the contact mechanics in several configurations. The first part is the formulation of the problem and how it can be solved by taking some assumptions into consideration. The second part is a review of the previous studies on the fretting fatigue mechanics in general along with the experiments those have been done on this subject, then specific researches on the titanium alloy are addressed to be compared with the results of this study, and finally the fatigue predictive parameters are covered.

2.1. Contact Mechanics

As shown in Figure 1.1 the fretting fatigue configuration can be modeled by a cylindrical-end body in contact with a flat body which is a cylinder with infinite radius, this configuration is shown in details in Figure 2.1, the specimen is represented by a rectangular with cross sectional area A, thickness d, half thickness b, and this specimen is subjected to an axial load equal to σ_{axial}. The fretting pad is represented by a semi rectangular whose one of its faces is an arc with a constant radius r, and it is also subjected to a normal load P. As a result there will be a reacted tangential load Q, and a contact area which has a length known as a contact-width 2a, where a represents the contact half-width. The configuration shown in Figure 2.1 is an incomplete contact which depends on the applied load, it has no singularity at the edges, the contact half width is

assumed very small relative to the bodies radius (a << r), and the two bodies are elastically similar.

In the contact area there are three zones, the first two zones are the slip zones those are located on both sides where the relative tangential motion occurs and the shear stress is given by:

$$q(x,y) = - f\, p(x,y) \tag{2.1}$$

where f is the coefficient of friction, and p is the direct stress. The second zone, which is located in the middle between the two previous zones, is the stick zone where the particles of the two bodies are adhered, and the applied shear force Q is less than the resulted friction force:

$$Q < f\, P \tag{2.2}$$

where P is the normal load.

When the two bodies are in contact with each other and there is an application of normal force P in y-direction and shearing force Q in x-direction, Hills and Nowell [1] found that the relative displacement in normal direction $v_1(x) - v_2(x)$ is given by:

$$\frac{1}{A}\frac{\partial h}{\partial x} = \frac{1}{\pi}\int \frac{p(\zeta)d\zeta}{x-\zeta} \quad - \beta\, q(x) \tag{2.3}$$

where h(x) is equal to $v_1(x) - v_2(x)$, and known as the amount of overlap that would occur if the contacting bodies could freely interpenetrating each other, A represents the composite compliance

$$A = 2\left\{ \frac{1-\nu_1^2}{E_1} + \frac{1-\nu_2^2}{E_2} \right\} \tag{2.4}$$

and β Dundurs' parameter is given by :

$$\beta = \frac{1}{A} \left\{ \frac{(1-2\nu_1)(1+\nu_1)}{E_1} - \frac{(1-2\nu_2)(1+\nu_2)}{E_2} \right\} \quad (2.5)$$

where E and ν are the material modulus of elasticity and Poisson's ratio respectively.

In a similar way the relative tangential displacement $u_1(x) - u_2(x)$ is equal to g(x) and equation 2.3 can be expressed in terms of g(x) as follow:

$$\frac{1}{A}\frac{\partial g}{\partial x} = \frac{1}{\pi}\int \frac{q(\zeta)d\zeta}{x-\zeta} + \beta\, p(x) \quad (2.6)$$

Since the two bodies are similar and they have the same properties, then the term β will be zero and equations 2.3 and 2.6 can be simplified to:

$$\frac{1}{A}\frac{\partial h}{\partial x} = \frac{1}{\pi}\int_{-a}^{a} \frac{p(\zeta)d\zeta}{x-\zeta} \quad (2.7)$$

$$\frac{1}{A}\frac{\partial g}{\partial x} = \frac{1}{\pi}\int_{-a}^{a} \frac{q(\zeta)d\zeta}{x-\zeta} \quad (2.8)$$

where the contact patch x extend from –a to a, and the contact load distribution can be found by taking the inverse of equation 2.7:

$$p(x) = -\frac{\omega(x)}{A\pi}\int_{-a}^{a} \frac{h'(\zeta)d\zeta}{\omega(\zeta)(\zeta-x)} + C\omega(x) \quad (2.9)$$

where h'(x) = δh / δx, C is a constant and it is assumed to be zero in this case because there is no singularity at the edges, and at the same time the weight function ω(x) can taken to be :

$$\omega(x) = \sqrt{a^2 - x^2} \quad (2.10)$$

2.2 Hertz Analysis

From the equations mentioned in the previous section the contact-half-width and the peak value of contact load can be determined by using Hertz solution. The amount of overlap in freely interpenetrating bodies h(x) is assumed to be as:

$$h(x) = \Delta - \frac{1}{2} k * x^2 \tag{2.11}$$

where Δ is a constant, k is the curvature given by:

$$k = \frac{1}{R_1} + \frac{1}{R_2} \tag{2.12}$$

and R_1 and R_2 are the radii of the contacting surfaces.

From equation 2.11, h'(x), which was mentioned in equation 2.9, can be found to be:

$$\frac{dh}{dx} = -k * x \tag{2.13}$$

after applying equations 2.10 and 2.13 in equation 2.9 the result will be:

$$p(x) = -\frac{\sqrt{a^2 - x^2}}{A\pi} \int_{-a}^{a} \frac{k\zeta \, d\zeta}{\sqrt{a^2 - \zeta^2}(\zeta - x)} \tag{2.14}$$

this equation can be integrated to give the distribution load as follows:

$$p(x) = -\frac{k}{A} \sqrt{a^2 - X^2} \tag{2.15}$$

however, the half contact-width a is unknown here, but to be in equilibrium state with the applied normal load P, the distributed load in equation 2.15 can be integrated on the total contact length to get:

$$P = \frac{\pi k a^2}{2A} \tag{2.16}$$

and this gives the solution for the contact half-width a, and the peak contact pressure as follows:

$$a^2 = \frac{2PA}{\pi k} \tag{2.17}$$

$$p(x) = -P_0 \sqrt{1-(\frac{x}{a})^2} \tag{2.18}$$

where P_0 is the maximum peak pressure found to be:

$$p_0 = \frac{2P}{\pi a} \tag{2.19}$$

As the fretting specimen is assumed to have a flat surface ($R_1=\infty$), equation 2.17 can be simplified as:

$$a = \sqrt{\frac{8PR_1}{\pi}\frac{1-\nu^2}{E}} \tag{2.20}$$

From the above analysis the axial stress resulting from the applied contact load P can be expressed in Cartesian coordinates as:

$$(\sigma_{xx})_{contact} = -p_0\{\frac{\sqrt{a^2-x^2}}{a}\} \tag{2.21}$$

The stick and slip zones are shown in Figure 2.2, the stick zone is bounded by –c and c, whereas slip zones are located between –a and -c as well as c and a. The stick zone is a portion where the particles of the fretting bodies, the specimen and the pad, move together, while there is a freely motion inside the slip zones. The stick zone in fretting fatigue configuration is determined simplistically by the contact geometry, contact pressure and coefficient of friction. The formation of the stick zone leads to an

amplification of remotely applied stresses in the vicinity of contact surface and premature crack initiation.

Before the application of the tangential force, the stick zone encompasses the entire contact from –a to a, and there is no tangential motion, so equation 2.8 will be equal to zero which gives the solution of the shear stress distribution along the contact surface as follows:

$$q(x) = \frac{C}{\sqrt{a^2 - x^2}} \tag{2.22}$$

where C=Q/π, and Q is the total shear stress along the contact length calculated by integrating the shear stress distribution as:

$$Q = \frac{fp_0\pi}{2a}(a^2 - c^2) \tag{2.23}$$

where f is the coefficient of friction and the stick zone size can be found as:

$$\frac{c}{a} = \sqrt{1 - |\frac{Q}{fP}|} \tag{2.24}$$

The stress distribution in x-direction as a result of the tangential load could be obtained as follows:

$$(\sigma_{xx})_{\text{tan}\,gential} = 2fp_0 - \frac{2}{\pi}\int_{-a}^{a}\frac{q'(x)}{x+a}dx \tag{2.25}$$

where

$$q'(x) = -\frac{fp_0 c}{a}\sqrt{1-(\frac{x-e}{c})^2} \tag{2.26}$$

and

$$e = \frac{\sigma a}{4fp_0} \tag{2.27}$$

where $$\sigma = \frac{E\varepsilon_{xx}}{1-\nu^2} \quad (2.28)$$

and ε_{xx} is the strain induced by the axial stress (σ_{axial}) under plane strain.

As a result the total axial stress along the contact surface between the fretting specimen and the fretting pad can then be expressed as:

$$\sigma_{xx} = (\sigma_{xx})\text{contact} + (\sigma_{xx})\text{tangential} + (\sigma_{xx})\text{axial} \quad (2.29)$$

A FORTRAN program named “Ruiz program” was written by Chan and Lee [2] to calculate the numerical solutions required by analytical analyses for variables such as contact half-width in equation 2.20, Hertzian Peak Pressure in equation 2.19, σ_{xx} in equation 2.21, and so forth. These solutions from both analytical equations and Ruiz program are computed to verify the finite element model used in this study in chapter IV and to compare with experimental results in chapter V.

2.3. Fretting Fatigue Configuration

The fretting fatigue configuration has been developed and simplified by several previous studies in order to give a complete understanding of the problem and make it easier to be solved. Figure 2.3 shows the test scheme of the general fretting fatigue configuration. In this figure the fretting specimen and the fretting pads are presented as two mechanical components in contact with each other, the specimen is gripped at one end and subjected to axial stress (σ_{axial}) at the other end, on the other hand, the fretting pads are pressed against the specimen by the applied contact load P which is perpendicular to the axial load.

The axial load and the contact load can be applied by a servo hydraulic machine which can control the loads with the magnitude, stress ratio, frequency, phase angle, and waveform, in order to simulate the load conditions as desired. The fretting fatigue contributing variables can be tested by using identical or dissimilar pad and specimen material, in room or elevated temperature, and with different pad geometry.

The tangential load Q, as a result of the contact mechanics, makes a partial slip condition instead of gross slippage, and its magnitude is the half of the difference between the applied axial load and the load measured at the gripped end of specimens. The side of the contact region near the fixed end is called leading edge, while the other side near the applied axial loads is defined as trailing edge. Contact half-width, a, incorporates both stick-zone (c) and partial slip zones, and the center of contact width is defined as the origin of x-direction. A similar fretting fatigue configuration, cylindrical-end pads in contact with a flat specimen, was used in this study, and the detailed experiment setup is elaborated in chapter III.

2.4. Fretting Fatigue Factors

Fretting fatigue is a very complicated phenomenon because there are as many as 50 factors that can affect the behavior of the material under fretting fatigue condition; such as; coefficient of friction, contact pad geometry, elevated temperature, axial load conditions, contact load conditions, interface shear stress, shoot-peening treatment, environment corrosion, etc., hence several studies have been conducted to investigate the

contribution of each factor on the fretting fatigue condition. Most of these factors will be discussed in the following sections:

2.4.1. Coefficient of Friction

The coefficient of friction, f, on a contact interface is mainly dependent on the applied normal load. The coefficient of friction can be determined firstly by applying the contact load P on the pad against the specimen, then increasing the axial load slowly on the specimen until gross slip occurs, at this time the resulting tangential load Q should be monitored and recorded immediately. The ratio between the tangential load and the applied contact load is known the dynamic coefficient of friction and this ratio can be found as follows:

$$f = Q/P \tag{2.30}$$

During fretting fatigue test, the coefficient of friction is usually stabilized after 5,000 to 10,000 fretting fatigue. Iyer and Mall [3] reported that the experimental stabilized static coefficient of friction was determined to be ranging among 0.37~0.46 for Ti-6Al-4V, the coefficient of friction may vary depending on the ratio of Q/P as postulated by Hills et al. [4]. This variation is needed for fretting fatigue analysis. Lykins et al [5], and Iyer and Mall [6] found that the variation of friction coefficient from 0.45 ~ 0.7 caused relatively small variation on fretting fatigue variables such as 20% increase in strain range, while Namjoshi [7] showed that by increasing coefficients of friction from 0.5 to 0.8 the following have been occurred; MSSR always predicted crack orientation at about ±45˚ for a cylindrical-end pad configuration, there was no effect on crack initiation

location prediction from MSSR parameter, and only about 32% increase in MSSR was observed under cylindrical-end pad geometry and average 12% increase in MSSR under flat-end pad geometry. Lee [8] found that the friction coefficient is equal of 0.34 and 0.45 when applying a 2224 N and 4448 N contact load respectively. From these results and in order to simplify the fretting fatigue analysis in finite element analysis, the coefficient of friction can be assumed to be constant. In this study the magnitude of 0.5 was used as the coefficient of friction in FEA.

2.4.2. Contact Pad Geometry

Varying pad geometry will affect the fatigue life of the material. Namjoshi [7, 9, and 10] investigated fretting fatigue mechanism of Ti-6Al-4V specimens in contact with three different radii and two different flat- end- with- radius- edge contact pad geometry. He noticed that the fretting fatigue life was significantly reduced compared to plain fatigue life despite pad geometry and by increasing the applied normal pressure on fretting pads the fretting fatigue life will decrease at a given applied axial stress. In this study Namjoshi showed also that the crack initiation location was found at the contact surface near the trailing edge with orientation at about either -45˚ or +45˚ under variation of ±15˚ from the direction perpendicular to the applied axial load, and there was no significant correlation between pad geometry/load conditions and crack initiation location/orientation.

On another hand, Madhi [11] investigated two pads geometry, 50.8 mm and 304.8 mm, on fretting fatigue behavior of IN-100 alloy and he reported that the pad geometry has less effect on the fatigue life of IN-100 alloy relative to titanium alloy.

2.4.3. Axial Load Frequency and Contact Pressure

Varying the magnitude of the applied contact load and the applied axial load frequency on Ti-6Al-4V has been looked into by Iyer [3]. Iyer found that when the contact load was increased from 1338 N to 3567 N, the fretting fatigue life has been reduced at 1 Hz and it hasn't been affected at 200 Hz. He noticed also that by increasing the axial load frequency from 1 Hz to 200 Hz and keeping the applied contact load at a constant value of 1338 N the fretting fatigue life reduced. In this study; at 1338 N applied contact load a wear/ plastic deformation across the entire contact region was found, while at 3567 N applied contact load a clear dominate stick zone and a narrow slip zone with little debris was observed , and the crack initiation location was found near the trailing edge in all tests on the contact surface.

The answer why the fretting fatigue life reduced when increasing the contact load can be found in [6] where the finite element analysis was conducted. In this study it was reported that fretting fatigue loading results in an amplified stress range in the vicinity of contact region due to the local build-up of compressive stresses upon loading and unloading. Furthermore, the decrease of fretting fatigue life by increasing the contact pressure can be related to the increase in the local stress range amplification along the

contact surface, without any regard to the increase in the local shear stress or slip amplitude.

In another study, Jutte [12] found that by increasing the contact load under unidirectional shear the fatigue life was reduced, while fretting fatigue life with variable contact loads was observed less than fatigue life for tests with equivalent constant contact loads under unidirectional shear tests. This reduction in fretting life is increased under bi-directional shear tests, however, fatigue life reduction was observed less distinguishable for tests with variable contact loads at higher magnitude under bi-directional shear tests. The crack initiation location in this study was also found near the trailing edge on contact surface, and crack initiation orientation was about -50˚.

Lee [8] conducted the effect of variable contact load on fretting fatigue behavior of titanium alloy. Lee found that the tangential load stayed in phase with the axial load and the contact load affected only the magnitude of the tangential load and it had no effect on the phase or the frequency of the tangential load. He noticed also that the fatigue life was primarily dominated by the axial load, the magnitude and frequency of the contact load had no significant effect on fatigue life and MSSR parameter, the crack initiated near the trailing edge, and the crack initiation orientation is the same as for the constant contact load.

2.4.4. Elevated Temperature

Lee et al. [13, 14] investigated Ti-6Al-4V specimens under influence of temperature at 25˚C, 100˚C, and 260˚ C. He showed that there was no effect on fretting

fatigue life from rising temperature up to 260˚. For all entire tests, the multiple-crack initiation pattern was observed, and the cracks always initiated at the trailing edge on the contact surface. In this study, most of the scar surface was basically covered by debris/oxides, and no noticeable effect on changing the coefficient of friction was observed. The stress relaxation phenomenon has been noticed somehow away from the contact region for all specimens that failed at 25˚C, 100˚C and 260˚C. In addition, higher temperature as well as longer exposure time induced larger stress relaxation.

2.4.5. Environment Corrosion

As the environment affects the behavior of crack initiation and crack propagation of fretting fatigue condition and the resistance strength of the material, fretting fatigue should be investigated under some environmental situation. Waterhouse and Dutta [15] found that fretting fatigue life under 1% NaCl solution corrosion is reduced at higher alternating stresses but it is improved at lower stress regime when compared to tests under dry conditions. This phenomenon has been explained by Wharton and Waterhouse [16]. They found that at higher stresses, environment corrosion increases crack propagation, resulting in a reduced fatigue life, but the protective corrosive debris which remained on the fretting contact surface under lower stresses can retard crack initiation and improve fatigue life. Hoeppner et al. [17] also found that a greater reduction on fatigue life in 3.5% NaCl solution than in distilled water or air.

Lietch [18] found that under dry and seawater conditions, seawater corrosion fretting fatigue life is reduced under low cycle fatigue; on the other hand it improved

under high cycle fatigue He also showed that fretting crack initiated at the trailing edge on the contact surface among his tests.

2.5. Fatigue Parameters

During previous researches the predictive parameters were developed on the basis of stress or strain history of the plain fatigue configuration, and then these techniques have been extended to fretting fatigue data. In fretting fatigue, these parameters can be used to predict the location of the initiation crack, its angle, and after how many cycles this crack will occur. The fretting fatigue behavior, under low cycle fatigue regime, can be described by the critical plane approach that based on the maximum damage plane which is formulated during the fatigue. During fretting fatigue conditions the fatigue life is mostly spent in crack nucleation till the crack is getting a detectable size while a small life time is spent in crack propagation to the critical size. The fretting fatigue life is reduced compared to the plain fatigue [5, 11, and 19]. On the other hand an alternative approach is needed to predict the High Cycle Fatigue (HCF) crack initiation behavior of the fretting fatigue condition.

2.5.1. Plain Fatigue Techniques

In plastic area the relationship of fatigue life in low cycle regime as showed in Coffin [20] and Manson [21] can be expressed as follows:

$$\left(\frac{\Delta\varepsilon}{2}\right)_p = \varepsilon_f^{'}(2N_f)^{c'} \tag{2.31}$$

where $(\Delta\varepsilon/2)_p$ is the plastic strain amplitude, ε_f' is the fatigue ductility coefficient, N_f is the number of strain reversals to failure (1/2 cycle =1 reversal) and c' is the fatigue ductility exponent.

For the elastic area Basquin [22] found that stress vs. fatigue life relationship can be correlated as follows:

$$\left(\frac{\Delta\varepsilon}{2}\right)_e = \frac{\sigma_f^{'}}{E}(2N_f)^{b'} \tag{2.32}$$

where $(\Delta\varepsilon/2)_e$ is the elastic strain amplitude, σ_f' is the fatigue strength coefficient, E is modulus of elasticity, N_f is the number of strain reversals to failure (1/2 cycle =1 reversal) and b' is the fatigue strength exponent.

From above the strain life equation can be found to be as follows:

$$\varepsilon_a = \frac{\sigma_f^{'}}{E}(2N_i)^{b'} + \varepsilon_f^{'}(2N_i)^{c'} \tag{2.33}$$

where ε_a is total strain amplitude, N_i is the cycles to crack initiation. This equation can only be applied under constant strain ratio conditions but it does not hold for different strain ratios. For different strain ratio the Walker shift formula [23] can be used to collapse data from different strain ratios onto a single curve can be written as:

$$\varepsilon_{\max,R_\varepsilon} = \varepsilon_{\max}(1-R_\varepsilon)^m \tag{2.34}$$

where $\varepsilon_{max,R\varepsilon}$ represents the maximum strain corrected for the strain ratio, ε_{max} is the maximum strain, R_ε is the strain ratio ($R_\varepsilon=\varepsilon_{min}/\varepsilon_{max}$), and m is the material fitting parameter that was chosen to collapse plain fatigue crack initiation data at different strain ratios, however; Lykins [5]showed that this parameter could predict the number of cycles

to crack initiation and crack initiation location along a contact surface very well, but not for crack initiation orientation prediction.

2.5.2. Stress Range and Effective Stress

The stress range for the applied axial load can be expressed as:

$$\Delta\sigma = \sigma_{\max} - \sigma_{\min} \tag{2.35}$$

in this equation there is no effect from mean stress or stress ratio, however; Namjoshi et al. [4] found another method using effective stress to account for the effects from stress ratio as well as residual stress as follows:

$$\sigma_{eff} = (\sigma_{\max} + \sigma_{residual}^{tensile})(1 - \frac{\sigma_{\min} + \sigma_{residual}^{tensile}}{\sigma_{\max} + \sigma_{residual}^{tensile}})^{m} \tag{2.36}$$

where σ_{eff} is the effective stress, and m was found by Lykins [5] to be 0 .45. This equation only collapse fretting fatigue life data into a single curve as shown in Mall et al. [10, 24], while Andrew [11] showed that this equation was able to collapse fretting fatigue life into a single curve under variable contact load as will as constant contact load conditions, and Lee et al. [12] observed that it worked well in fretting fatigue life prediction under elevated temperature up to 260˚ C.

The above two equations 2.35 and 2.36 didn't include the stress concentration effect occurring at the trailing edge of contact region and multi-axial loading conditions induced by fretting fatigue. This explains why critical plane-based predictive parameters, as to be described in the subsequent sections, formulated on local stress distribution are needed.

2.5.3. Critical Plane

The in-plane principal stresses acting at a specific point can be expressed as follows:

$$\sigma_{1,2} = \frac{\sigma_{xx} - \sigma_{yy}}{2} \pm \sqrt{(\frac{\sigma_{xx} - \sigma_{yy}}{2})^2 + \tau_{xy}^2} \tag{2.37}$$

$$\tau_{\max} = \sqrt{(\frac{\sigma_{xx} - \sigma_{yy}}{2})^2 + \tau_{xy}^2} \tag{2.38}$$

where σ_1 and σ_2 are the maximum and minimum principal normal stresses that acting on the principal planes. σ_{xx}, σ_{yy}, τ_{xy} are stress components at a local point, and τ_{max} is the maximum shear stress which acts on a plane with 45^o from the orientation of principal planes.

The local normal and shear stresses can be computed as follows:

$$\sigma = \frac{\sigma_{xx} + \sigma_{yy}}{2} + \frac{\sigma_{xx} - \sigma_{yy}}{2}\cos(2\theta) + \tau_{xy}\cos(2\theta) \tag{2.39}$$

$$\tau = -\frac{\sigma_{xx} - \sigma_{yy}}{2}\sin(2\theta) + \tau_{xy}\cos(2\theta) \tag{2.40}$$

where θ is evaluated from -90^o to $+90^o$. These two equations can formulate the critical plane to help predicting fatigue life, and crack initiation location and orientation.

2.5.4. Smith-Watson-Topper Parameter (SWT)

The Smith-Watson-Topper (SWT) parameter can be found by the following equation:

$$SWT = \frac{\left(\sigma_f^{'}\right)^2}{E} * \left(2N_i\right)^{2b'} + \sigma_f^{'} \varepsilon_f^{'} \left(2N_i\right)^{b'+c'} \quad (2.41)$$

where $\sigma_f^{'}$ is fatigue strength coefficient, b_f' is fatigue strength exponent, ε_f'is fatigue ductility coefficient, c' is fatigue ductility exponent, E is the elasticity modulus, and N_i is cycles to crack initiation. This equation has been modified by Szolwinski and Farris [25] by using critical plane approach as follows:

$$SWT = \sigma_{\max} \varepsilon_a \quad or \quad \max(\sigma_{\max} \varepsilon_a) \quad (2.42)$$

where σ_{max} is the stress normal to a critical plane, and ε_a is the normal strain amplitude to a critical plane. SWT parameter asserts crack initiation occurs on the plane where the product of σ_{max} and ε_a is maximal. Using the computed local stress and strain from finite element analysis of the fretting fatigue experiments, this parameter was calculated at all planes ranging from $-90^o \leq \theta \leq +90^o$, which provided this parameter's maximum value. However some previous studies [10, 24, 25, and 26] found that SWT parameter was effective in predicting the number of cycles to crack initiation and crack initiation location with strong dependence on pad geometry. However, it didn't provide good agreement with crack initiation orientation.

2.5.5. Shear Stress Range Parameter (SSR)

For computing Shear Stress Range Parameter (SSR), the shear stress should be calculated along all planes ranging from $-90^o \leq \theta \leq 90^o$ from the state of stress (σ_{xx}, σ_{yy}, τ_{xy}) computed from FEA by applying the following equation:

$$\tau = -\frac{\sigma_{xx} - \sigma_{yy}}{2} \sin 2\theta + \tau_{xy} \cos 2\theta \tag{2.43}$$

This will give the parameter SSR as, $\Delta\tau = \tau_{max} - \tau_{min}$ at all planes and at all points in the contact region, where $\tau_{max} - \tau_{min}$ are maximum and minimum shear stresses, and because there is an effective from mean stress and stress ratio this parameter can be explained by:

$$(SSR = \Delta\tau_{crit}) = \tau_{\max}(1 - R_{\tau})^{m} \tag{2.44}$$

where τ_{max} is the maximum shear stress, R_τ is the shear stress ratio (τ_{min} / τ_{max}) at the critical plane, and m is a fitting parameter determined as mentioned before to be 0.45. Mall et al. [10, 24] showed that SSR, for specimens with different pad geometry, was useful in conjunction fretting fatigue life with plain fatigue life. In addition, this parameter can also correlate crack initiation location and orientation with experimental observations very well.

2.5.6. Findley Parameter (FP)

Findley's study [27] found that there is a multi-axial fatigue parameter affected from the normal stress on a critical plane in addition to the shear stress as shown in the following equation:

$$FP = \tau_a + k\sigma_{\max} \tag{2.45}$$

where k is an influence factor calculated from [10] to be 0.35, and τ_a is stress amplitude defined as $\tau_a = (\tau_{max} - \tau_{min})/2$. FP was calculated at all planes ranging from $-90^o \leq \theta \leq +90^o$

from computed stresses and strains obtained from finite element analysis. These calculations provided the critical plane, where this parameter is the maximum.

In Mall et al. [10, 24] they found that for specimens with different geometry pads under fretting fatigue conditions, FP could predict crack initiation location well but was not able to predict fretting fatigue life from plain fatigue data. In addition, the predicted crack orientations were different from experimental observations

2.5.7. Modified Shear Stress Range Parameter (MSSR)

As seen in previous section another parameter is needed to predict the crack initiation location, the fatigue cycles to occur, and the crack initiation orientation at the same time. This can be found by modified SSR parameter by combing maximum normal stress on a critical plane of maximum SSR:

$$MSSR = A\Delta\tau_{crit}^{B} + C\sigma_{\max}^{D} \tag{2.46}$$

where $\Delta\tau_{crit}$ found from equation 2.43, and σ_{max} is the maximum normal stress on the critical plane of the SSR parameter. A, B, C, D are fitting constants determined by curve fitting approach. These constants are determined empirically by [10] as A = 0.75, B = 0.5, C = 0.75, and D = 0.5. MSSR was calculated at all planes ranging from $-90^{o} \leq \theta \leq +90^{o}$ from computed stresses and strains obtained from finite element analysis. These calculations provided the critical plane, where this parameter is the maximum.

As in previous studies [10,19,24] the MSSR was found to be the only critical plane-based parameter eligible in predicting fatigue life, crack initiation location, and crack initiation orientation Therefore, MSSR parameter was determined to be an

appropriate fatigue predictive parameter while investigating crack initiation behavior of Ti-6Al-4V under fretting fatigue phenomenon. Also Namjoshi et al. [7] showed that MSSR was able to satisfactorily characterized fretting crack initiation orientation and location independent of contact geometry for two values of coefficient of friction, 0.5 and 0.8. So in this study, MSSR was adopted as the fatigue parameter to be investigated in fretting fatigue behavior prediction.

2.6. Summary

In summary, fretting fatigue occurs between two components in contact with each other and reduces the fatigue life when compared to the plain fatigue. Analytical solutions have been developed and several researches have been conducted to give a better understanding of fretting fatigue phenomenon by varying some of the contributed factors that have an effect on the fretting fatigue behavior.

These several studies, as seen in the previous sections, tried to analyze different contributing variables, such as coefficient of friction, fretting pad geometry, shot-peening process, elevated temperature, environmental corrosion, axial load condition with different frequencies, and contact load condition. Most of these previous studies have been conducted on titanium alloy under a constant applied contact load conditions, while a little effort has been done with a variable contact load with different frequencies with respect to the axial load. This study focused on the variable contact load with a phase difference between the axial and the contact load condition and the different between the fretting fatigue and the plain fatigue on fretting fatigue condition.

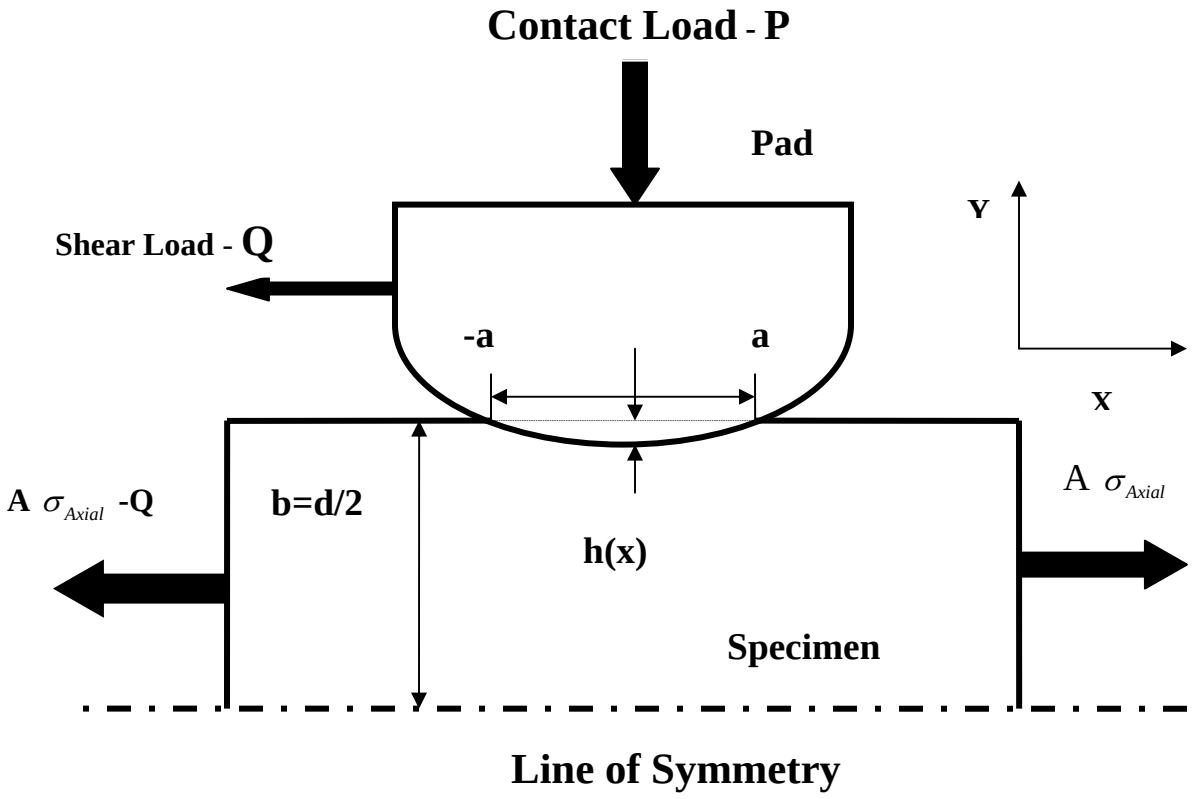

Figure 2.1 Bodies under fretting fatigue loads

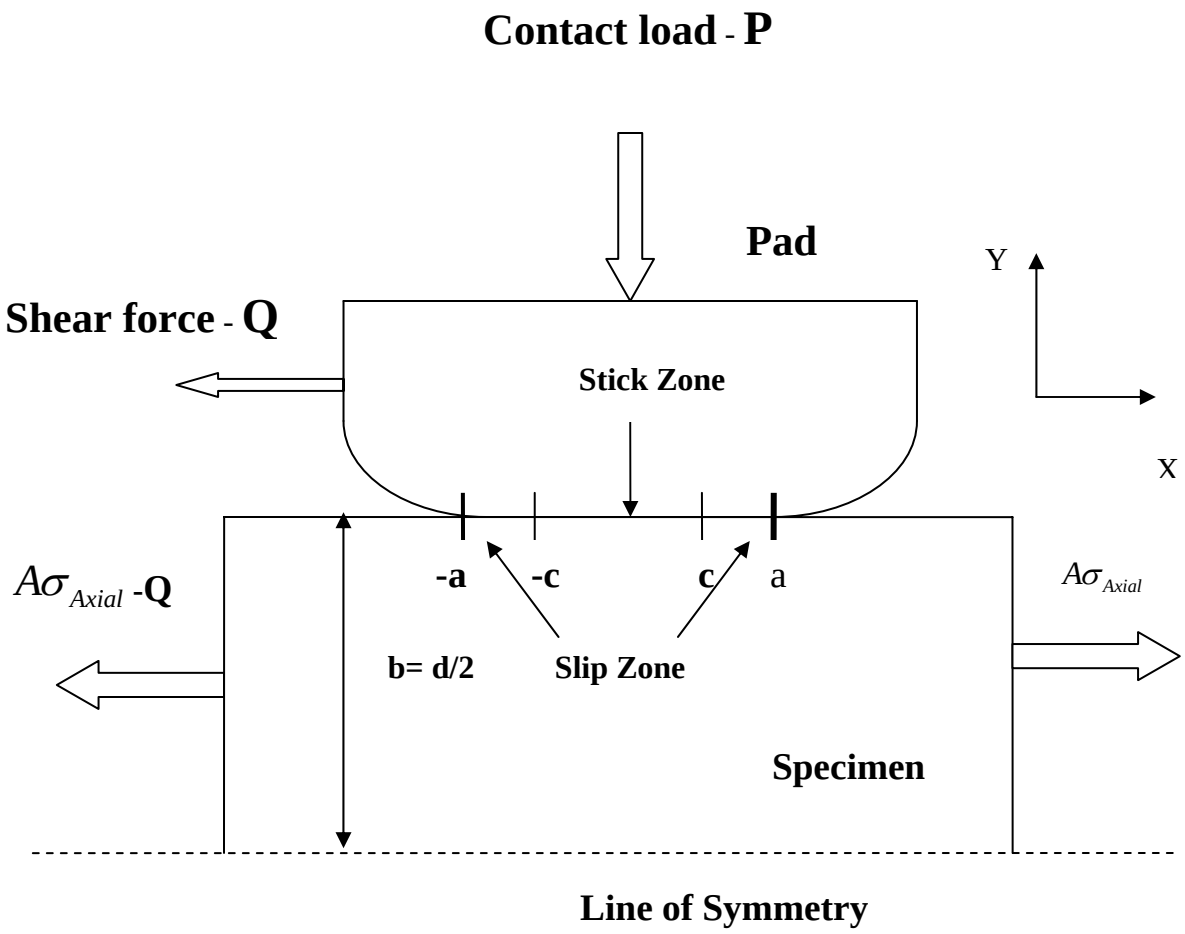

Figure 2.2 Stick and slip zones for deformed bodies

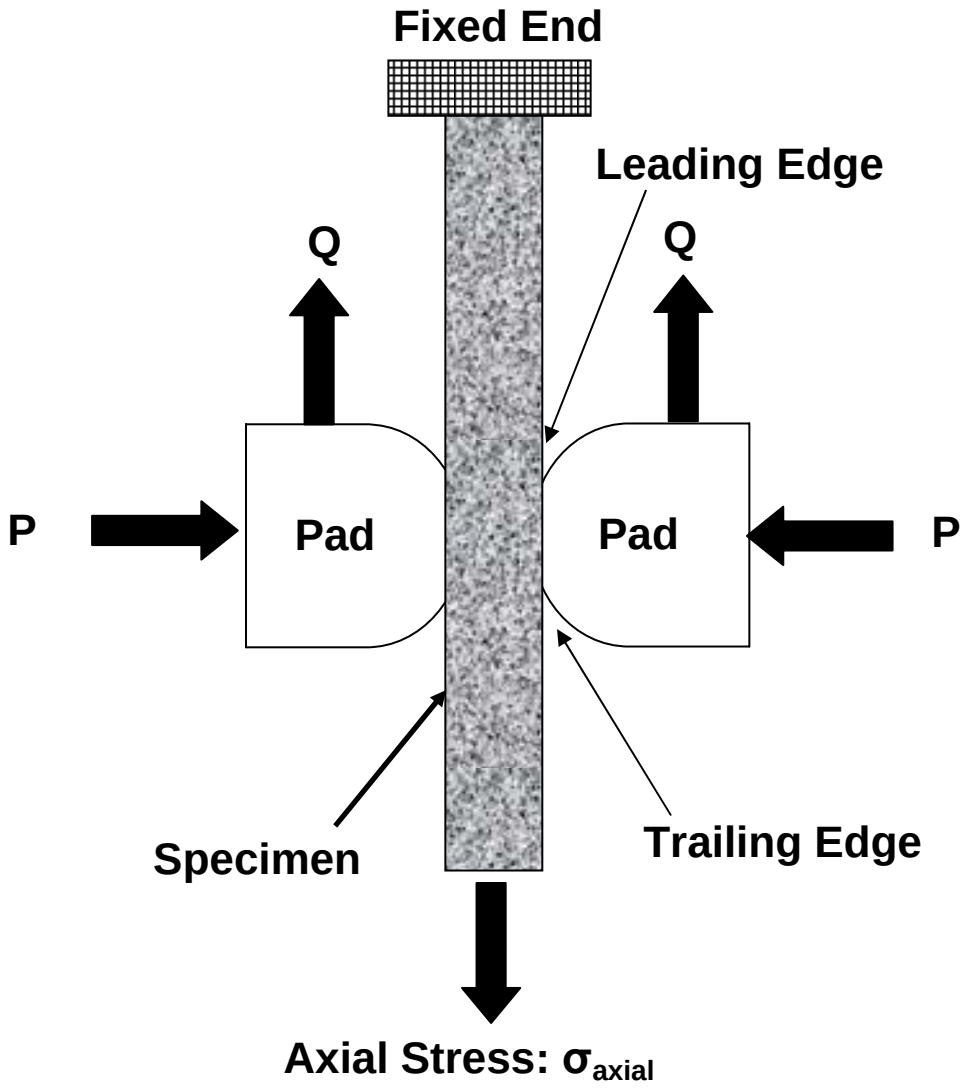

Figure 2.3 Schematic fretting fatigue configurations

3. Experiments

The experimental details used in this study are addressed in this chapter. The test set up is discussed first, followed by the material details and the geometry of both the specimen and the pad which were used in this work, then the test procedure and load determination will be discussed, and finally the details to determine the crack initiation and the crack initiation orientation experimentally will be covered.

3.1. Test Set-up

To investigate the effects of the phase difference between the applied contact load and the axial load and the combination of the plain and the fretting fatigue conditions on the titanium Ti-6A1-4VA specimen, a bi-axial servo-hydraulic test machine shown in Figure 3.1 was used. This test machine consists of a rigid steel fixture frame, a 100 kN lower axial hydraulic servo actuator, and a 5 kN contact hydraulic servo actuator. These two actuators are controlled by Multi Test System MTS 793.10 Multi-Purpose Test Software (MPT) which allows the users to vary the magnitude, frequency, waveform, and phase lag between these two actuators which were used to apply both the axial and the contact loads at the same time.

A schematic diagram of the above test machine is shown in Figure 3.2. This diagram shows that the fretting fixture holding the blocks to keep a pair of pads in the precise alignment and prevent them from moving freely. The axial load is controlled by the 100 kN hydraulic servo actuator and its variation is measured by the lower axial

servo-hydraulic load cell, while the applied contact load is controlled by the left fretting servo-hydraulic and its variation is measured by the left servo load cell. It is necessary to note here that the pad alignment is very important to ensure that both loads are perpendicular to each other.

3.2. Specimen and Pad Geometry and Material Properties

The dimensions of dog-bone specimen and the pad are shown in Figure 3.3. The specimen's length is 228.6 mm, thickness 3.81 mm, width 6.35 mm, and cross section area is $24.1935\,mm^2$, while the pad geometry has one cylindrical end with radius of 50.8 mm at one end and with a flat end at the other side, and its thickness and width are the same of 9.525 mm.

Both the specimens and the pads used in this study were made up from the same material, and this material is forged titanium alloy, Ti-6A1-4V. This alloy was preheated and treated in a solution at 935^oC for 105 minutes, then cooled in air, afterwards vacuum annealed at 705^oC for two hours, and cooled again in argon. The resulting micro structure showed 60 % by volume of α (HCP) phase (platelets) and 40 % by volume of β (BCC) phase matrix. The measured grain size was about 10 μm. The yield strength (σ_y) of the material is 930 MPa, Poisson's ratio (υ) of 0.33, elastic modulus (E) of 126 GPa, and Brinell hardness number of 302. Both the dog-bone specimens and the pads are cut by the wire electrical discharge method.

3.3. Test Procedure

In this study two types of fretting fatigue tests were investigated; the first one is to investigate the effect of phase difference between the axial load and the applied contact load on fretting fatigue conditions. In this type of test; the frequency of both axial load and applied contact load was chosen to be the same, i.e. 10 Hz. The minimum magnitude of the applied contact load was 2224 N and the maximum one was 4448 N, while the axial load was applied in a tension- tension loading condition and the axial mean stress was varied at a constant stress ratio of 0.1 as shown in Table 3.1. The values in this table these were used with in-phase and out of phase angles between the axial load and the applied contact load. In the second type of fretting fatigue test; various combinations of fretting fatigue and plain fatigue were investigated under constant applied contact load of 3336 N and cyclic axial load with maximum value of 564 MPa and minimum value of 56.4 MPa with a frequency 10 Hz.

The desired procedure for each test is programmed in multi-purpose test; however there are some steps that should be done before running this procedure. Starting with installation of one pair of pads into the holding blocks that were affixed to a fixture frame, and then aligning these pads to ensure that the contact surfaces of the pads were orthogonal to the specimen and the axial load was perpendicular to the applied contact load. After that the specimen is removed from the fixture and a warm up procedure programmed in multi-purpose test is executed for at least 30 minutes to ensure that there is no hydraulic malfunction. Once warm-up is done, the specimen is mounted and

clamped into the test fixture through the upper and lower grips. Afterwards the selected procedure will be ready to run.

The first step in each procedure was set by applying the contact load gradually till the magnitude of the applied contact load reached the maximum value, followed by application of the axial load gradually also till its magnitude reached the maximum. After that, the cyclic load (sinusoidal wave) between the maximum and the minimum values of both the applied axial load and the applied contact load (if required) with a frequency of 10 Hz is applied until the failure occurred. While the desired procedure is running the following parameters are recorded; the lower axial load, the running time, the upper axial load, the fretting fatigue cycles, the displacement, and the applied contact load. After the specimen failed, the number of fretting fatigue cycles was taken down as the specimen's fatigue life.

3.4. Load Determination

During each test, the peak-valley compensator (PVC) was activated for both contact load and axial load to reduce variation between command and feedback signals sensed by the test machine. The axial loads, and the contact loads were monitored and recorded continuously until a specimen failure occurred. The tangential load can be calculated from the following formula:

$$Q = \frac{V_{lower} - V_{upper}}{2} \tag{3.1}$$

where V_{lower} is the lower axial load, V_{upper} is the upper axial load, and Q is the tangential load. The tangential loads were plotted with respect to the axial loads for a desired number of cycles as shown in Figure 3.4. The curve in this Figure, which known as the fretting hysteresis loops, indicates that the partial slip conditions have been met after approximately 100 fretting fatigue cycles.

The maximum and minimum tangential loads were also plotted versus the life cycles as shown in Figure 3.5. From these curves, it can be seen that the test started to be in a steady state condition at the first hundreds cycles of fretting fatigue cycles. So the magnitude of the maximum and minimum tangential loads suspending to the maximum and minimum axial loads respectively were taken at a 10,000 cycles as an input to the analytical solution of Ruiz program as well as the Finite Element Analysis (FEA) as it will be presented in chapter IV.

On the other hand, the coefficient of friction, f, can be found as the ratio between the tangential load Q and the applied normal load P as follows:

$$f = Q/P \tag{3.2}$$

in this study and based on the absolute maximum ratio of tangential load to the corresponding contact load in each test, this coefficient of friction was found to be ranged between 0.2397 ~ 0.5033 for in-phase condition tests and 0.1568 ~ 0.2144 for out of phase condition tests. The Q/P ratio for tests # 2 (in-phase) and 3 (out of phase) were plotted versus the fretting fatigue cycles as shown in Figure 3.6, in this figure it can be confirmed also that the steady state condition reached after about 100 fretting fatigue cycles.

3.5. Crack Initiation and Orientation

After the failure of the specimen occurred, the contact region and the fracture surface of the failed specimen was investigated. In order to locate the crack initiation a lower magnification microscope was used to take a photo of the scar, which resulted from the contact mechanism between the specimen and the pad, and this microscope was also used to take a general picture of the fracture surface of the specimen. In all fretting fatigue tests of the investigation in this study, the crack, in the case of fretting fatigue failure, always initiates at or very near the trailing edge of the contact region where the stress concentration in the x-direction is maximum and x/a =1 as shown in Figure 3.7. This photo shows that the location of the crack initiation for test # 4 is near the trailing edge, and the contact-half- width for this test was measured experimentally to be approximately 0.77 mm for the maximum contact load, while the analytical solution from Ruiz program predicted that the contact half-width, a, is 0.801 mm for the maximum contact load. This value of the contact half- width is needed in FEA to find the required stresses at the contact area.

Figure 3.8 shows a general picture of the fracture surface area that was taken by a lower magnification microscope. In order to be able to see this area in a higher magnification a Scanning Electron Microscope (SEM) was used, but in order for the specimen to be fit inside the SEM it should be cut along the y-direction by using a saw machine to reach a length of around 10 mm in x-direction.

On the other hand, the crack initiation orientation along the contact surface can be evaluated also by using the SEM to show that the crack initiation zone is the area with

discoloration on the failed specimen surface. Firstly the saw machine was used to cut the failed specimen while it is sectioned laterally in the x-axis as close as possible to the center of the estimated crack initiation zone. Then a trimming machine was used to shave the cutting area of the fracture surface until a clear SEM picture allows the investigation of the crack orientation. Finally the trimmed cutting part of the specimen was put inside the SEM in order to measure the crack initiation orientation angle.

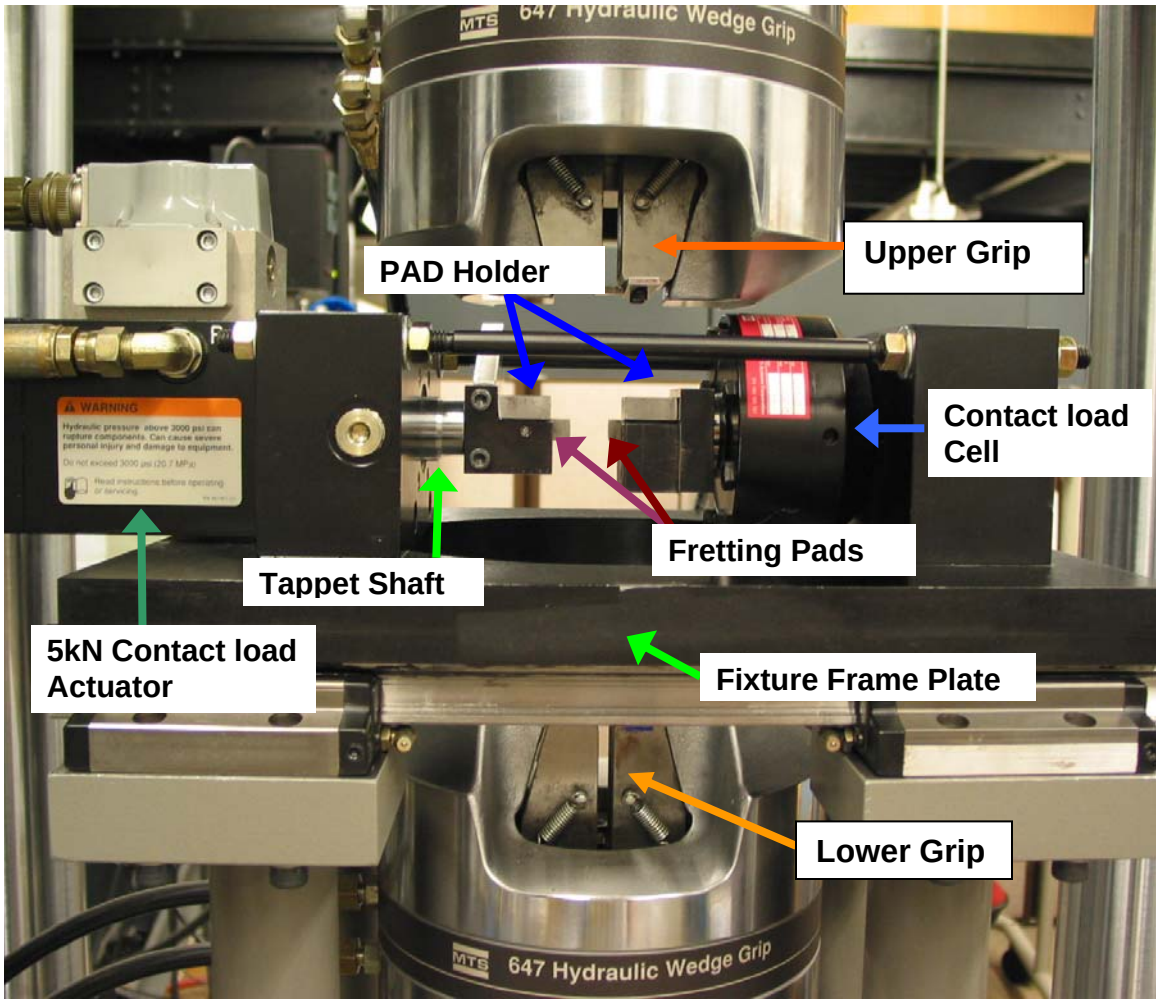

Figure 3.1 Bi-axial fretting fatigue test machine

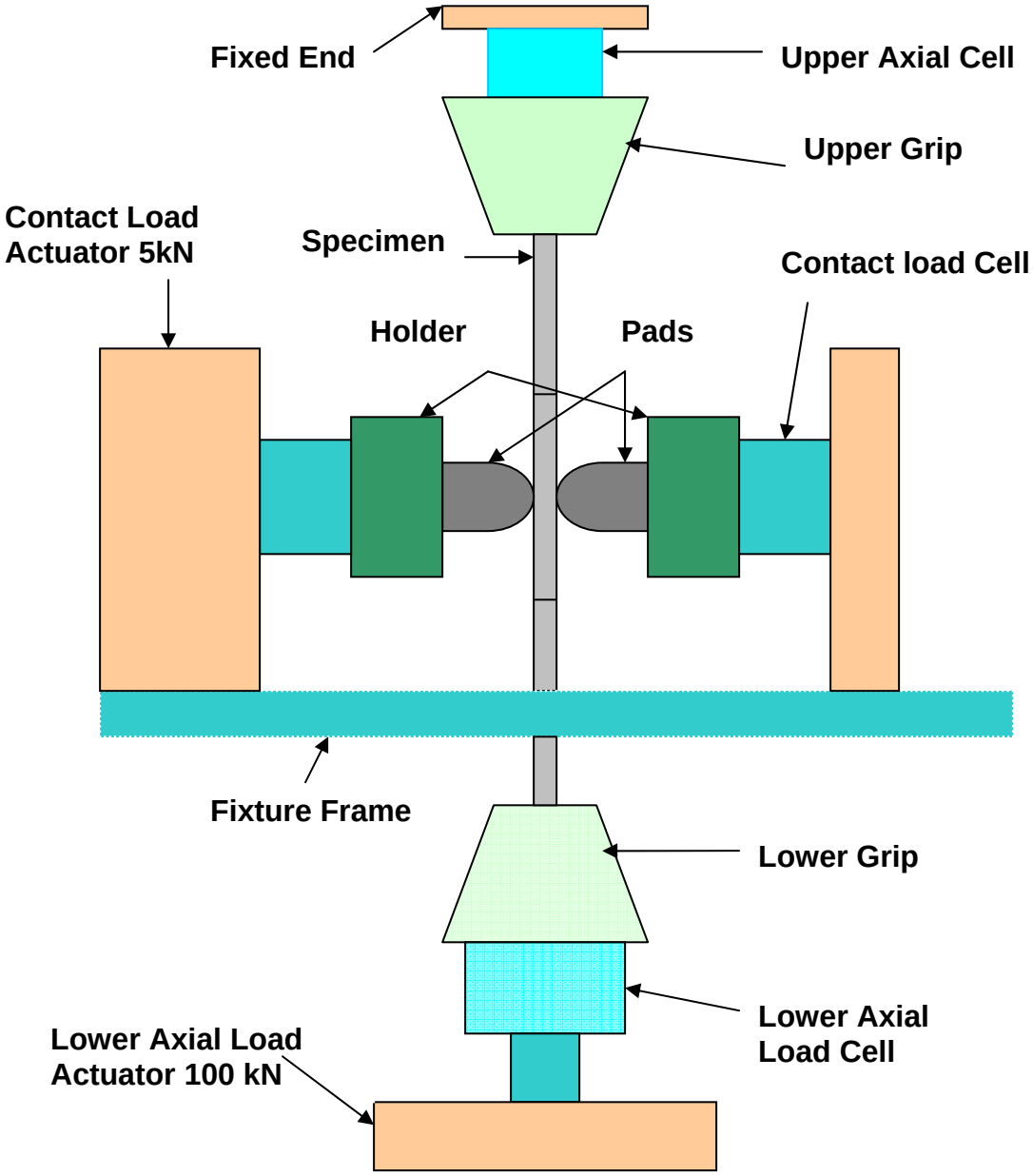

Figure 3.2 Schematic diagram of bi-axial test machine

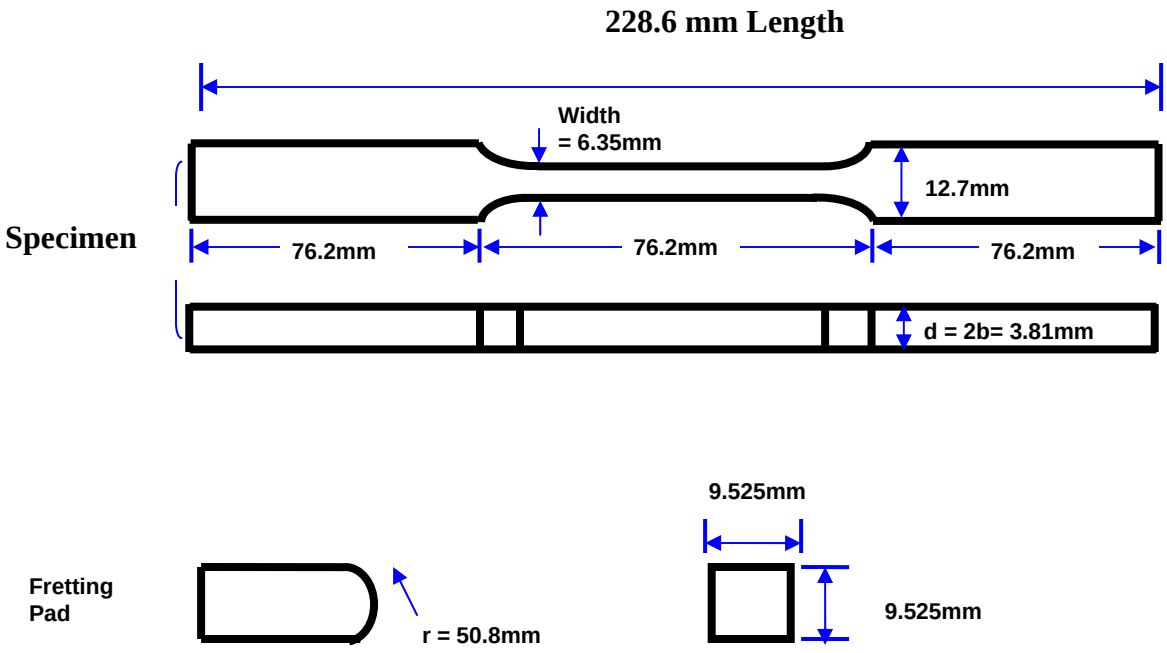

Figure 3.3 Specimen and pad dimensions and geometry

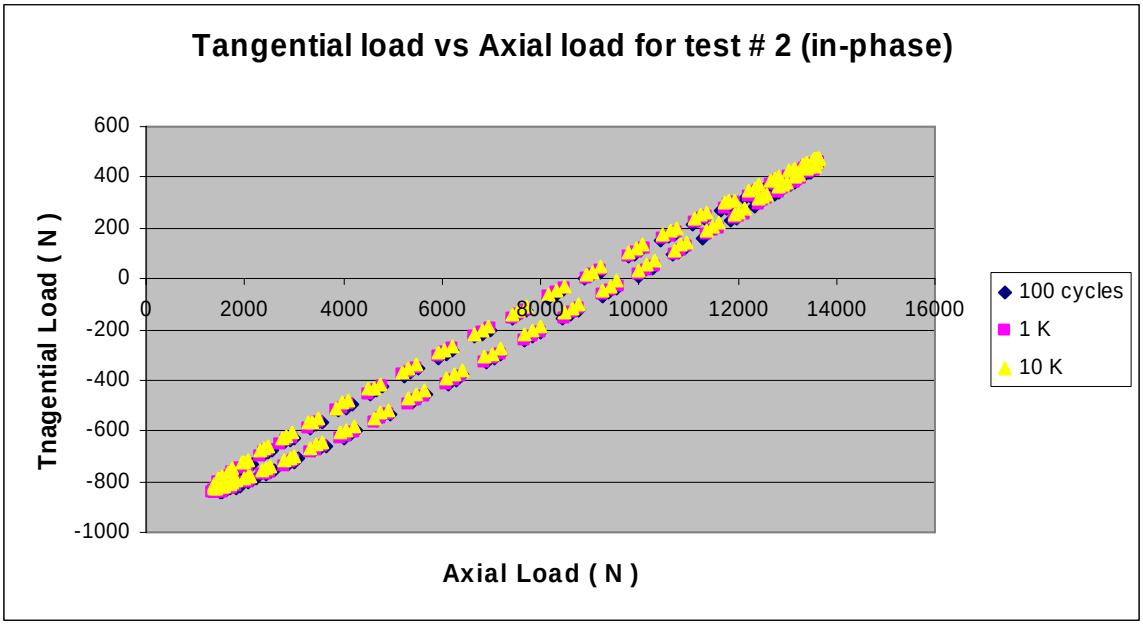

In-phase

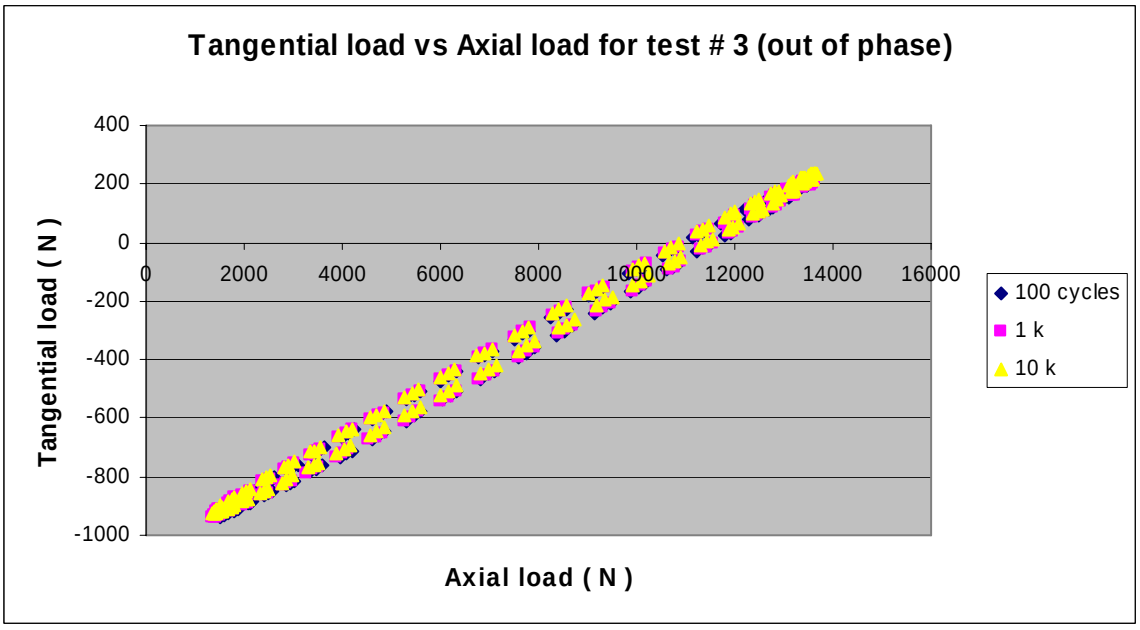

Out of phase

Figure 3.4 Tangential load vs. axial load for test#2 (in-phase) & test#3 (out of phase)

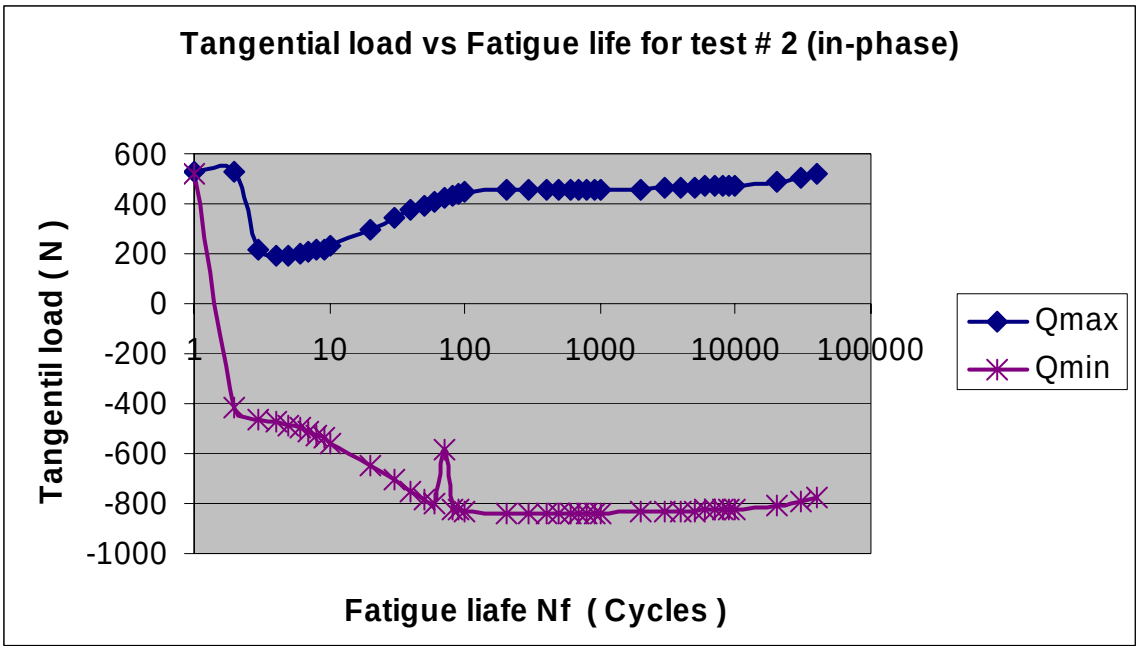

In-phase

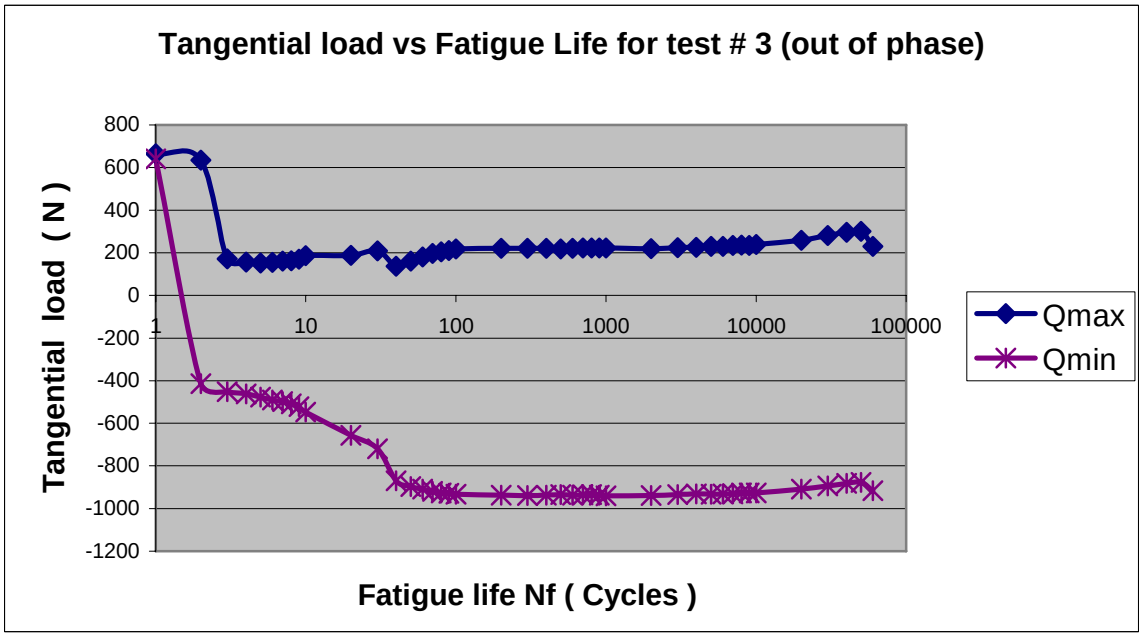

Out of phase

Figure 3.5 Tangential load vs. cycles for test#2 (in-phase) & test#3 (out of phase)

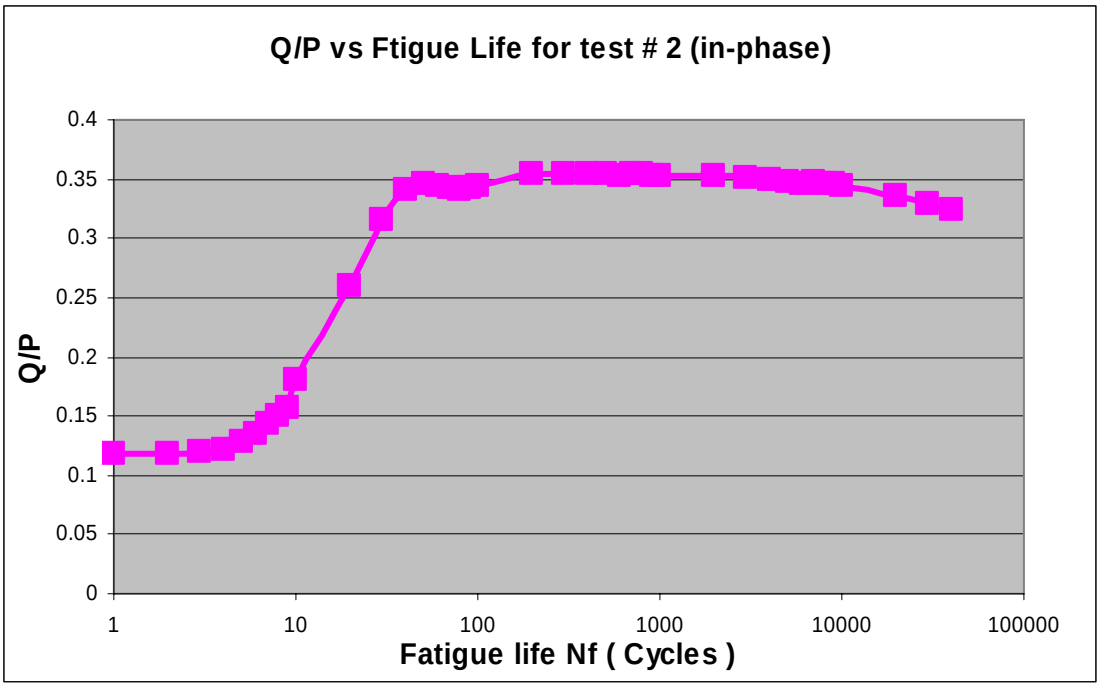

In-Phase

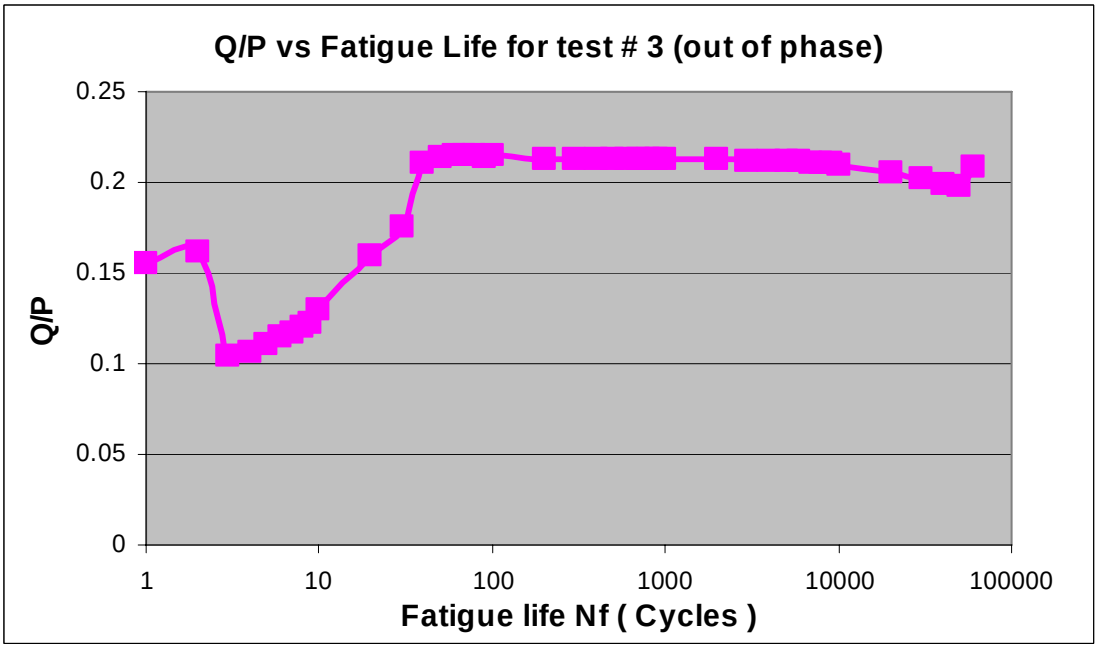

Out of Phase

Figure 3.6 Q/P vs. cycles for test#2 (in-phase) & test#3 (out of phase)

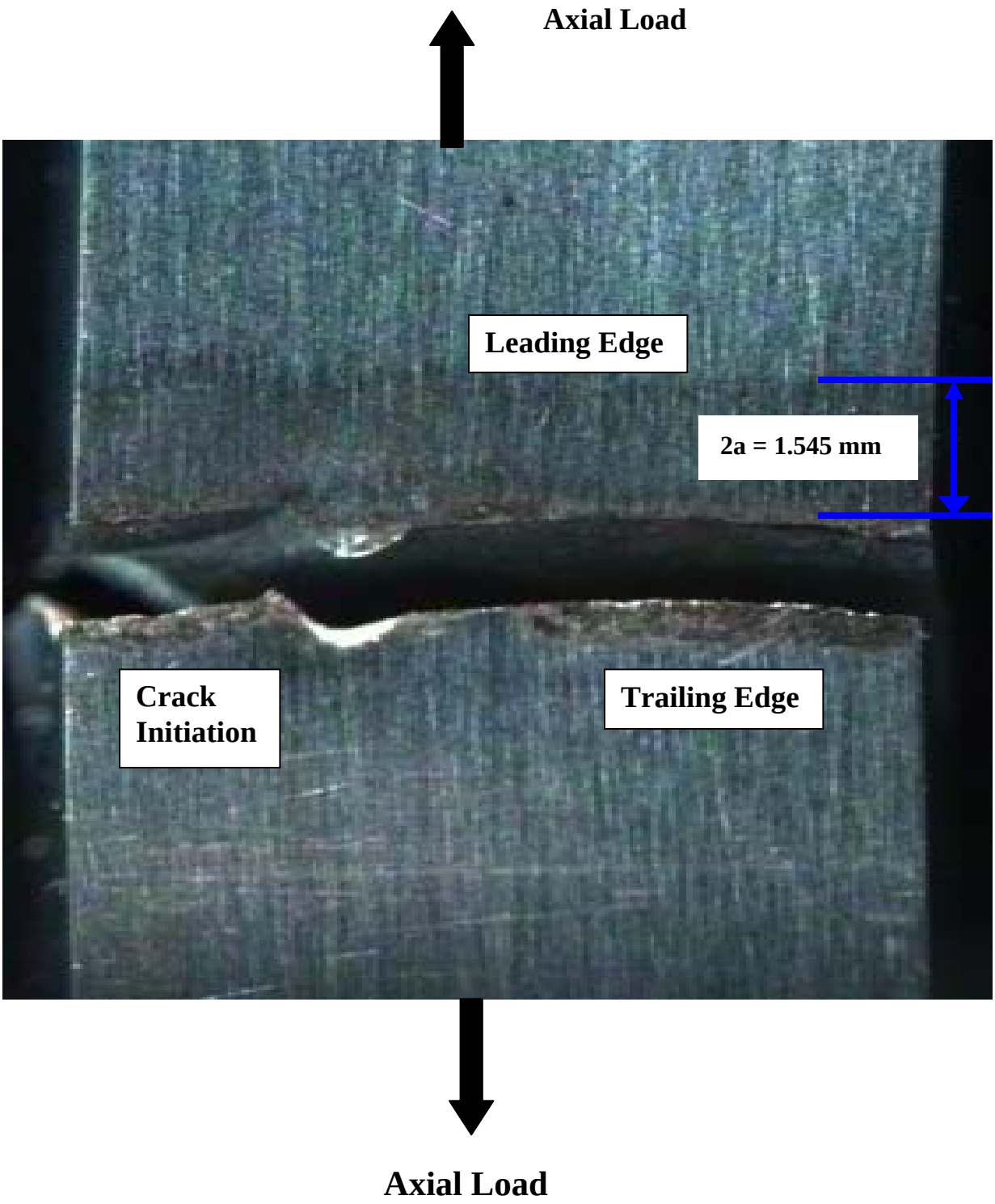

Figure 3.7 Crack initiation location for test # 4

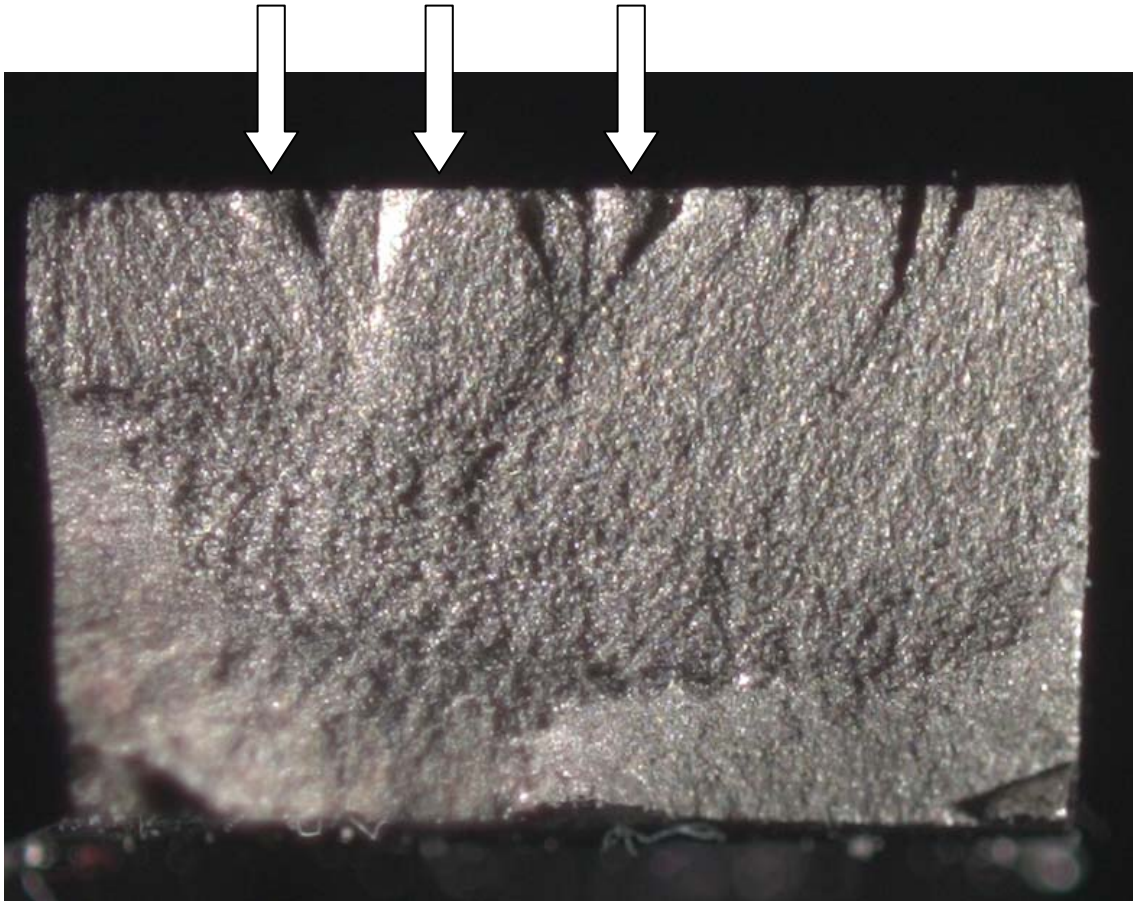

Figure 3.8 Fracture surface of failed specimen of test # 2

Table 3.1 Input loads and phase angles used in this study

Test #	σ_{max} MPa	σ_{min} MPa	P_{max} N	P_{min} N	$phase\_angle(\phi)$ Degree
1	**760**	**76**	**4448**	**2224**	**0**
2	**564**	**56**	**4448**	**2224**	**0**
3	**564**	**56**	**4448**	**2224**	**90**
4	**413**	**41**	**4448**	**2224**	**0**
5	**413**	**41**	**4448**	**2224**	**90**
6	**376**	**37**	**4448**	**2224**	**0**
7	**376**	**37**	**4448**	**2224**	**90**
8	**282**	**28**	**4448**	**2224**	**0**
9	**564**	**56**	**3336**	**3336**	**0**
10*	**564**	**56**	**3336**	**3336**	**0**
11**	**564**	**56**	**3336**	**3336**	**0**
12	**564**	**56**	**4448**	**2224**	**60**
13	**564**	**56**	**4448**	**2224**	**105**
14***	**564**	**56**	**3336**	**3336**	**0**
15	**330**	**33**	**4448**	**2224**	**90**

* Test done first with 21,320 fretting fatigue cycles and then under plain fatigue
** Test done with 5,000 fretting cycles followed by 10,000 plain cycles, then repeated
*** Test done with 1,000 fretting cycles followed by 200,000 plain cycles, then repeated

4. Finite Element Analysis

Finite Element Analysis (FEA) is a numerical procedure that was used to determine the fretting fatigue parameters by calculating the state of stress, strain, and displacement at the contact area. Why and how FEA is used in this study will be described in this chapter. This includes the requirements of FEA, FEA model, load inputs, and the model validation. In addition; the MSSR calculation is covered at the end of this chapter.

4.1. Requirement for FEA

In FEA, the rigid body can be represented by a discrete system containing many elements which are connected to each other by the nodes, and at these nodes the governing equations can be solved to give the solution of the stress, strain, and displacement at the contact interface. As mentioned previously, the configuration, that was used in this study, is a two cylindrical bodies, pads, on a flat body, specimen, and their radii are assumed very large in comparison to the contact width ($r >> a$) to be able to use the analytical solution. The infinite half-space assumption required that the specimen thickness, b, is more than ten times of the contact half-width, a, while in this study the maximum ratio of (b/a) was determined approximately of 3.43 and this makes the half infinite assumption invalid. Hence another procedure, that doesn't require an infinite half space assumption, is required to have a solution of the fretting fatigue parameters. So FEA, as a numerical analysis, can be used to achieve this goal, and the result of FEA can

be checked to match the analytical solution obtained from “Ruiz” program. This explains why finite element analysis is vital for conducting quantitative analysis in this study. The governing variables of fretting fatigue, such as contact stress, strain and displacement, were adopted to develop fretting fatigue predictive parameters which will be addressed in the following chapters.

4.2. Finite Element Model

The fretting fatigue configuration used in this study can be modeled as shown in Figure 2.1 by using the commercially available software, ABAQUS, where four nodes plain strain quadrilateral elements were used. This model mainly consists of three parts: the fretting pad, the fretting specimen, and the rigid body to constrain the pad from rotation. Also a Multi-Point Constraint (MPC) was applied to keep the specimen and the pad from rotating around x or y directions during the application of the loads. This model is formulated in two dimensions and because of its symmetry about x-axis, only one half of the contact configuration has been modeled to save the time and the memory resources. In contact region, the master segment and slave nodes were used to establish the contact algorithm that was used to determine how the loads were transferred. The master surface is chosen to be the fretting pad while the slave one is the fretting specimen.

The material properties for the pad and the specimen were 126 GPa as modulus of elasticity and 0.33 as a Poisson’s ratio, while the stiffness of the rigid constraint body was selected very small of 5 Pa as a modulus of elasticity and 0.3 as Poisson’s ratio, and this selection is to ensure that it has a minimum effect on the pads and the specimen in order

to improve the convergence of the finite element analysis. The half thickness b of the specimen is 1.905 mm, the length of specimen is 19.05 mm, and the width for all three parts is the same of 6.35 mm.

In fretting fatigue condition, the contact region is the most critical area where it is required to find the governing variables; such as the stress, strain, and displacement, in an accurate way. So the mesh for both the pad and the specimen is refined incrementally from the center of contact surface, on the other hand a course mesh far away from the contact region is designed in order to save the time as well as the memory resources.

Since the previous studies as [18] reported that a slight difference in a coefficient of friction doesn't generate much deviation in stress profile, contact half-width, and so forth, and also the experimental stabilized static coefficient of friction was found to be ranged between 0.37~0.46 for Ti-6Al-4V, the coefficient of friction of 0.5 was used in all calculations in this study, and this value is higher than the largest magnitude of the calculated of Q/P ratio in order to have a converging numerical solution.

4.3. Load Inputs

The fretting fatigue steady state condition was always met after the first hundreds cycles of fretting fatigue cycles. In order to insure that all fretting fatigue variables including coefficient of friction, contact load, tangential load, and axial load were selected from the stable condition. Therefore, the load conditions at 10,000 cycles in all tests, which don't contain a plain fatigue condition, were selected to be as inputs to FEA.

To avoid the gross slip condition, the maximum contact load was applied initially at the first step and kept constant until step 2. At the second step, the maximum axial load and the corresponding tangential load were applied for in-phase condition as shown in Figure 4.2, while for the condition of out of phase, the minimum value of axial and tangential loads were applied as shown in Figure 4.3. However; in the condition where the phase angle was 60 degree or 105 degree, the input values for the axial and the tangential loads were the corresponding values related to the contact load at that time as shown in Figure 4.4. The frequency for all loads in all conditions of this study was constant of 10 Hz. After Step 2, the applied loads were simulated as a sinusoidal wave function with predetermined peak/valley values for the axial, the contact, and the measured tangential loads. Table 4.1 shows the values of the input loads for all tests, while Figures 4.2, 4.3, and 4.4 show the details of the applied loads sequence and the numbering systems for the seven steps that were needed for the all tests in this study.

.

4.4. Model Validation

In order to insure that the finite element analysis model is working well, the output results from FEA model were compared with the output from the “Ruiz” FORTRAN program which was developed on the basis of infinite half-space assumption under static applied contact and axial loads. This comparison has been done only for two tests; one for in-phase condition and the other for the out phase condition. Each test validation was also compared for two conditions; one for the maximum axial load condition and the second for the minimum axial load condition. The load values for Ruiz

program were also picked at 10,000 cycles of fretting fatigue cycles which is the same as the FEA input load conditions. The results from this comparison are shown in Figures 4.5 through 4.9.

From this comparison the following can be noticed:

a) The contact half-width ($a_{analyticl}$) was found to be 0.801 mm by using equation 2.20 or Ruiz program, while this value was found in FEA to be 0.82 mm for test # 3 and this gives a very small variation of 2 %. Hence the contact half-widths which were calculated from equation 2.20 and the Ruiz program were identical to each other and very close to the FEA solution, and since the contact half-width is subjected to change all the time under variable contact loads the contact half-width, $a_{Ruiz,max}$, calculated from the Ruiz program at a step where a maximum axial occurred concurrently is used as a reference in this study.

b) Figure 4.5 shows that the stress profile from FEA and Ruiz program is very close to each other where the maximum value of axial stress is 986 MPa at x/a = 0.961 from step 2 of FEA and 899 MPa from Ruiz program, and this gives 8.8 % difference in stress value and 3.9 % in location.

c) Figure 4.6 shows that the Hertzian peak pressure, p_o , from FEA and Ruiz program. p_o was determined from FEA to be 571 MPa, while p_o from Ruiz was 557 MPa which gives only variation of 2.4 %.

From this validation, it can be noticed that there is a good agreement between the analytical solution and the numerical solution calculated from FEA.

4.5. Steady State Condition

During the entire tests, the axial load and the contact load were applied in a sinusoidal pattern, and it would take a small time for this application to converge into a steady state. Since the frequency for both the axial and the applied contact load is same i.e. 10 Hz, only seven steps were needed to reach this convergence. Figures 4.7 to 4.9 show the stress profiles of test # 2 for σ_{xx} , σ_{xy} , and σ_{yy} which resulted from Ruiz program and FEA results. These figures show that σ_{yy} doesn't vary at all and σ_{xy} is subjected to more variation than σ_{xx} during the transition from unsteady to steady state. Step 2 in all tests is almost identical to the analytical solution and this is because step 2 indicates a quasi-static state; while there is much deviation in steps 4 and 6. For this reason FEA was elected and analyzed after the state becomes steady.

4.6. MSSR Calculation

As it has been discussed in section 2.7.2, the MSSR parameter was the most effective parameter in predicting the fretting fatigue life, crack initiation orientation, and crack initiation location, and also MSSR can take the effects of multi-axial loading and the stress concentration at the trailing edge, which is the case in the fretting fatigue condition, into consideration. So MSSR is adopted in this study as the only critical plane-based parameter. The MSSR calculation was conducted by using the FEA stress outputs superimposed with the corresponding residual along all planes ranging from

$-90^{o} \le \theta \le 90^{0}$ at 0.1^{0} increment throughout the whole specimen, where θ is the orientation at which stress state in material is observed.

Only two steps are needed to calculate the MSSR and these steps were computed as the maximum and minimum values at the peak and the valley of the axial, tangential, and contact loads. After calculating the all MSSR of each test over the seven steps, as shown in Table 4.2, the MSSR with the greatest value was designated as the maximum MSSR parameter of this test and it is then, as shown in the next chapter, analyzed for its location, orientation, and correlation with fretting fatigue life under cyclic axial and variable contact load conditions.

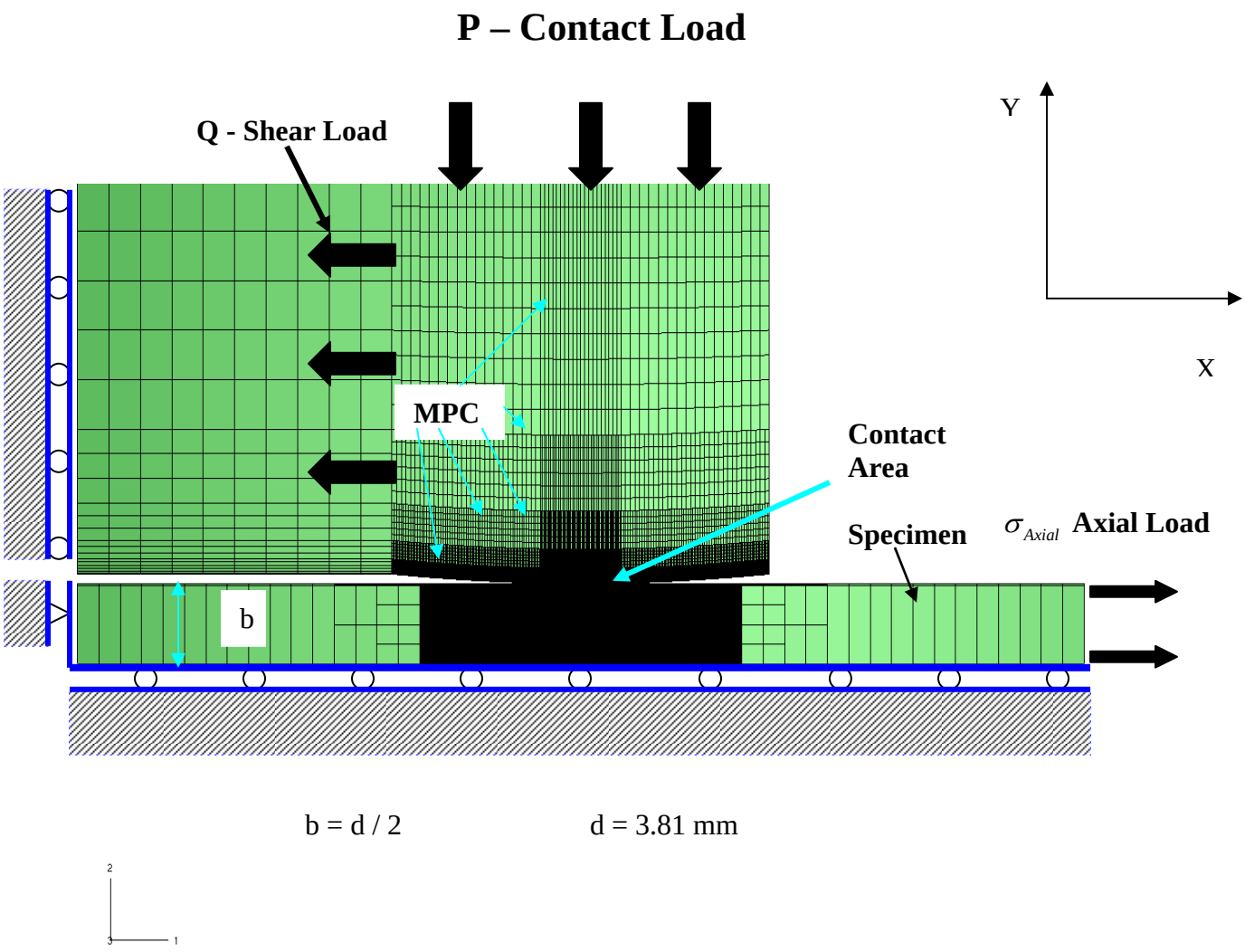

Figure 4.1 FEA Model with load and boundary conditions

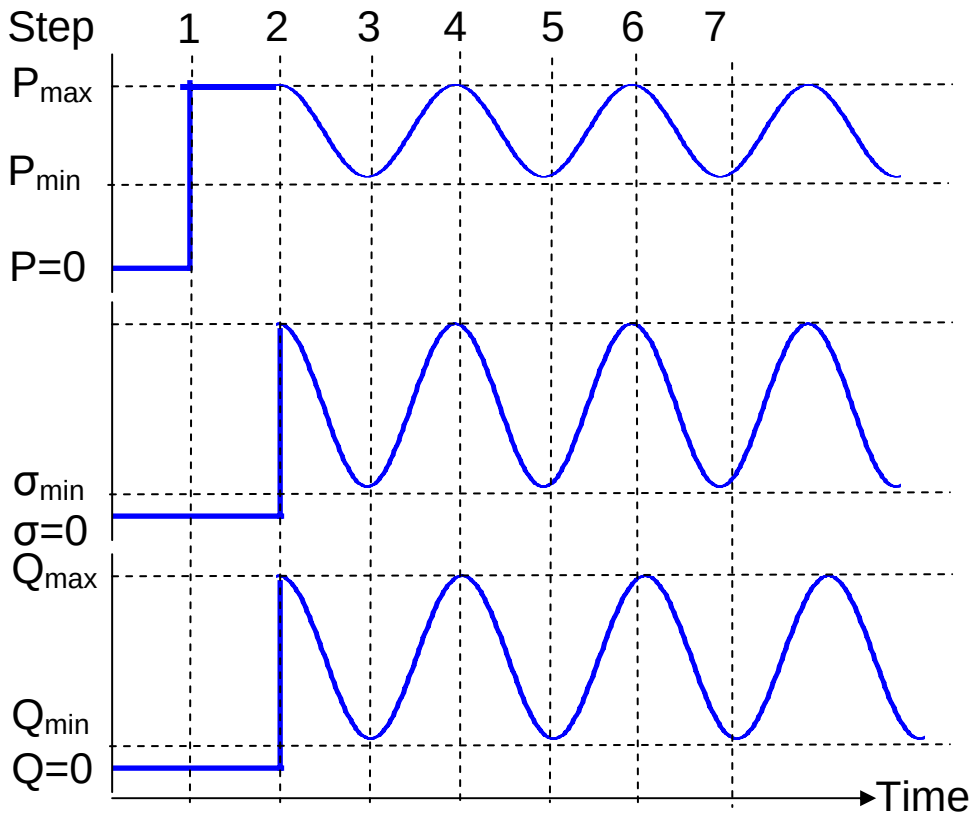

Figure 4.2 Load step used in FEA for in-phase condition

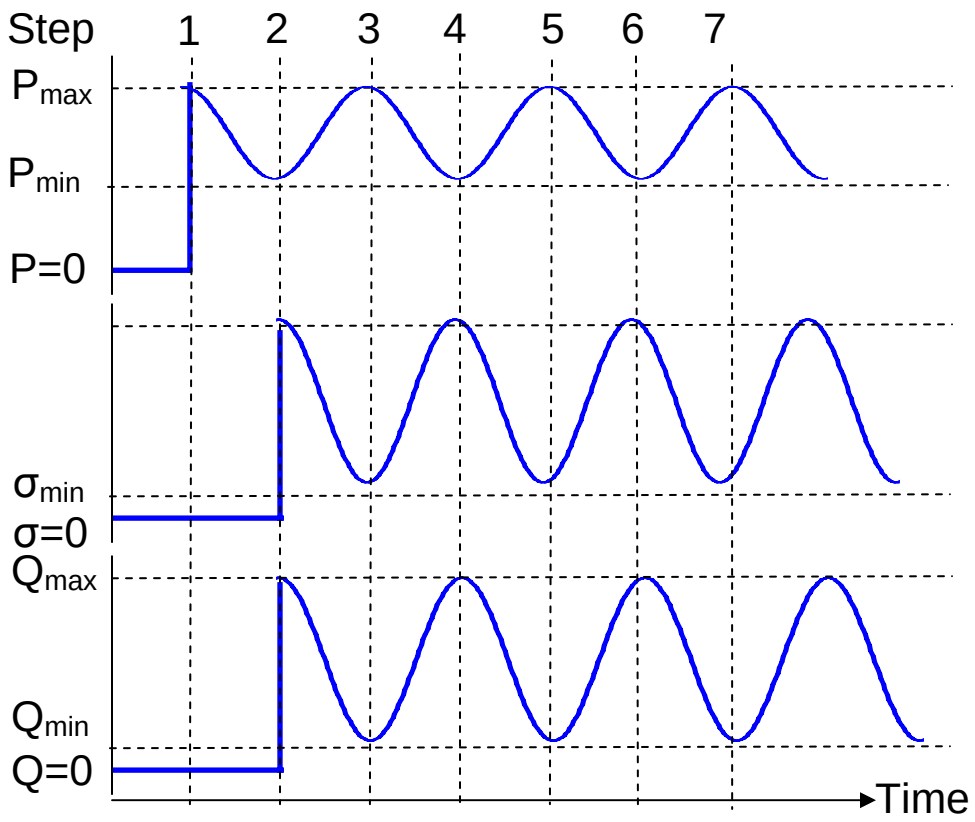

Figure 4.3 Load step used in FEA for out-phase condition

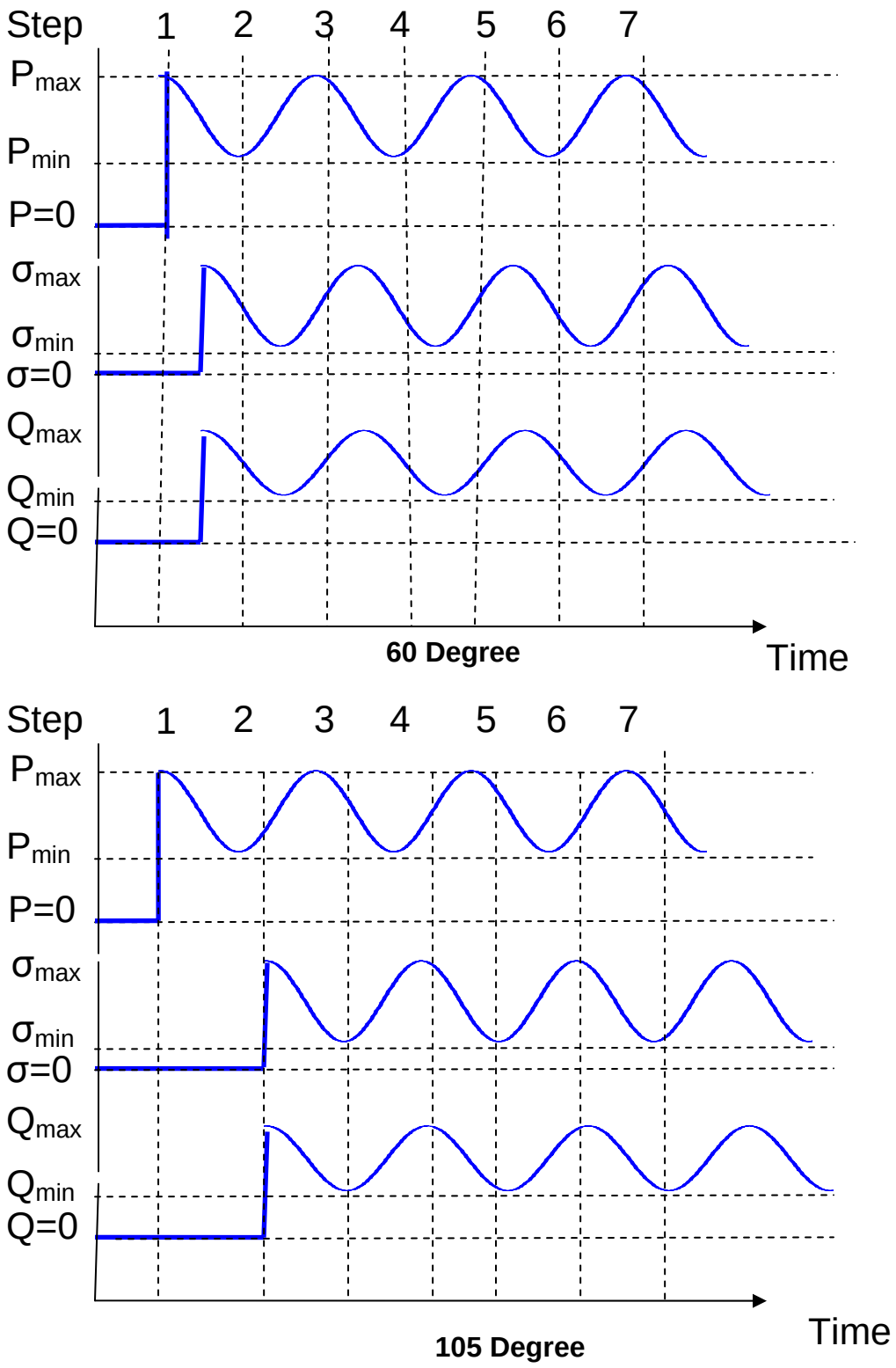

Figure 4.4 Input loads for 60 and 105 degree

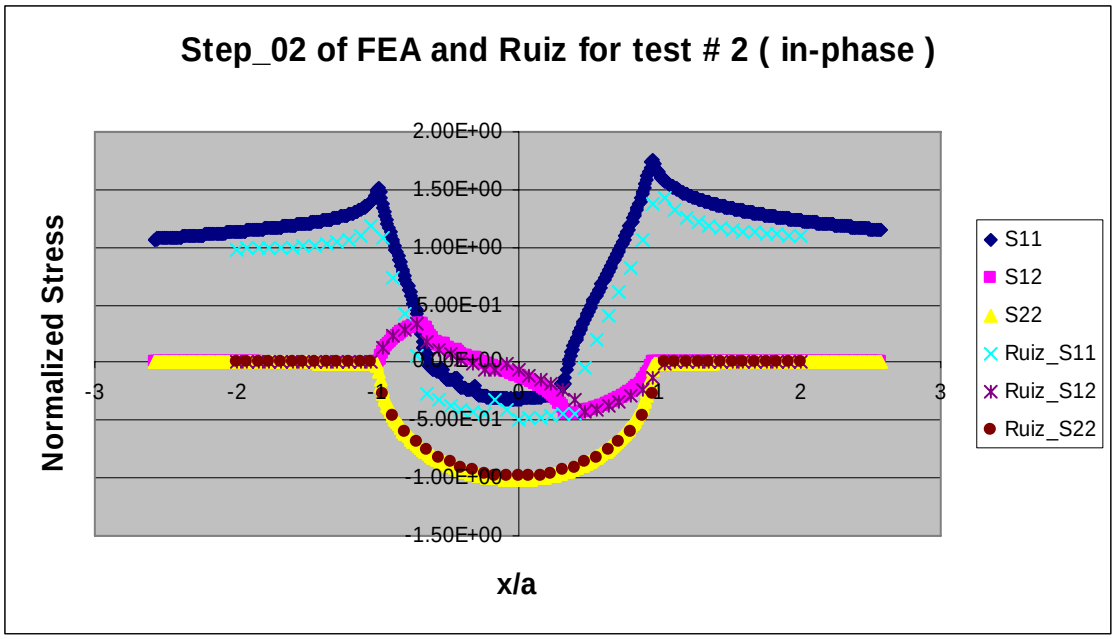

Figure 4.5 Test # 2 FEA and Ruiz profile stress

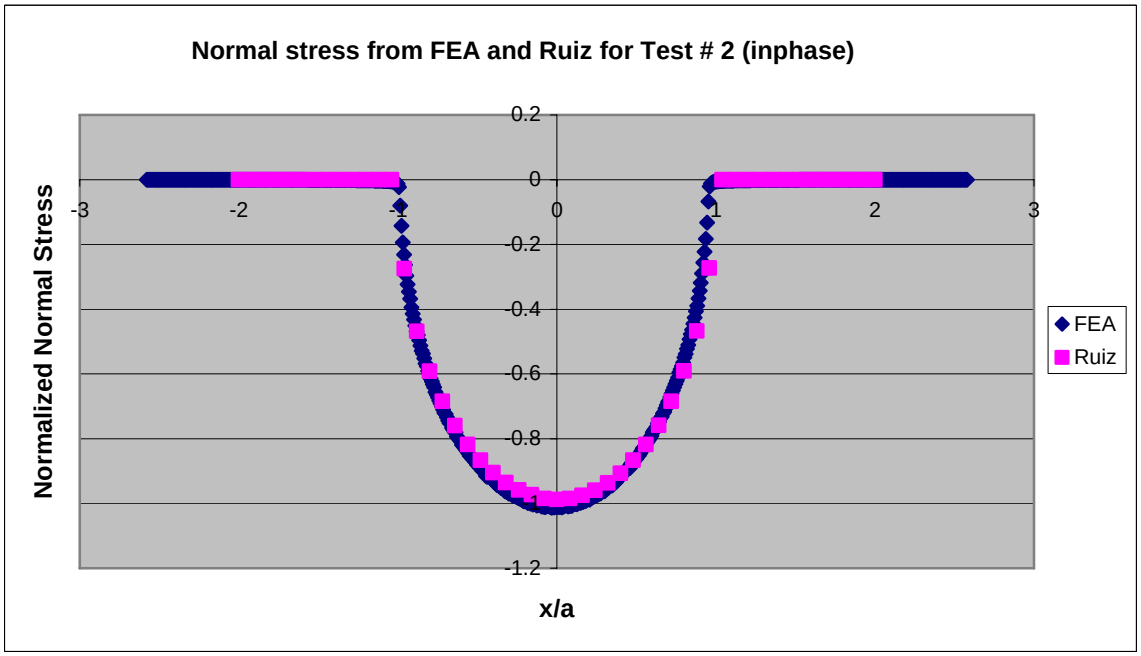

Figure 4.6 Test # 2 FEA and Ruiz Heratzian peak pressure

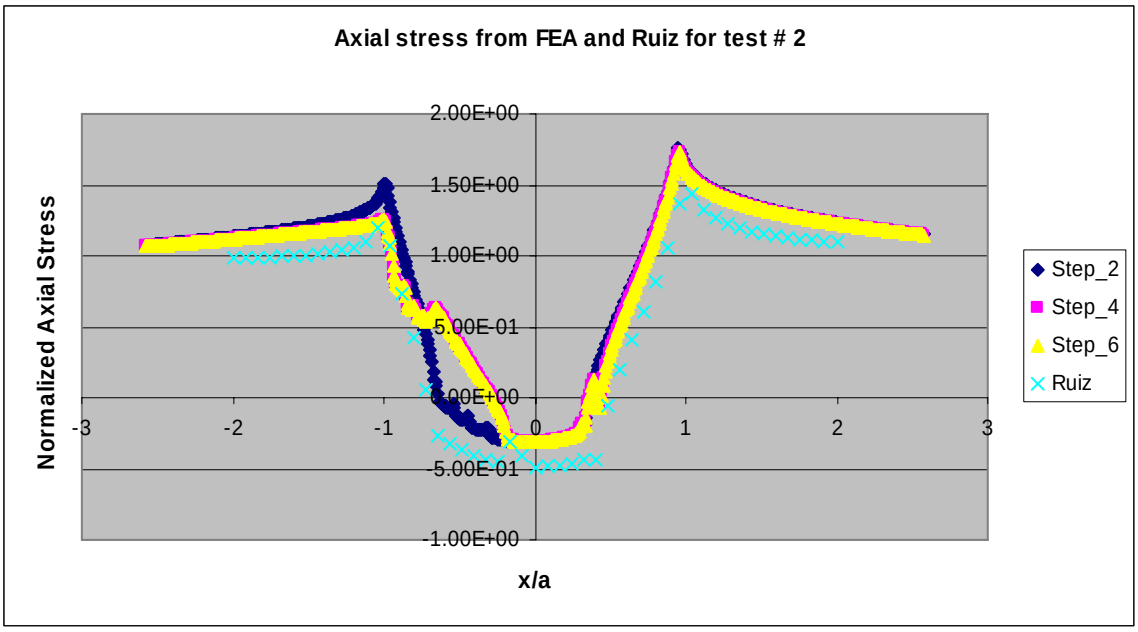

Figure 4.7 Axial stress profiles (σ_{xx}) of test # 2 for FEA and Ruiz

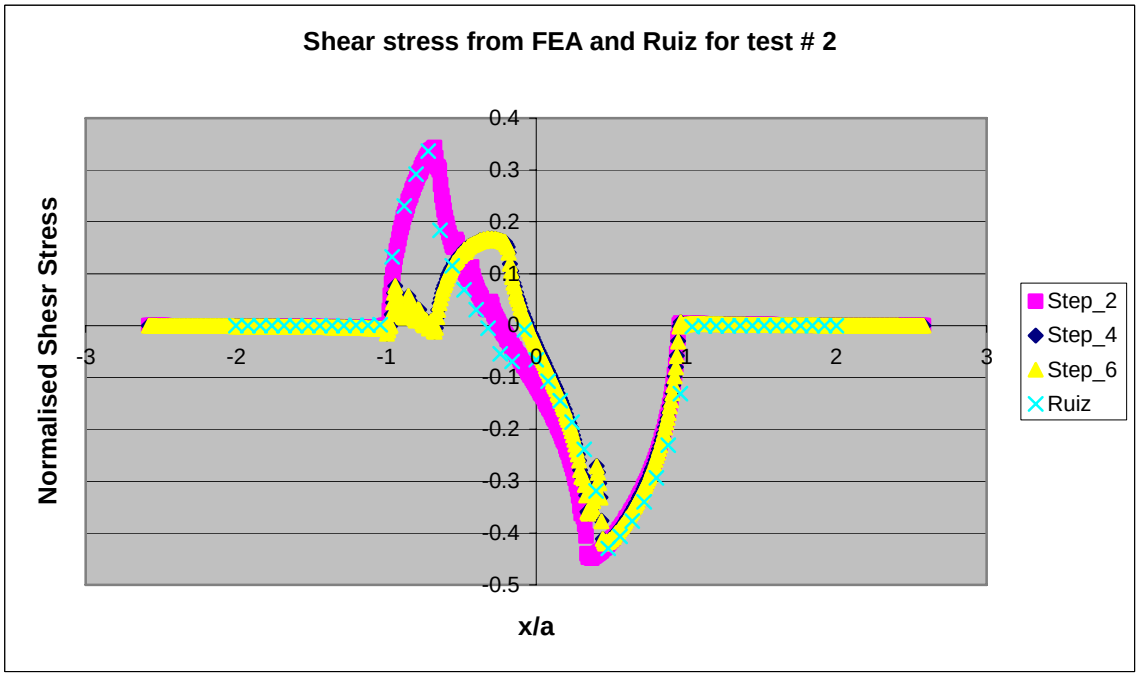

Figure 4.8 Shear stress profiles (σ_{xy}) of test # 2 for FEA and Ruiz

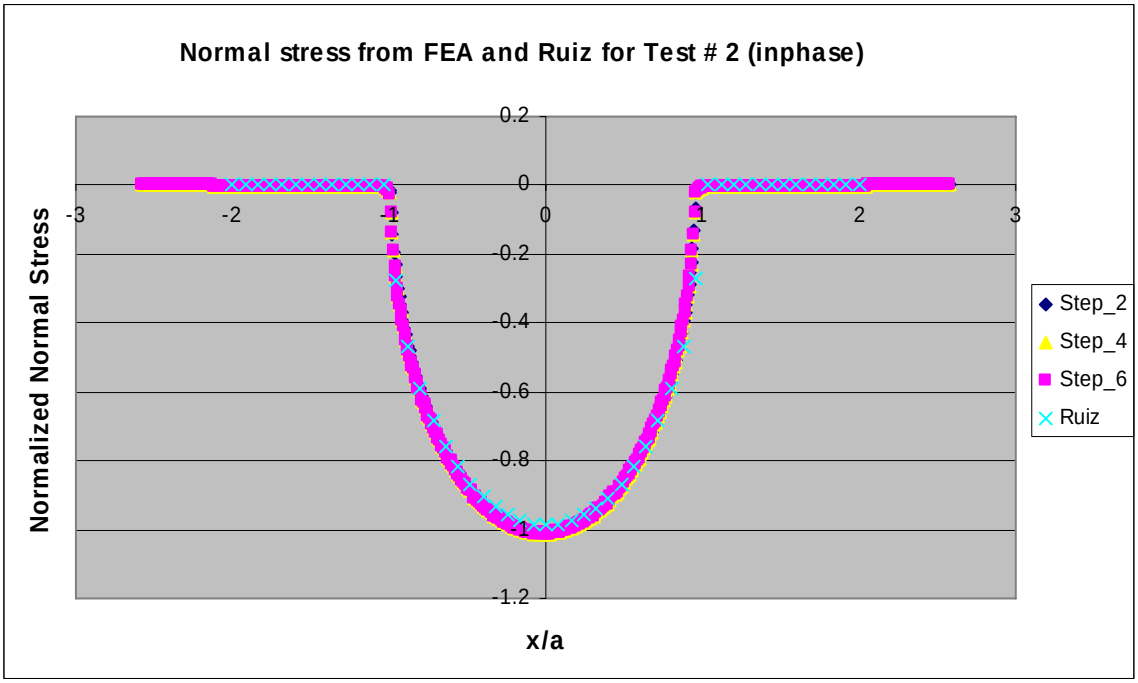

Figure 4.9 Normal stress profiles (σ_{yy}) of test # 2 for FEA and Ruiz

Table 4.1 Input loads for FEA

Test #	σ_{max} MPa	σ_{min} MPa	P_{max} MPa	P_{min} MPa	Q_{max} MPa	Q_{min} MPa	$phase\_angle(\phi)$ Degree
1	723.322	72.305	73.546	36.77	6.2467	-20.167	0
2	564.267	56.427	73.546	36.77	8.0531	-13.955	0
3	564.267	56.447	36.77	73.546	3.6956	-15.43	90
4	413.244	41.286	73.546	36.77	6.8189	-9.4044	0
5	413.203	41.003	36.77	73.546	1.8616	-12.114	90
6	376.019	37.48	73.546	36.77	3.7163	-10.983	0
7	375.985	37.39	36.77	73.546	0.986	-11.556	90
8	282.161	28.227	73.546	36.77	-6.743	-18.506	0
9	563.86	56.254	55.158	55.158	12.776	-8.2392	0
12	172.665	470.12	73.546	36.77	1.2962	-9.4251	60
13	62.0252	548.08	73.546	36.77	7.0051	-12.355	105
15	351.598	35.115	36.77	73.615	8.4323	-3.9921	90

Table 4.2 MSSR calculations of test # 4 (in-phase)

Between Steps	MSSR	$\Delta\tau$ MPa	$\Delta\tau_{crit}$ MPa	θ Deg	$R_{\Delta\tau}$	σ_{max} MPa	σ_{min} MPa	x in	x/a max	x/a min
2 - 3	***30.41998***	394.4825	408.3885	40.8	0.061047	414.1774	29.31292	0.111286	0.949931	1.344338
3 - 4	30.17404	388.9283	402.8145	40.5	0.061793	406.4989	29.58133	0.11129	0.950058	1.344517
4 - 5	30.17608	389.162	402.9234	40.5	0.061229	406.4989	29.29717	0.11129	0.950058	1.344517
5 - 6	30.14837	388.9117	402.673	40.5	0.061266	405.2615	29.29717	0.11129	0.950058	1.344517
6 - 7	30.15083	389.1947	402.8049	40.5	0.060583	405.2615	28.95516	0.11129	0.950058	1.344517

5. Results and Discussion

The results of this study are discussed in this chapter. In the first part the experimental results of both the phase difference between the axial and the contact loads and the combinations of fretting and plain fatigue are addressed, followed by the Finite Element Analysis FEA and MSSR outputs, and finally the fretting fatigue predictive parameters, fatigue life, crack initiation mechanism, and phase difference effect are covered.

5.1. Experimental Results

In this study fifteen experiments have been conducted on titanium alloy Ti- 6A1-4V; eleven of them were done under the phase difference between the axial load and the applied contact load at different axial stress range and different phase angle, while the remaining four experiments were done with different combinations of the fretting fatigue and the plain fatigue by keeping the applied contact load constant and varying the application load ratio between the plain and fretting fatigue. The details of these tests and their results are tabulated in Table 5.1. As shown in this table the samples in test # 8 (in-phase) and test # 15 (out of phase), which were done at low axial stress range of 254 MPa for in-phase condition and 351 MPa for out of phase condition, didn’t fail due the low magnitude of the applied axial stress and the tangential load. There was a partial slip condition in all tests.

On the other hand tests # 10, 11, and 14, which were done under different combinations of fretting fatigue and plain fatigue. The steady state condition changes as the load conditions change from fretting fatigue to plain fatigue, were not included in FEA or MSSR analysis.

In this section the experimental results of the following are discussed: The fretting fatigue condition, Q/P ratio, the tangential load, the fracture surface, the contact half-width a, the crack initiation location, and the crack initiation orientation. The results of fatigue life will be discussed in later section.

5.1.1. Fretting Fatigue Condition

The hysteresis loops between the tangential and the axial loads can be used to determine the fretting fatigue condition. Figures 5.1 through 5.4 show the hysteresis loop of different tests, while Figures 5.5 to 5.10 show the maximum and minimum tangential load variation with respect to the fatigue cycles. Clearly from these figures it can be noticed that the partial slip condition of the fretting fatigue was met after a few hundreds of the fretting fatigue cycles.

In the combination between the fretting fatigue and the plain fatigue condition; Figure 5.8 for test # 9, which was done under constant contact load condition, shows that the steady state condition has been met after a few hundreds of cycles and the maximum tangential load converge approximately to 800 MPa, while Figure 5.9 for test # 10, which was done initially with 21,320 fretting fatigue cycles, this number represents the half of the fretting fatigue cycles of test # 9, followed by a plain fatigue condition, shows also

that the tangential load became stable around 800 MPa and it went down to zero immediately after the applied contact load was released and the plain fatigue condition started. On the other hand; Figure 5.10 for test # 11, which was done in an alternate condition between fretting fatigue with 5,000 cycles and plain fatigue with 10,000 cycles, shows that as the fretting fatigue condition appeared and the contact load is reapplied on the specimen, and the tangential load goes back to the same magnitude of 800 MPa, while at the plain fatigue condition this tangential load became also zero.

So the steady state condition of the fretting fatigue in all tests that were conducted in this study was met after a few hundreds cycles of fretting fatigue cycles even in the tests those contained a plain fatigue configuration. This result insures that all fretting fatigue variables including applied contact load, coefficient of friction, resulted tangential load, and axial load were in a steady state condition till the failure of the specimen occurred.

5.1.2. Q/P

The ratio of Q/P, as shown in equation 3.2, can be determined by dividing the tangential load by the corresponding contact load. The maximum value of Q/P in each test is considered to be the static coefficient of friction between the two bodies, the specimen and the pad. The largest value of static coefficient of friction has barely reached 0.5 in any test and hence this value was used in FEA. Table 5.2 shows the maximum value of Q/P for all tests those have been done at the same axial stress range condition. This table shows that the greatest value of Q/P was found to be at the in-phase condition,

while the least value in the out of phase condition, and this indicates that the out of phase condition has less friction than other conditions and the in-phase condition has the most friction. Figure 5.11 shows the variation of Q/P with respect to the time for test # 2 at 10,000 fretting fatigue cycles. This variation is a sinusoidal wave as it follows the variation of the axial and the tangential loads.

So the Q/P ratio under fretting fatigue condition is varying over time and could not be treated as a constant at all, hence the coefficient of friction for tests conducted in this study was selected to be 0.5 to be used in finite element analysis and it wasn't beneficial to investigate the effect of varying the coefficient of friction on the fretting fatigue behavior in this study.

5.1.3. Tangential load

As mentioned in chapter III; the tangential load can be determined as the half of difference between the lower applied axial load and the load measured at the upper grip. So it was expected that the tangential load will follow the axial load in frequency, phase, and the sinusoidal pattern. The conditions where there was no phase lag between the axial and the contact loads, all the loads; tangential, axial, and contact, vary in the same manner at the same time and at the same angle as shown in Figure 5.12, while in the conditions where there was a phase lag between the contact load, which is the reference, and the axial load, the tangential load varies in the same manner as the axial load and there was no effect from the applied contact load on the phase of tangential load, and this

can be seen in Figures 5.13 through 5.15. So the contact load only affects the magnitude of the tangential load and it has no effect on its phase angle or wave shape.

The global tangential load range, which is the difference between the maximum and the minimum tangential load, increased by increasing the applied axial load for both in-phase condition and out of phase condition, but as shown in Figure 5.16 the rate of increase for the out of phase condition is less than the rate of increase for the in-phase condition. Figure 5.17 shows the relation between the phase angle and the normalized tangential load range ($\Delta Q/P_{max}$) for the tests those were done at the same axial load condition and it can be noticed that the tangential load range decreases by increasing the phase lag until the phase angle reaches 90^O then the tangential load range starts to increase. So the least magnitude of the tangential load range is under the out of phase condition and the greatest one is at the in-phase condition. Hence the phase lag in general reduces the tangential load range which could have the most effect on fretting fatigue.

5.1.4. Contact Half-Width

The applied contact load is the only parameter that affect the contact-half-width, a, as shown in equation 2.20 and there was no effect from the axial load conditions. Figure 5.18 is a photo of the specimen from test # 3 which shows the partial slip zones and stick zone at the contact region. It was very difficult to measure the contact half-width , a, from the experiments because it has a very small length, and also due to the severe slip condition at the final stage of fretting fatigue test, so different magnitudes of the contact half-width were determined each time during the measurement even for the same test,

however; most of these values ranged between 0.76 mm ~ 0.818 mm for the variable applied contact load and 0.67 mm ~ 0.725 mm for the constant applied contact load and these values were tabulated in Table 5.3.

On the other hand from Ruiz program; the contact half-width for the variable applied contact load condition was determined to be 0.801 mm at the maximum value of the applied contact load and 0.566 mm at the minimum value of the applied load. While for the constant applied contact load condition this contact half-width, a, was 0.693 mm. By comparison between the analytical solution and the experimental one, it can be noticed that the maximum deviation is around 5.1 % for the variable contact load condition and 4.6 % for the constant contact load condition, and these deviations are reasonable values. Hence, in order to save time and extra work, Ruiz program which was developed with infinite half space assumption is a practical tool for estimating the contact half-width under variable contact load conditions as well as constant applied contact load conditions.

5.1.5. Fracture Surface Area

The Scanning Electron Microscope (SEM) was used to examine the fracture surface of the cross sectional area of the specimens by taking a higher magnification pictures. Figure 5.19 is a photo of the lower side of the failed specimen from test # 4; this photo, which was taken under a lower magnification microscope, shows the fracture surface along with its four distinguishable regions that were created during the crack initiation and propagation. These regions can be seen, by using the Scanning Electron Microscope,

in Figures 5.20 through 5.23 which show that there was debris in region 1 due to the created wear from the damaged surface of the contact mechanism that nucleates the initial crack as seen in Figure 5.20. Figure 5.21 shows striations of region 2, which represents the main region for the crack propagation; Figure 5.22 shows the large dimples with grain boundary of region 3, while as shown in Figure 5.23 there is a catastrophic fracture of region 4 where the final and the unstable crack occurred.

5.1.6 Crack Initiation Location

One of the important issues in fretting fatigue investigation is to determine the location of the initiated crack. In all tests those conducted in this study which failed due to fretting fatigue condition, the crack initiation location always occurred at or very near the trailing edge of the contact region where x/a = +1 along the x-direction. Figure 5.24 for test # 2 shows that the crack initiated at the trailing edge of the contact area, while Figure 5.25 shows, for test # 2 also, that this crack has been initiated at the contact surface where it is shown as darker area than other areas. On the other hand this crack initiation can be illustrated, under high magnification, as the darker region on the failed specimen as in Figure 5.26.

Since the trailing edge area corresponds to the point where the maximum axial load is applied, this axial load will propagate any crack that was initiated with a critical size at the trailing edge area. But the question is how this crack can be initiated? Magaziner reported in his study [28] that the crack nucleates in the trailing edge area due to the

stress concentration forming at the boundary of the stick zones due to the shifting of the stick zone.

5.1.7. Crack Initiation Orientation

The crack initiation orientation for titanium Ti-6Al-4V alloy under constant applied contact load is known, from the previous studies. [7, 9, and 10] to be about $+45^o$ or $-45^o \pm 15^o$. On the other hand Lee; in his study[8] for the test conducted under variable applied contact load with frequency of 2.5 Hz, while the axial load frequency is 10 Hz, found that the crack orientation was -50^o which is equivalent to 40^o. So he documented that the variable contact load under different frequencies didn't alter crack initiation orientation significantly from constant contact load.

In this study; two tests were examined for the crack initiation orientation by using SEM, the first one is test # 2 which was under in-phase condition and the second one is test # 3 which was under out of phase condition. The crack initiation orientation for test # 2 was found to be 48^o as shown in Figure 5.27. This value is very close to the one of the previous studies. However the orientation crack of test # 3 was 63^o as shown in Figure 5.28 and this is a little bit higher than the expected value with a deviation of 10^o. This deviation is due to the change of the shear stress and the contact stress from in-phase to out of phase conditions. Hence the orientation of the initiation crack for the out of phase condition is about $+55^o$ or $-55^o \pm 15^o$.

5.1.8 Effect of out of phase

The effect of out of phase condition on fretting fatigue can by summarized as follows; the partial slip condition of the out of phase was met at the first hundreds cycles of fretting fatigue cycles and this was also true for the in-phase condition. The Q/P ratio was found to be smaller in this case than in-phase condition. Under both in-phase or different phase condition the tangential load was varying in the same manner as the axial load and the only effect from the contact load was on the magnitude of the tangential load. Under any phase condition the crack initiation location always found to be at the trailing edge of the contact region and the fracture surface topography was containing four distinguishable areas. The crack initiation orientation for in-phase condition was similar to the previous studies, however for the out of phase condition the crack initiation orientation deviated with 10^{o} from the previous studies.

5.2. Finite Element Analysis Results

As mentioned in chapter IV, Finite Element Analysis (FEA) model has been used to determine numerically the stress, strain, and displacement distribution within the contact region of the specimen. The load condition of the applied axial and contact loads, and the corresponding tangential load, at 10,000 fretting fatigue cycles for each test, were used as the input into FEA, and these values were shown in Table 4.1. In this section the stress state and the effect of out of phase on fretting fatigue behavior are discussed by comparing two tests condition, in-phase and out of phase, with the analytical solution.

5.2.1. Axial Stress State, σ_{xx}

Equation 2.39 showed that the total axial stress along the contact surface between the fretting specimen and the fretting pad depends on the applied contact load and the resulting tangential load as well as the applied axial load. Figure 5.29 shows the axial stress σ_{xx} for tests # 2 (in-phase) and 3 (out of phase), those have been conducted under the same applied axial stress. This figure represents both the Ruiz output and step 2 of FEA output for these tests. The maximum axial stress for test # 2 was found to be 807 MPa at x/a = 1.04 from Ruiz program and 994 MPa at x/a = 0.9397 from FEA, while the maximum axial stress for test # 3 was found to be 740 MPa at x/a = 1.04 from Ruiz program and 837 MPa at x/a = 0.9845 from FEA output.

From this figure the following can be noticed:

a) The maximum stress for both tests from Ruiz program has a deviation of 8.3 %, however; this was located at the same value of x/a for both tests which is 1.04. On the other hand; the stress concentration factor in axial stress is 1.345 for test # 2 and 1.233 for test # 3 with a deviation of 8.3 % also. So the axial stress value and the stress concentration factor for the out of phase condition is less than the in-phase condition.

b) From FEA the deviation of the maximum axial stress between both tests is 15.79 % in magnitude and 4.5 % in location. The stress concentration factor is 1.6567 for test # 2 and 1.395 for test # 3 with a

deviation of 15.79 %. This also emphasizes that the stress of the out of phase condition is less than the in-phase condition.

c) The deviation between the Ruiz out put and FEA out put for each test can be found as follow: 18.8 % in maximum axial stress magnitude with 9.9 % in location for test # 2, and 11.59 % in maximum axial stress magnitude with 5.34 % in location for test # 3. These results show that the out of phase condition is closer to the analytical solution than in-phase condition.

In summary, the maximum axial stress magnitude for the out of phase condition is less than that of the in-phase condition, and this gives a less concentration factor in axial stress which could affect the fretting fatigue life.

5.2.2. Distribution of Normal Stress σ_{yy}

The distribution of the normal stress σ_{yy} of Ruiz output and FEA output for tests # 2 and 3 can be seen in Figure 5.30. In this figure it is clearly seen that there is no deviation or correlation between Ruiz program and FEA out put results and they seem to be close to each other. However; there is a big difference between the in-phase conditions and the out of phase conditions, for example the maximum magnitude of $\boldsymbol{\sigma}_{yy}$ for test # 2 is 557 MPa from Ruiz and 570 MPa from FEA with a small deviation of 2.2 %, while magnitude for test # 3 is 394 MPa from Ruiz and 399 MPa from FEA with a very small deviation of 1.2 %. These values give a deviation between the in-phase condition and the

out of phase condition of 29.26 % from Ruiz program and 30 % from FEA. This result makes sense because during the in-phase condition; if the axial load was at its maximum magnitude, the contact load would be at its maximum magnitude, and this was true also for the minimum condition. However; during the out of phase condition if the axial load was at its maximum magnitude the contact load would be at its minimum one.

5.2.3. Distribution of Shear stress σ_{xy}

The results from the above two sections bring up this question. Based on which load, axial or contact, is the maximum load condition met? To answer this question it is better to look into the previous studies. Most of these previous studies were done under a constant contact load, so the maximum condition was based on the maximum axial load. In those studies where the applied contact load was variable, the maximum load condition was based on the maximum axial load also and this was because the maximum contact load was met at the same time when the maximum axial load was met and this was because these studies were conducted under the in-phase conditions. So what should be the maximum load condition under the out of phase case?

Since the distribution for both the axial stress and the normal stress didn't give an answer to that, the answer could be looked from the distribution of the shear stress. For test # 2 (in-phase); step no.2 is the maximum load condition for both the maximum axial load and the maximum contact load. For test # 3 (out of phase); step no.2 represents the maximum axial load condition and the minimum contact load condition, and step no.3 is the minimum axial load condition and the maximum contact load condition. The σ_{xy} at

these steps are shown in Figure 5.31. In this figure step 2 for both tests are close to each other while step 3 for test # 3 has a different pattern. The maximum axial load condition of both in-phase and out of phase conditions gives almost the same shear stress. The minimum contact load condition of the out of phase condition gives different shear stress from the in-phase condition. Hence the maximum axial load condition in this study was also assumed the maximum load condition.

5.2.4. Stress Profiles

In this section the stress profile for test # 2 (in-phase) and test # 3 (out of phase) are discussed. As it has been shown above that the maximum load condition is met at the maximum axial and tangential loads conditions, so in test # 3 this maximum condition was met at steps 2, 4, and 6 where the contact load was at minimum magnitude. Figures 5.32 to 5.34 show the stresses profile of steps 2, 4, and 6 for test # 3. Figure 5.32 shows that the maximum magnitude of σ_{xx} is 837 MPa, 836 MPa, and 834 MPa at the same location of x/a = 0.9845 for steps 2, 4, and 6 respectively, which gives a maximum deviation of only 0.3 % between steps 2 and 6. Figures 5.33 and 5.34 show the same that the stress profile is almost identical for each load, and this gives an indication that there was no effect from the sequence of the applied loads and the only effect is coming from the magnitude of the applied loads. This also can be seen at the minimum load condition for test # 3 as shown in Figure 5.35.

Figures 5.36 to 5.38 show the stress profile at the maximum load condition of axial, normal, and tangential stress for steps 2, 4, and 6 of test # 2. There was no effect from the

step load sequence on the normal stress profile as shown in Figure 5.38. However; there were a deviation between step 2 and steps 4, and 6 in the axial stress that results in a deviation in tangential stress. This deviation is only in the magnitude of the axial stress and it is not in the location. The maximum axial stress is 994 MPa in step 2 and 978 MPa in steps 4, and 6 at the same location for all steps which is x/a = 0.9534, and this gives a deviation of 1.6 %. The tangential load was 193.6 MPa at x/a = -0.675 and -238 MPa at x/a = 0.4753 in step 2 and this tangential load changed to 94.6 MPa at x/a = -0.3338 and 237 MPa at x/a = 0.4597 in steps 4, and 6. So there was a big difference at the leading edge for the tangential load of about 51 % in magnitude and 50 % in location, and this can be shown in Figure 5.37. On the other hand the minimum condition of test # 2 didn't indicate any deviation in the magnitude or the location of all stress profiles as shown in Figure 5.39.

So the only difference between step 2 and step 4 is in the maximum condition of test # 2. The only explanation for this is that the contact load in all tests in FEA was applied at step1 and it was kept constant till step 2, as seen in Figure 4.2, only for the tests which were done under in-phase condition, afterwards it goes in a sinusoidal pattern to step 3 and so forth. In the tests those were done under out of phase condition; at step 2 the contact load was at its minimum value, so it is less from its maximum at step 1 to minimum at step 2, as seen in Figure 4.3. In other words; the sinusoidal pattern starts at step 1 for out of phase condition. Hence this difference is appeared to be because prior the starting of step 2 the contact load was constant in in-phase condition and not variable.

5.2.5 Out of phase effect on stress profile

In summary; the maximum load condition of the out of phase condition can be assumed, as the in-phase condition, at the maximum axial load condition. The stress profile of the out of phase condition is a little bit closer to the analytical solution than the in-phase condition. At the same axial stress, the axial stress concentration factor for the out of phase condition is lower than the in-phase condition. There was no effect from the sequence of the applied loads and the only effect is from the magnitude of these loads.

5.3. MSSR Calculation

The MSSR parameter was adopted in this study to predict the material fatigue life, the crack initiation location, and the crack initiation orientation. For each test; the results from finite element analysis were obtained to be used as an input into the MSSR calculations. The calculation of MSSR needs only two steps of the load application; one is at the maximum magnitude, while the other one is at the minimum magnitude. So the MSSR was determined five times for each test since each test has seven steps and step 1 is not included. In this section the determination of the maximum MSSR, the effect of MSSR on the crack initiation location, and the crack initiation orientation are discussed, while its effect on the fatigue life will be discussed in a latter section.

5.3.1. Maximum MSSR Calculation

Since the determination of the MSSR needed two steps and each test has seven steps, it is required to calculate the MSSR between different step pairs of the all steps. This will give a total of five values of MSSR for each test. Hence for the effectiveness of the MSSR is to be studied, the maximum value of the MSSR in each test should be taken into consideration, and this value will be the greatest value among the calculated five values.

Table 5.4 shows the calculation of MSSR for test # 2 (in-phase) and test # 3 (out of phase), and table 5.5 shows the maximum MSSR for all tests those failed due to fretting fatigue. The data from these tables have been plotted in Figures 5.40 through 5.42. Figure 5.40 shows the max MSSR for tests those conducted under in-phase and out of phase conditions. It is seen in this figure that the MSSR for the out of phase condition is higher than the in-phase condition and the reason for that is the MSSR depends on both the axial stress and shear stress as shown in equation 2.46 and it doesn't depend on the maximum of any of them but it depends on the combination between them as well as the arbitrary constants A, B, C, and D.

Figure 5.41 shows the MSSR variation with the applied axial stress for both in-phase and out of phase conditions. In general there is a proportional relationship between the axial load and the MSSR, so as the axial load increases the MSSR also increases for both cases. However at a specific axial load the MSSR for the out of phase condition is greater than the one of the in-phase condition. In Figure 5.42 the relation between the maximum MSSR and the phase angle is plotted. This figure shows that as the phase angle

increases the maximum MSSR increases also till the phase angle reaches 90^o degree (out of phase) and after that the MSSR starts to decrease. So the maximum value of MSSR was at the out of phase condition while the minimum one was at the in-phase condition.

5.3.2. Crack initiation location

The contact half-width, a, which determines the leading and trailing edges area, is mainly dependent on the applied contact load. Since the applied contact load is variable and it has maximum and minimum contact half-width. The result of the crack initiation location from the MSSR calculation should be divided by both the maximum and the minimum contact half-width magnitude and this will give two locations of the crack initiation. These results are tabulated in table 5.5. This table shows two values of the crack initiation location. In this table; the maximum value of the crack location for the tests under in-phase condition was at x/a = 1.373 and the minimum one was at x/a = 0.945. On another hand; the maximum value of the crack location for the test under out of phase was at x/a = 0.99 and the minimum one was at 0.683. So which one of these values should be taken as the actual location of the crack initiation.

Theoretically; for the in-phase condition and when the maximum load condition occurred, that includes all loads, axial, tangential, and normal, the value of the contact half width, a, will be the maximum one. Hence the result of the crack location of the MSSR should be divided by the maximum value of contact half-width and this will result in the minimum value of x/a. So the crack location of the in-phase condition will be at about x/a = .95. On the other hand for the out of phase condition the maximum load

condition occurred at the minimum value of the contact load. This results in a minimum contact half-width, and hence the result of the crack initiation location from MSSR, under out of phase condition, should be divided by the minimum value of contact half-width. This will result in the maximum value of x/a. So the location of the crack in this case will be at x/a = 0.99.

The above values of the crack initiation location are very close to the analytical solution. For instance; the crack initiation location for test # 2(in-phase) is 0.9535 and for test # 3 (out of phase) is 0.9845. These values give a deviation of 4.65 % for in-phase condition and 1.55 % for out of phase condition. These values of the contact half-width for both in-phase and out of phase conditions are also very close to the measured ones from the experiments.

5.3.3. Crack initiation orientation

Table 5.5 shows also the crack initiation orientation for all tests. For the in-phase condition; the crack initiation orientation angle ranged between $40.8^o \sim 42.8^o$ which is very close to the results from previous studies $(-45^o \text{ or } +45^o) \pm 15^o$ and the experimental measurement from this study. On the other hand the orientation crack angle for the out of phase condition is a little bit different with a range of $60.5^o \sim 67.8^o$. These values differ from the previous studies but they are close to the values from the experimental measurements of this study. So the range of the crack initiation orientation for the out of phase condition was, as the one from the experimental measurement, $(-55^o \text{ or } +55^o)$

$\pm 15^{o}$. In general the MSSR was an effective parameter in predicting the crack initiation details.

5.3.4 Out of phase effect on MSSR

In summary; the maximum MSSR occurred between different step pairs of each test and this step pairs differed from one test to another under the out of phase condition or the in-phase condition even though the frequency was kept constant at 10 Hz. The values of the MSSR at the same axial stress were higher in case of out of phase condition than in-phase condition and this is because the MSSR depends on both the axial stress and the critical shear stress range in addition to the arbitrary constants. Finally the MSSR was very effective in predicting the crack initiation location and the crack initiation orientation.

5.4. Fatigue Life

This section addresses the results of fatigue life that were determined from this study. The results from the combination between the plain fatigue and the fretting fatigue are discussed firstly, and then the results from the fretting fatigue of the phase difference conditions will be covered including the effect of the effective stress, the axial stress range, the average tangential load range, and the effect of the MSSR parameter on the fatigue life.

5.4.1. Plain fatigue and Fretting fatigue Life.

Four experiments were done under the combinations between the fretting fatigue and the plain fatigue condition. The fatigue life for these experiments was shown in table 5.1, while Figure 5.43 shows the comparison of the fatigue life between these experiments. Test # 9 was completely conducted under fretting fatigue condition with a constant contact load of 3336 N, and a cyclic axial load with maximum magnitude of 564 MPa and minimum magnitude of 56.4 MPa. The fatigue life of this test was 42,640 cycles and this is less than the fatigue life resulted from test # 2, which was done under a variable contact load condition with the same axial load, by 4,600 cycles. This gives around 10 % increase in fatigue life of variable contact load from constant contact load. This result was reported also in Lee. [8]

Test # 10 was done firstly under fritting fatigue condition with a number of cycles equal to the half of the cycles resulted from test # 9, and then followed by a plain fatigue condition. In this test the fatigue life was 10,049,531 cycles which is the same as the plain fatigue life of this material under the same axial load. So there was no effect from the fretting fatigue condition which was applied at the beginning. The reason for that is at 50 % of fretting fatigue life the crack did not initiate and this confirms that the life of the fretting fatigue condition is almost for the crack initiation.

Test # 11 was done under 5,000 cycles of fretting fatigue followed by 10,000 cycles of plain fatigue, and then the same condition was repeated. The life of this kind of combination was 79,695 cycles and this life includes total of 30,000 fretting fatigue cycles and total of 49,695 plain fatigue cycles. This result indicates that the crack

initiation started at 25,000 cycles~ 30,000 cycles of fretting fatigue life. So a low ratio of the plain fatigue cycles and the fretting fatigue cycles, which is 2 in this case, doesn't improve the total life of the material. For this reason test # 14 was conducted with a ratio of 200, the fretting fatigue cycles were 1,000 cycles followed by 200,000 cycles of plain fatigue. In this test the life was 3,301,122 cycles that include around total of 16,000 cycles of fretting fatigue. So as the ratio of plain fatigue to fretting fatigue cycles became higher the fatigue life of the material will be improved.

5.4.2. Fretting Fatigue Life

The fretting fatigue life of the remaining tests will be discussed in this section. The discussion will include the effect of the axial stress range and the effective axial stress as well as the shear stress range from the experimental side, the effect of MSSR parameter on fatigue life, and a comparison between this study and the previous studies.

5.4.2.1 Axial stress range and effective stress

The axial stress range is the difference between the maximum and the minimum axial stress, while the effective stress can be found from the following equation:

$$\sigma_{effective} = \sigma_{\max}(1-R)^{m} \tag{5.1}$$

where m is 0.45, hence the results of fatigue life with respect to the axial stress range and the effective stress for this study and the previous studies. [8, 12, and 29] were tabulated in tables 5.6, 5.7, 5.8, and 5.9. The values in these tables were plotted between the axial

stress range, or the effective axial stress, and the fatigue life as shown in Figure 5.43 through 5.46. Figures 5.43 and 5.44 show the results from this study; the pattern of both the effective stress and the stress range with respect to the fatigue life is the same. In other words; as the effective axial stress and the axial stress range decrease the fatigue life will increase. However; at the same axial load condition, the fatigue life with the phase difference condition is higher than that of the in-phase condition. In addition; test # 8 (in-phase) and test # 15 (out of phase) didn't fail at different axial stress, however the axial stress of the out of phase condition is higher than the one of the in-phase condition.

Figure 5.45 shows that the fatigue life of the out of phase condition is more than that of the in-phase condition at the same axial stress and it is seen also that as the axial stress decreases the fatigue life increases for both conditions. On the other hand Figure 5.46 represents the effect of the phase difference on the fatigue life of the tests; those were under same axial stress. In general; this figure shows that if there is a phase difference between the axial and the contact load the fatigue life will increase.

Figures 5.47 and 5.48 show a comparison between this study and the previous studies and it is noticed that the results from this study fall in the scatter band of the previous studies. But as shown in these figures the fatigue life for the out of phase condition or the phase difference condition is greater than other conditions at the same effective stress or the same axial stress range.

5.4.2.2 Tangential Load Range

The average tangential load range for each test is the difference between the maximum and the minimum tangential load. Table 5.10 shows the average tangential load range for all tests those conducted under fretting fatigue condition in this study. The S-N curve of the average tangential load with respect to the fatigue life is plotted as shown in Figure 5.49. This figure shows that the fatigue life increases as the tangential load range decrease despite of the phase condition even in-phase or out of phase condition. For example; at axial stress of 564 MPa the average tangential load range of test # 2 (in-phase) was 1300 N and this resulted in 47,298 fretting fatigue cycles. While at the same axial stress the average tangential load range of test # 3 (out of phase) was 1131 N and this resulted in 61,428 fretting fatigue cycles. So the tangential load range is an effective parameter in predicting the fatigue life under any phase condition.

5.4.2.3 MSSR effective of fatigue life

The MSSR parameter was adopted in this study as the most effective parameter in predicting the fatigue life, the crack initiation location, and the crack initiation orientation. As seen in the previous sections, MSSR was very effective parameter that was used to predict the crack initiation location and orientation. In this section the effect of MSSR on the fatigue life as a result from this study in addition to a comparison with the previous studies will be discussed.

Tables 5.11 through 5.12 show the result of MSSR calculation and the fatigue life for the titanium alloy from this study and previous studies. These tables represent the result from constant applied load condition and variable applied contact load condition from the previous studies as well as the phase difference condition from this study. The tabulated results of MSSR and fatigue life were plotted as shown in Figures 5.50 and 5.51. In Figure 4.50 the effect of MSSR on the fatigue life of this study is shown, and it can be noticed that at the same axial stress condition the fatigue life and the MSSR of the out phase condition are higher than those of the in-phase condition with a deviation between 10 % to 12 % in MSSR and 30 %, at high axial stress, to 160 %, at low axial stress, in fatigue life. Hence as the axial stress became low the fatigue life of the out phase condition will be more than double of the in-phase condition. Figure 5.51 shows that there was no significant distinction between the fatigue life of the in-phase condition and the previous studies and the values fall within the scatter band. However there was a small deviation for the results of the out of phase condition. This deviation appeared because at the out of phase condition the local critical shear stress range was higher than the in-phase condition as shown in table 5.4.

5.4.3 Effect of out of phase on Fretting fatigue

The main purpose of this work was to investigate the effect of out of phase on the fatigue life of titanium alloy. In general the phase difference between the axial and the contact loads improves the fretting fatigue life, however this improvement depends on the applied axial load; under high magnitude of applied axial stress, the improvement of the

fatigue life is not so much. On the other hand; under low applied axial stress condition the fatigue life might be doubled. Even though the MSSR was determined to be higher for the out of phase condition than the in-phase condition at the same axial stress, the fatigue life of the out of phase condition is higher. The results from this study were very close to the previous studies and most of the parameters were within the scatter band.

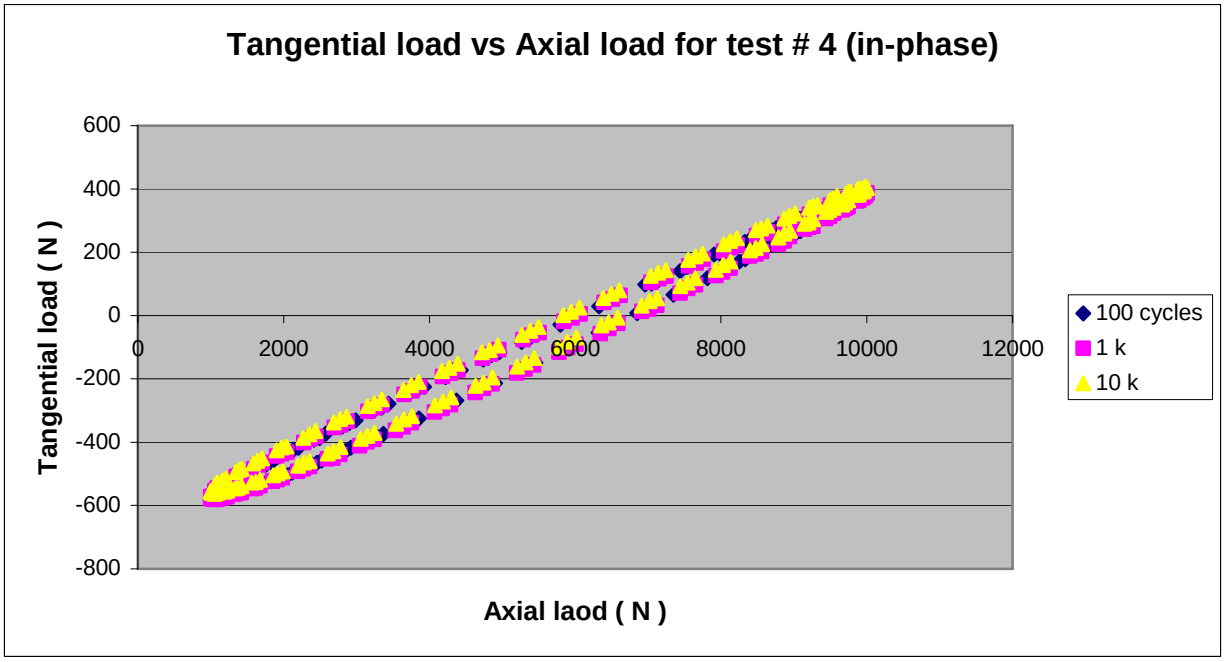

Figure 5.1 Hysteresis loop of test # 4 in-phase with axial load of 413 MPa

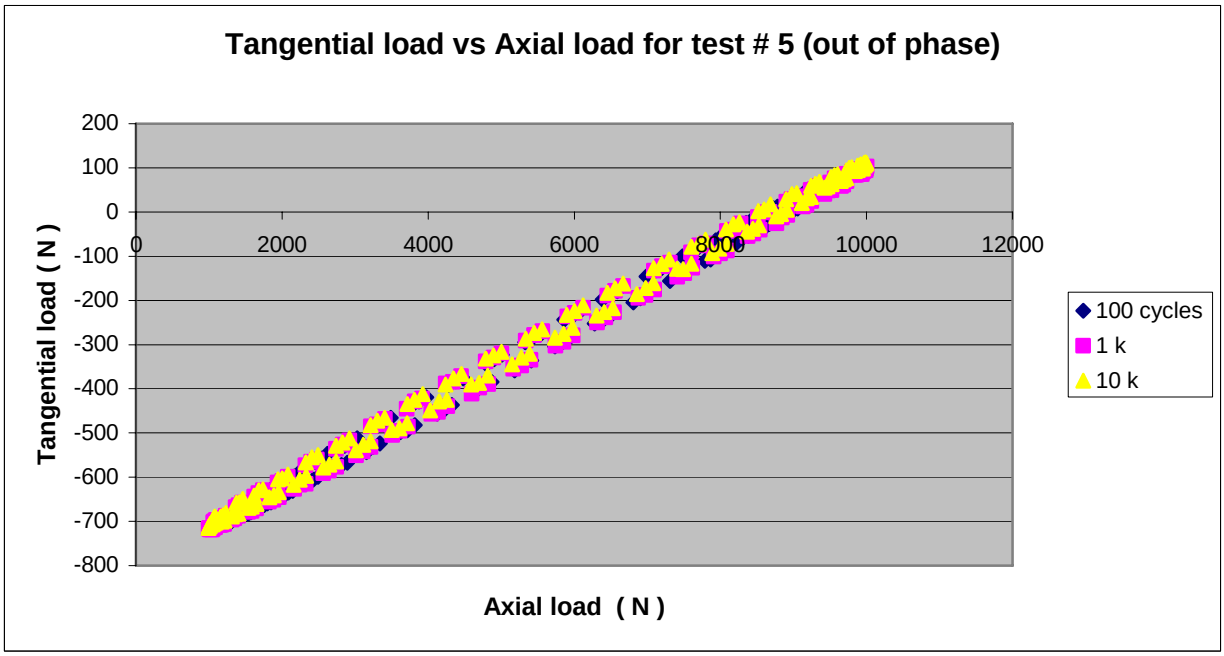

Figure 5.2 Hysteresis loop of test # 5 out of phase with axial load of 413 MPa

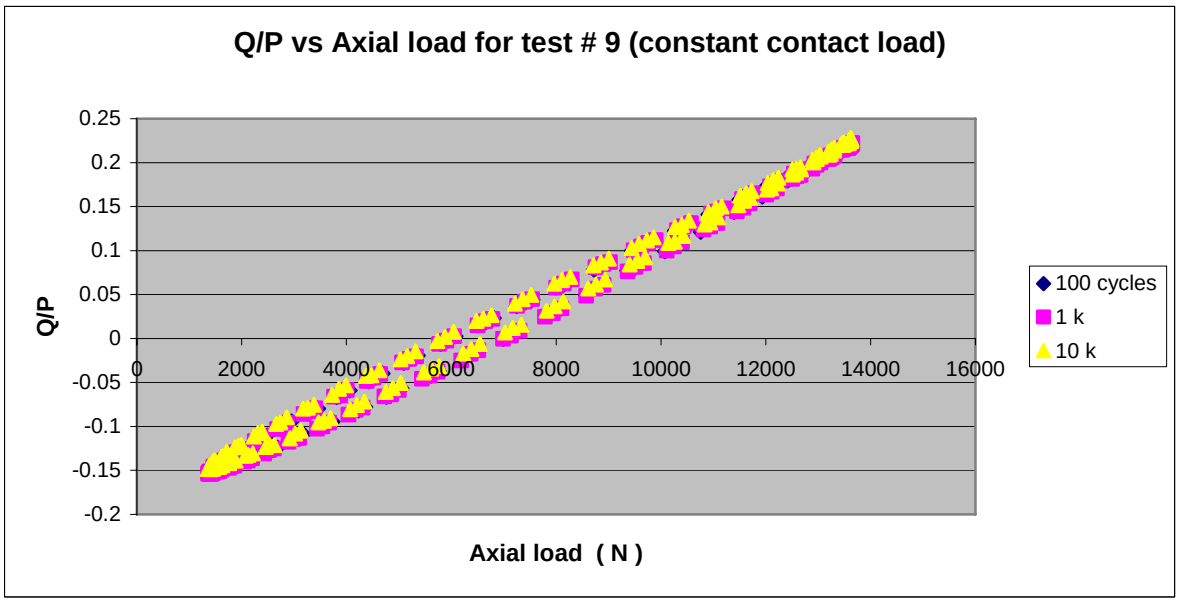

Figure 5.3 Hysteresis loop of test # 9 with constant contact load

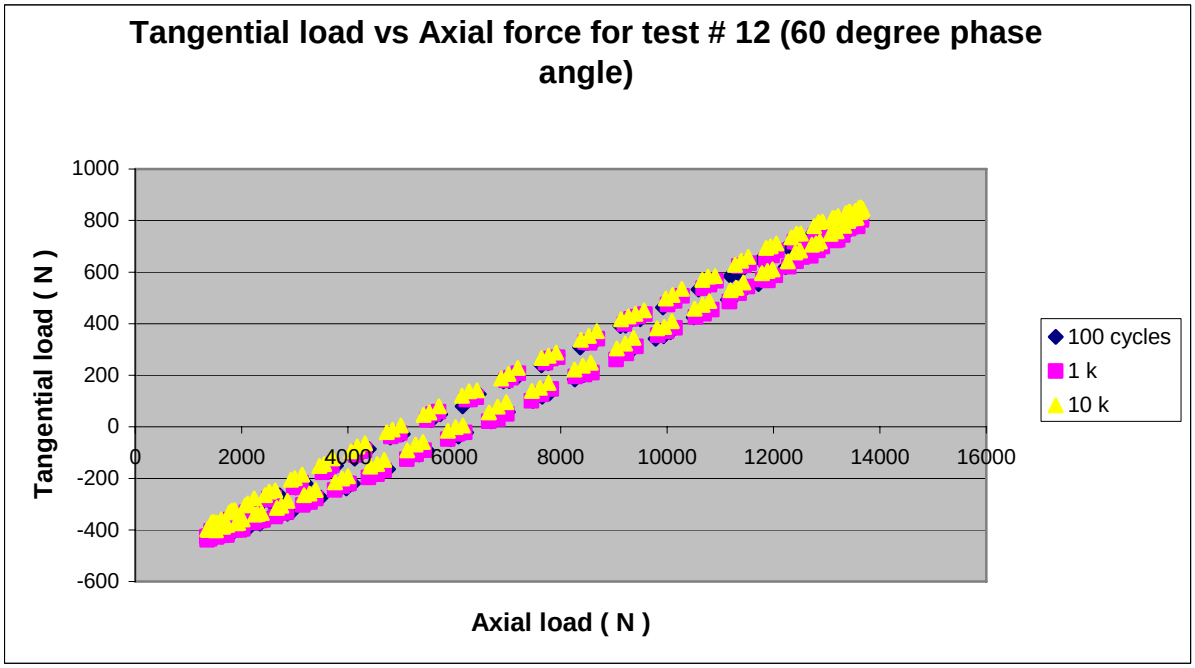

Figure 5.4 Hysteresis loop of test # 12 with 60 phase angle

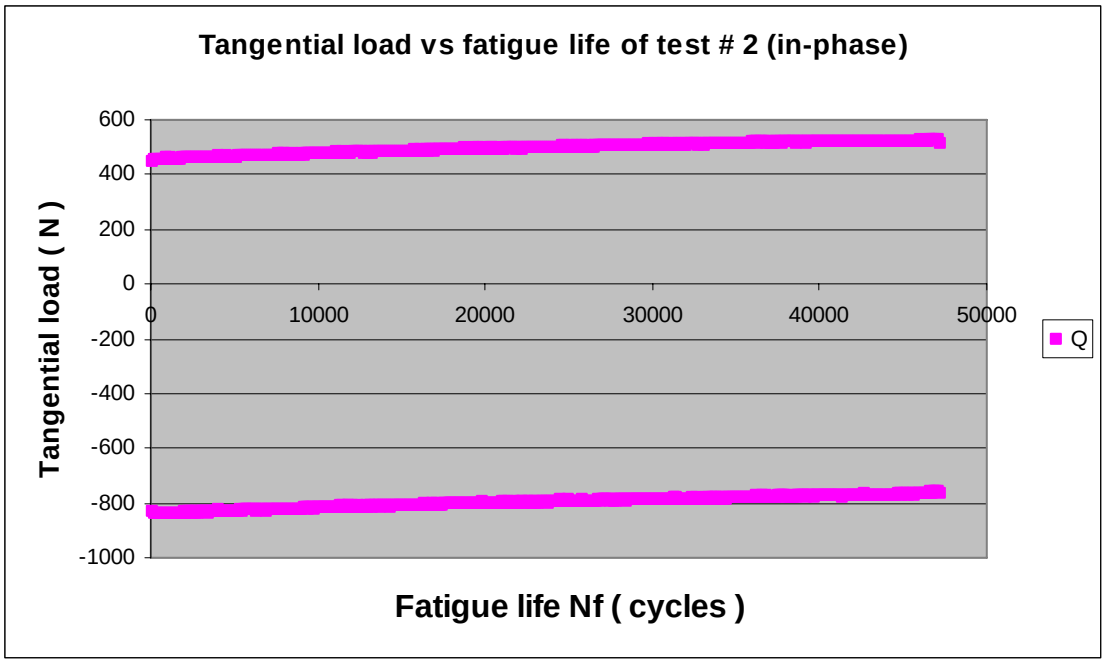

Figure 5.5 Shear load vs Cycles of test # 2 in-phase with axial of 564 MPa

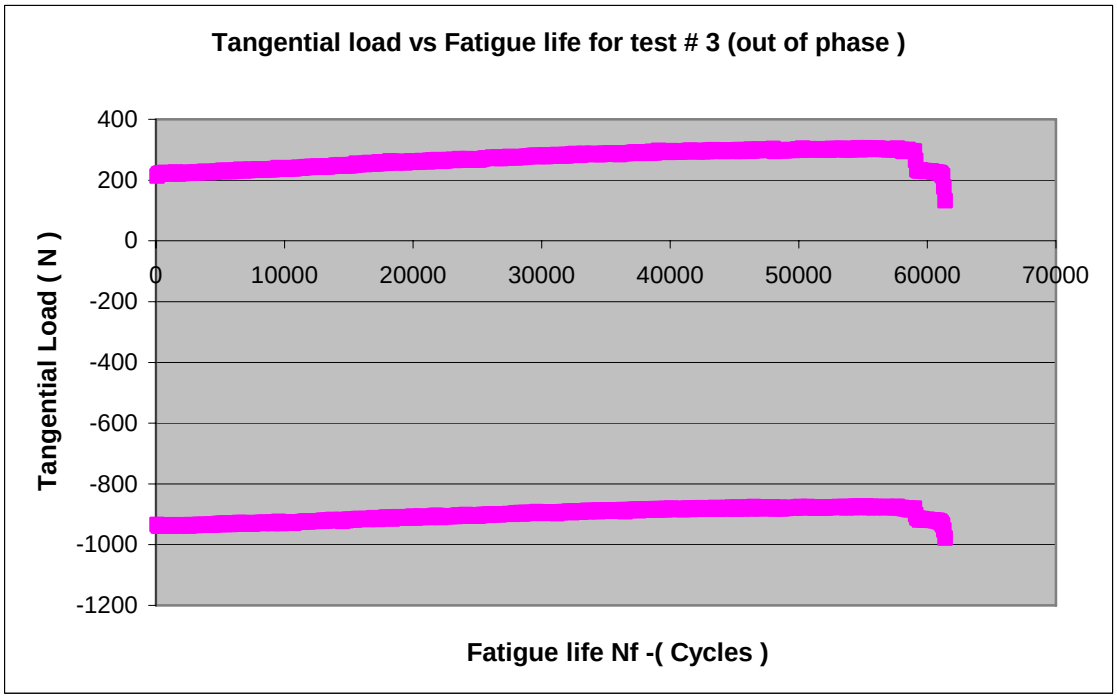

Figure 5.6 Shear load vs Cycles of test # 3 out of phase with axial of 564 MPa

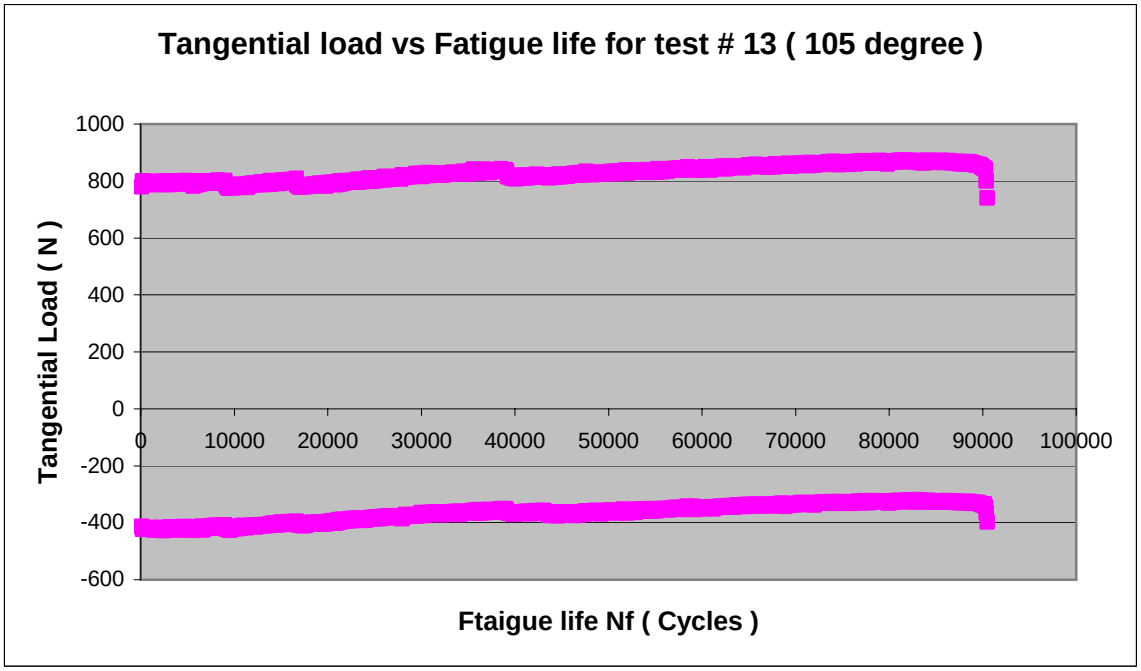

Figure 5.7 Shear load vs Cycles of test # 13 with phase angle of 105 degree

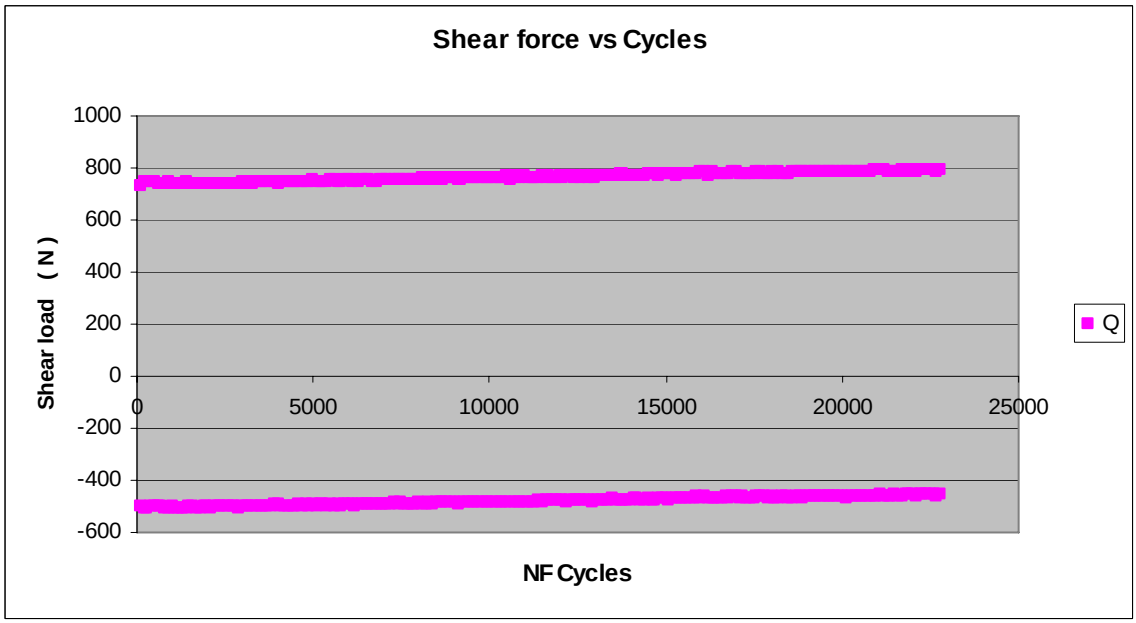

Figure 5.8 Shear load vs Cycles of test # 9 with constant contact load

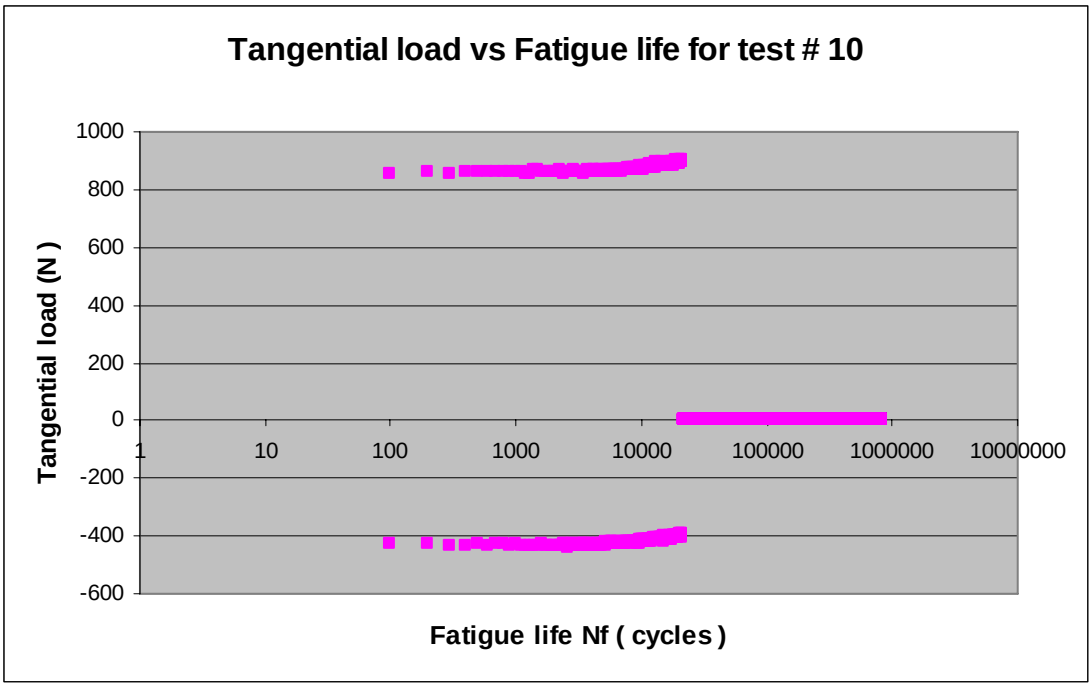

Figure 5.9 Tangential load vs Cycles of test # 10 starting with fretting fatigue followed by plain fatigue

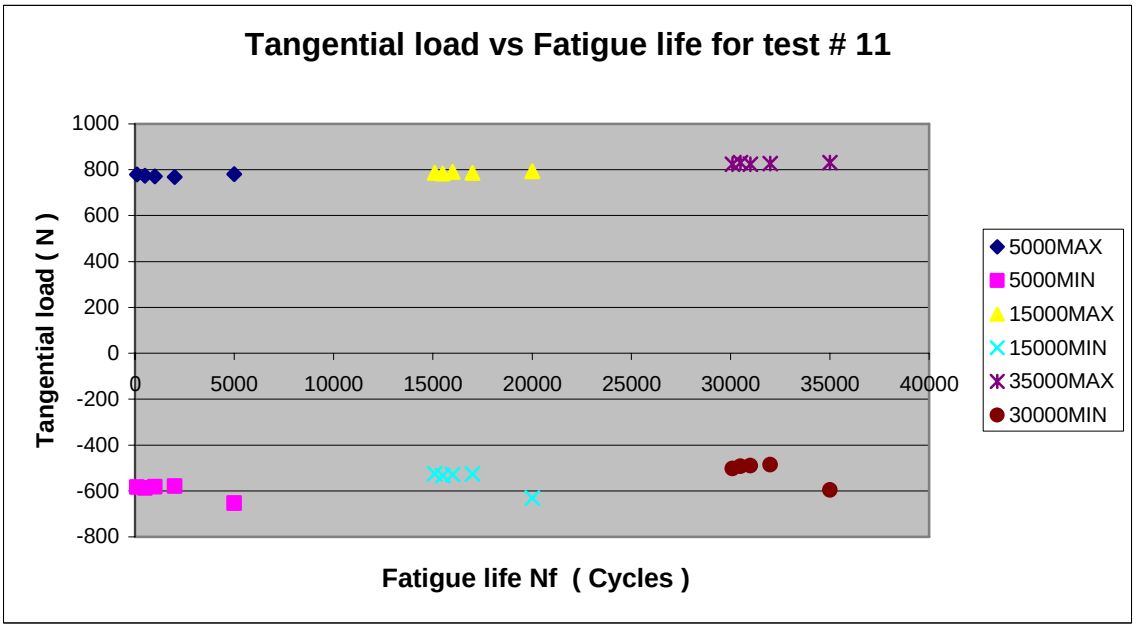

Figure 5.10 Shear load vs cycles of test # 11; 5,000 fretting cycles followed by 10,000 plain Cycles

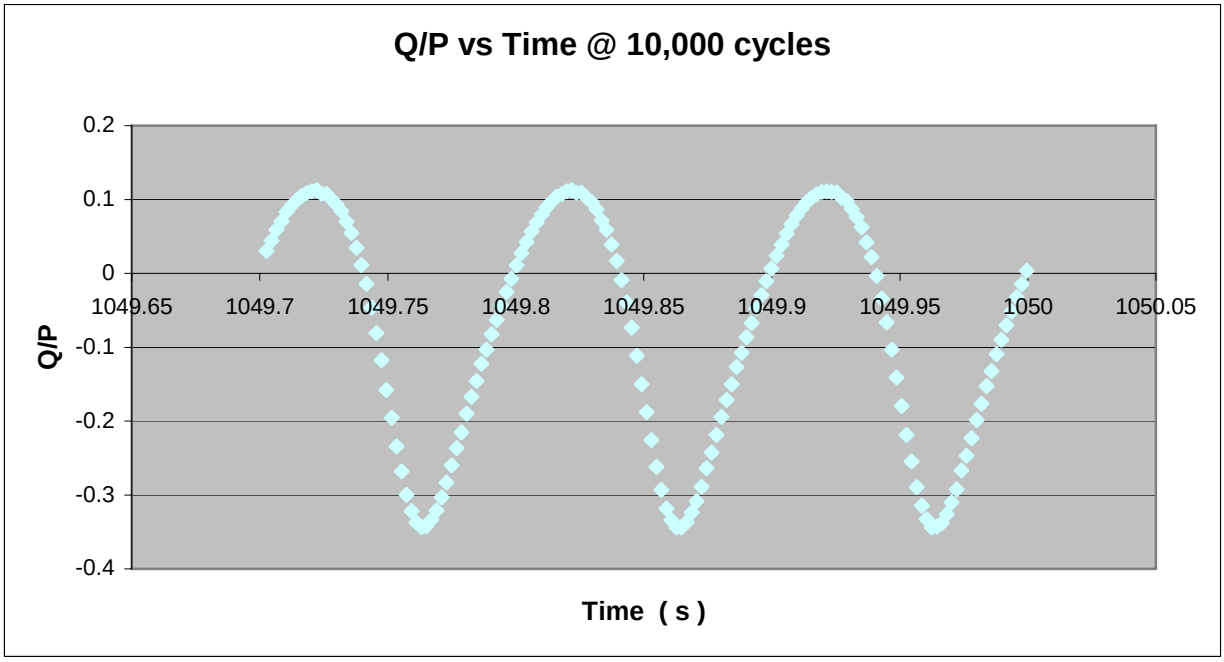

Figure 5.11 Q/P vs time for test # 2 in-phase at 10,000 cycles

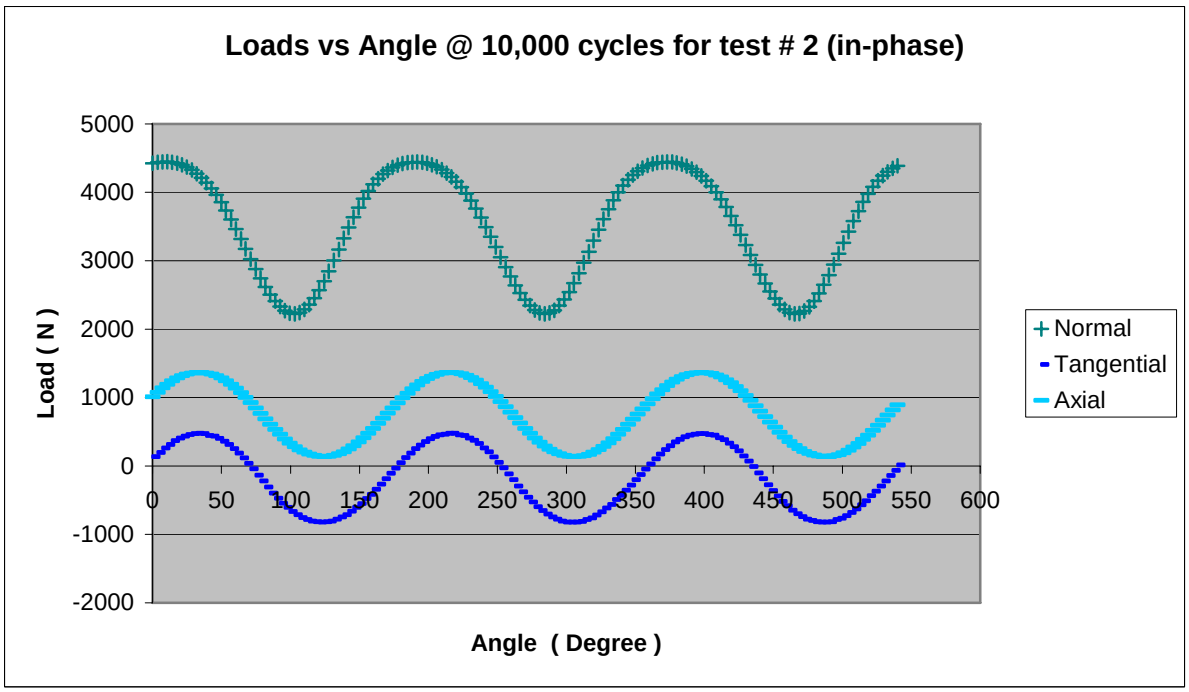

Figure 5.12 Loads vs angle for test # 2 (in-phase) at 10,000 cycles (in-phase condition)

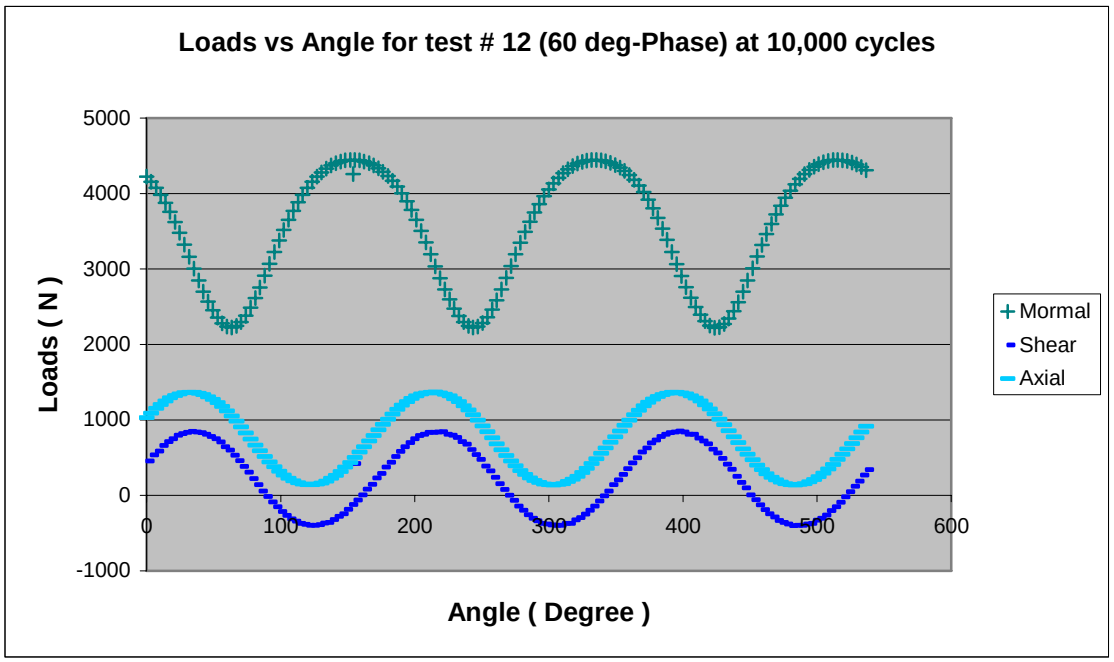

Figure 5.13 Loads vs angle for test # 12 at 10,000 cycles (60^{O} phase)

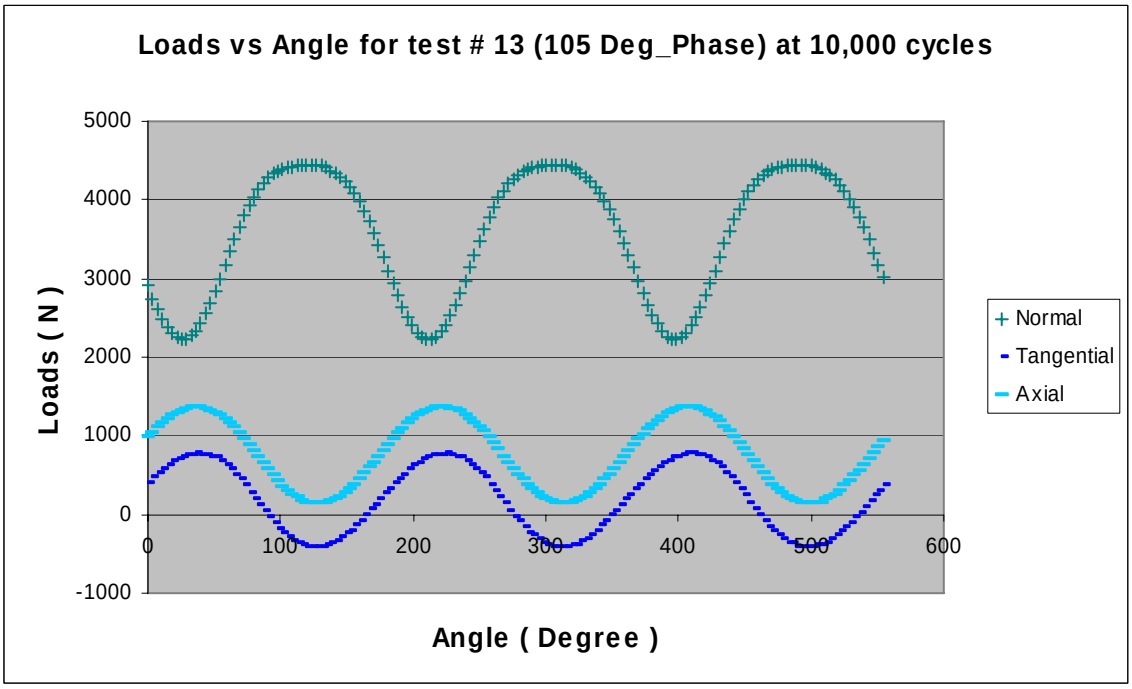

Figure 5.14 Loads vs angle for test # 13 at 10,000 cycles (105^{O} phase)

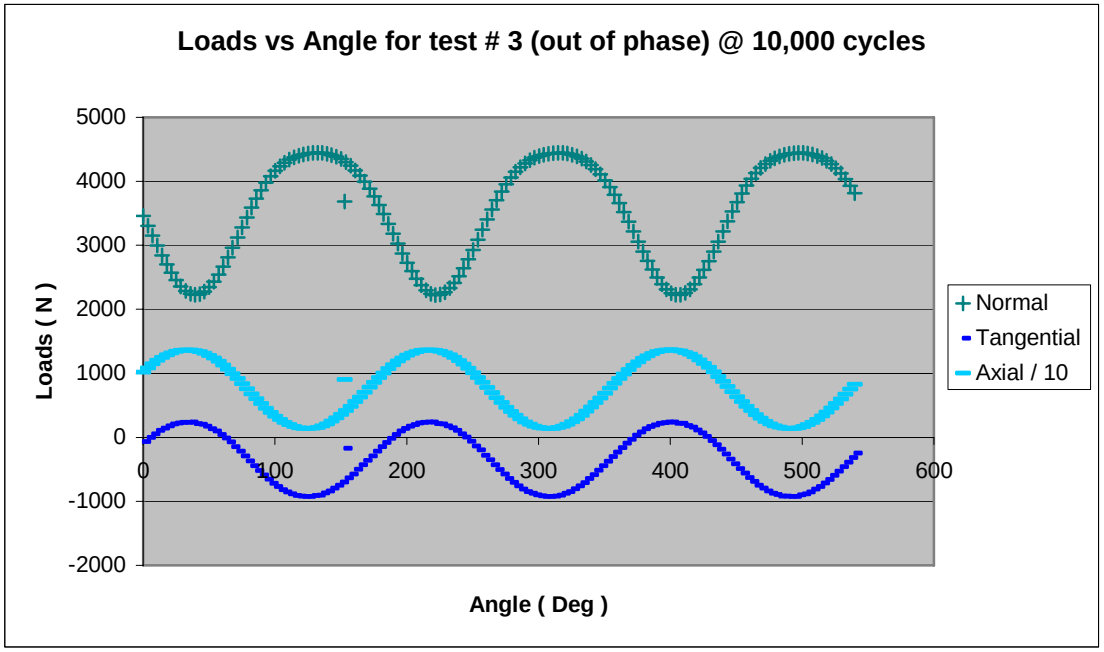

Figure 5.15 Loads vs angle for test # 3 at 10,000 cycles (out of phase condition)

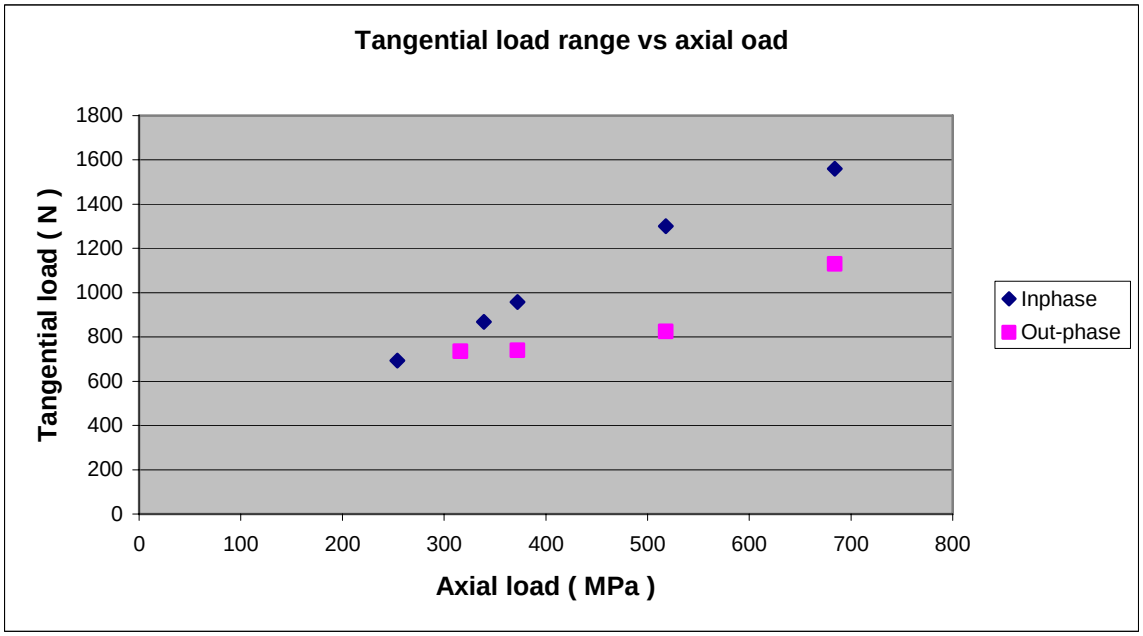

Figure 5.16 Shear range vs axial load in-phase and out of phase conditions

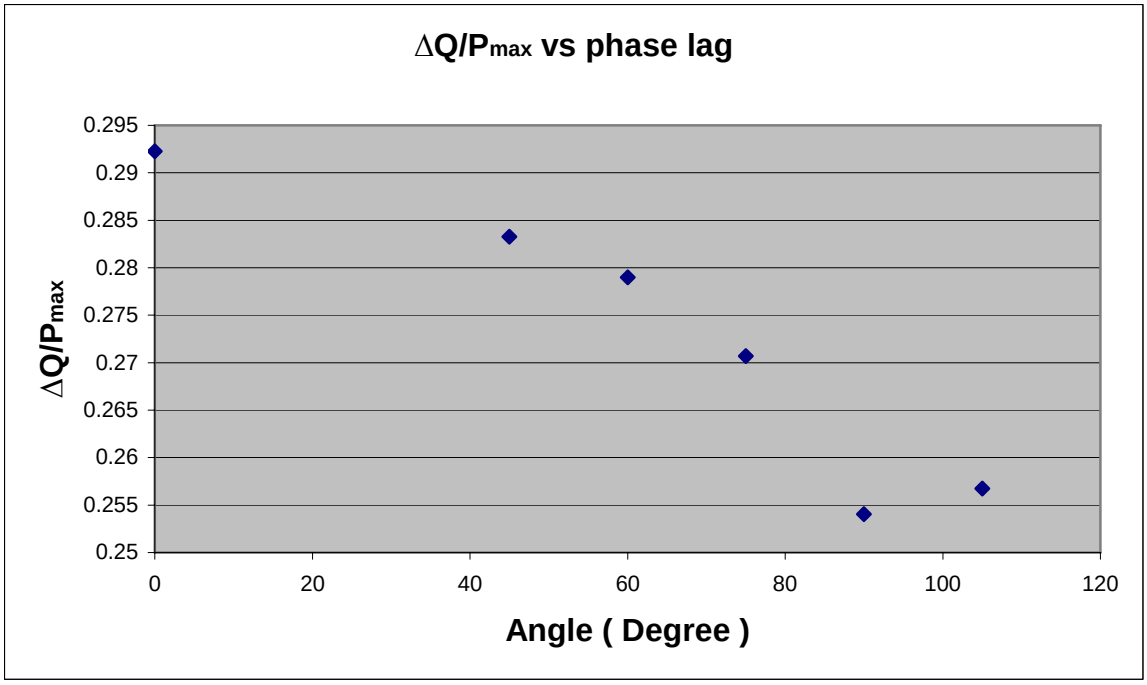

Figure 5.17 Normalized tangential load range ΔQ/P vs phase angle

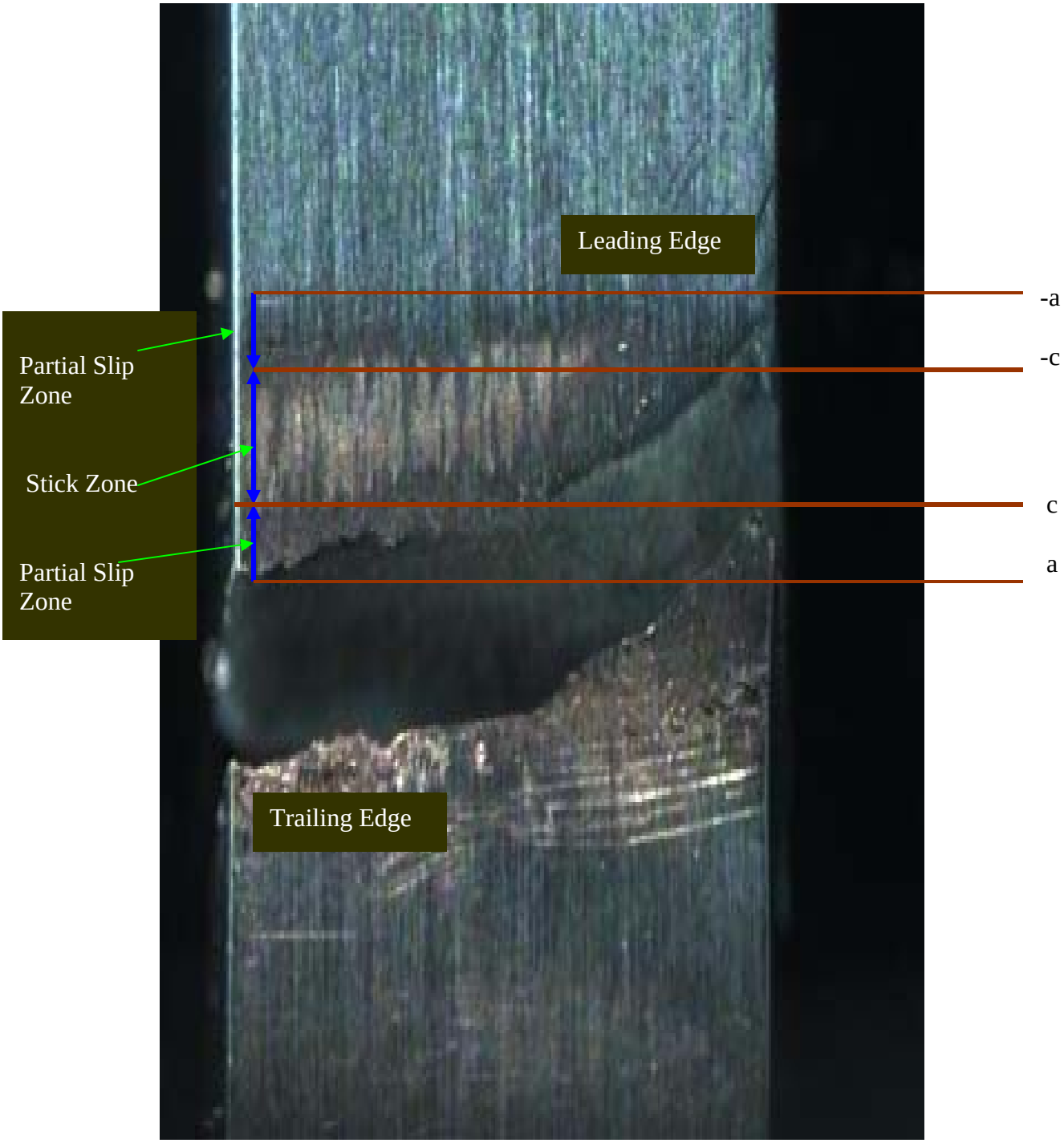

Figure 5.18 Partial slip and stick zones of test # 3

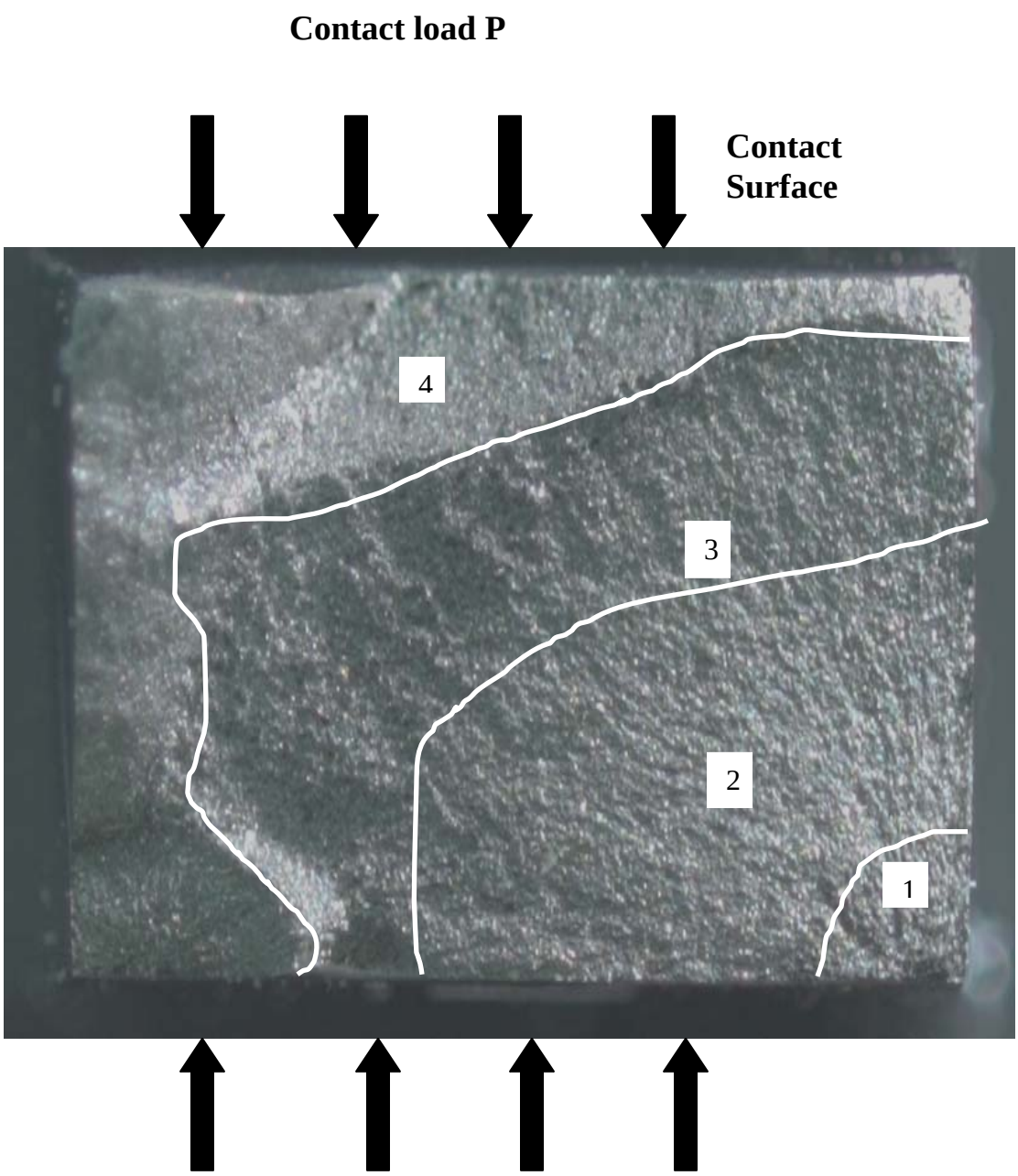

Figure 5.19 Fracture Surface for test # 4 along with four distinguishable regions

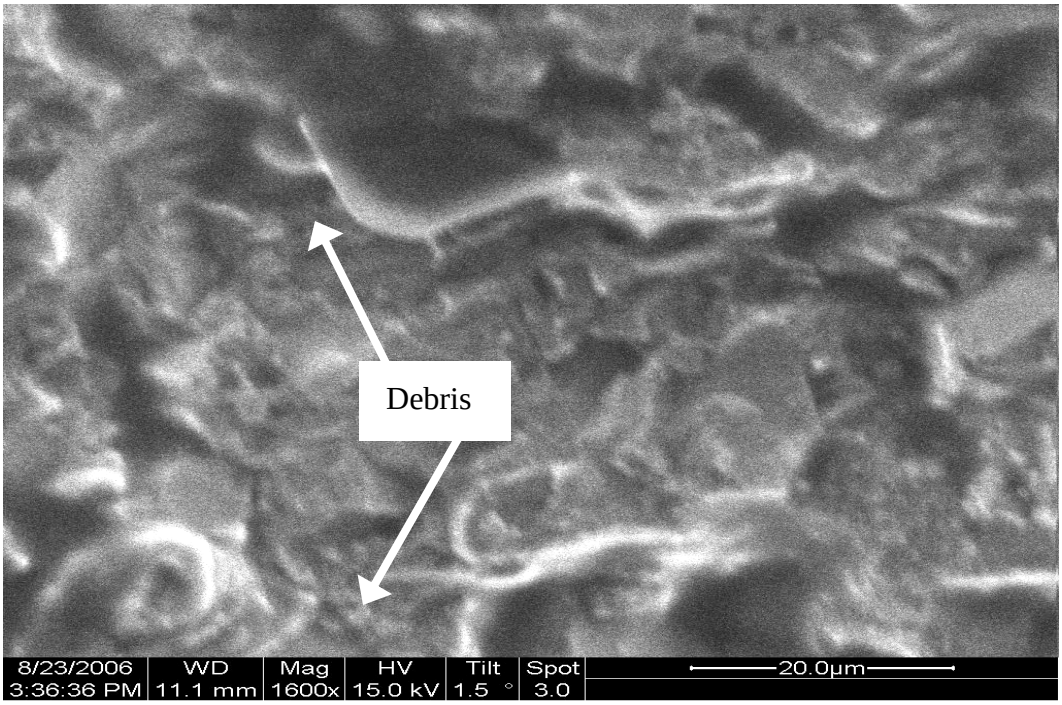

Figure 5.20 Region (1) with debris

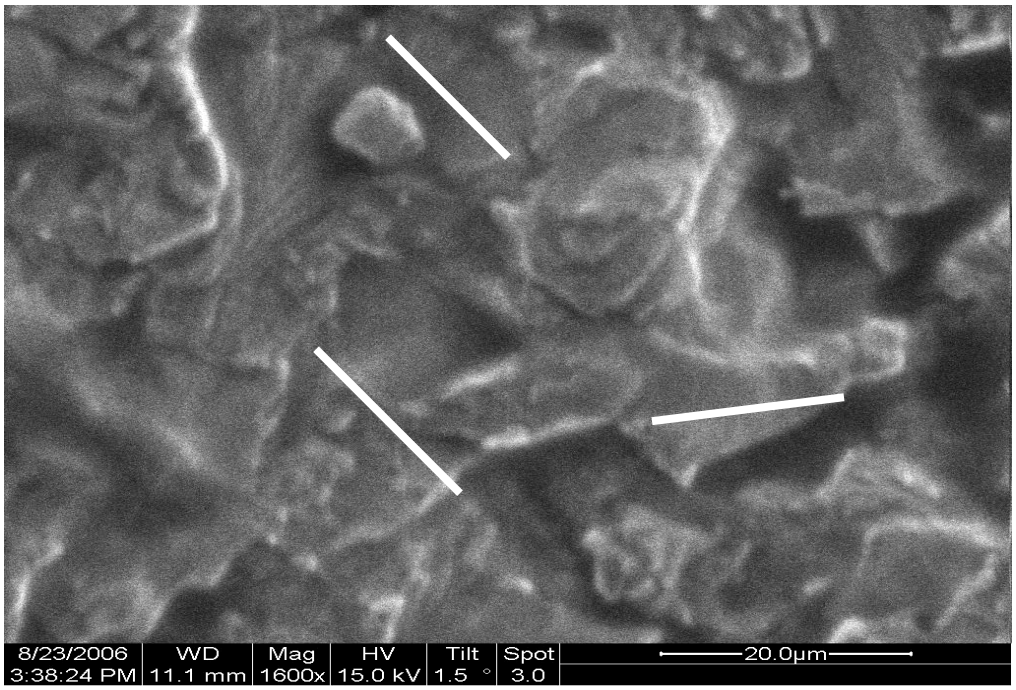

Figure 5.21 Region (2) striations

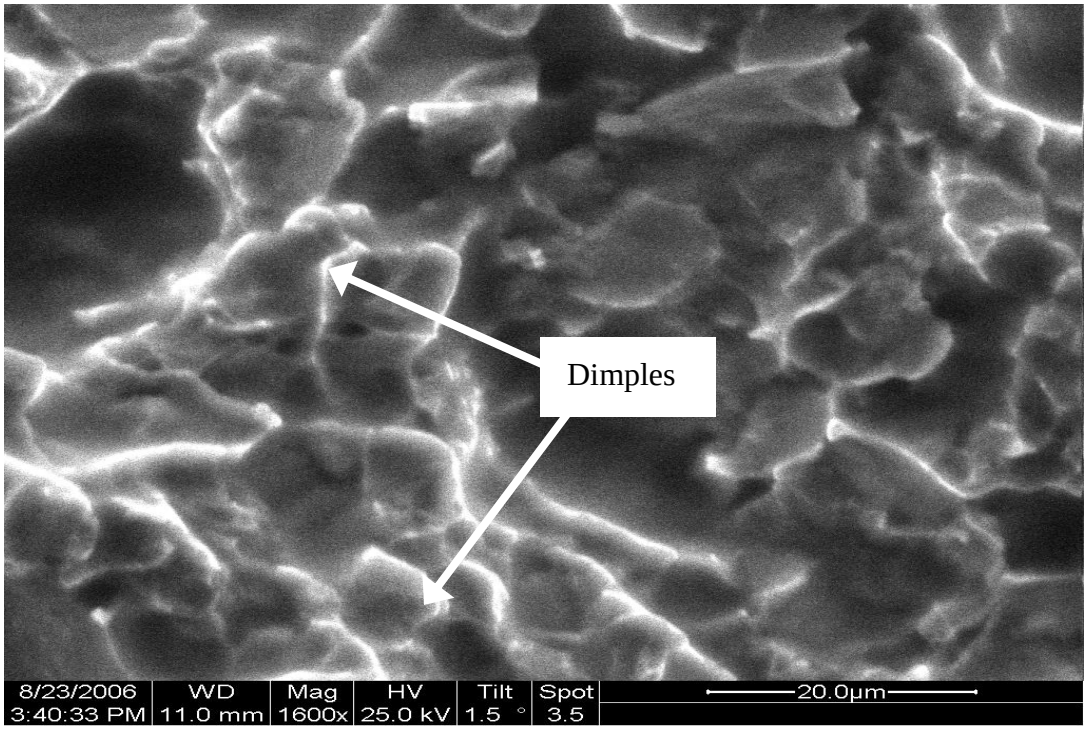

Figure 5.22 Region (3) large dimples

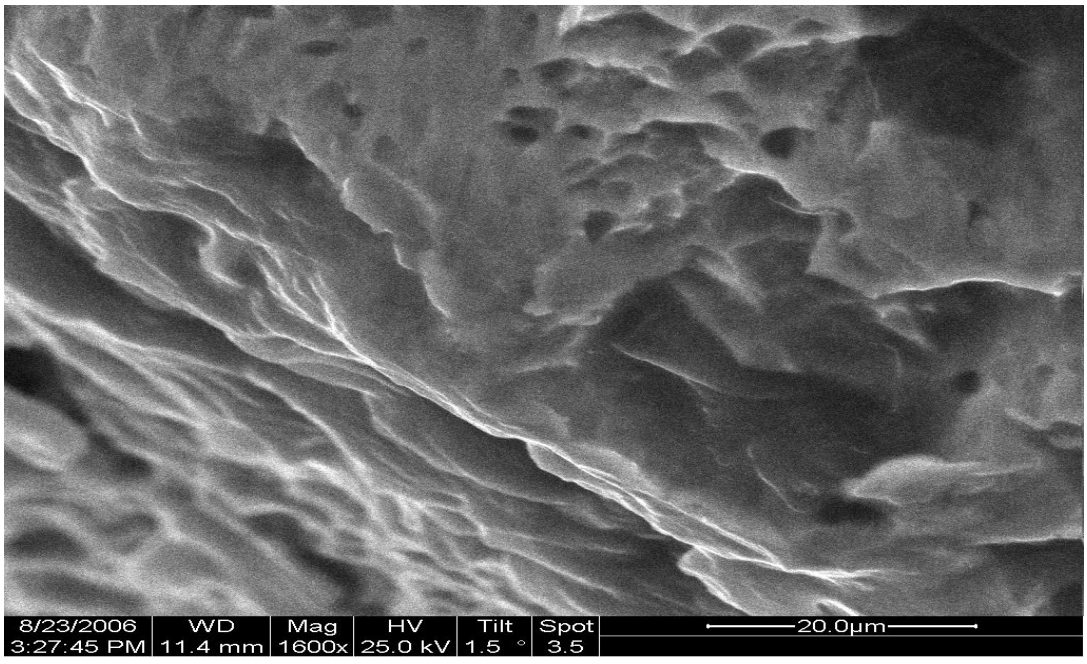

Figure 5.23 Region (4) catastrophic areas

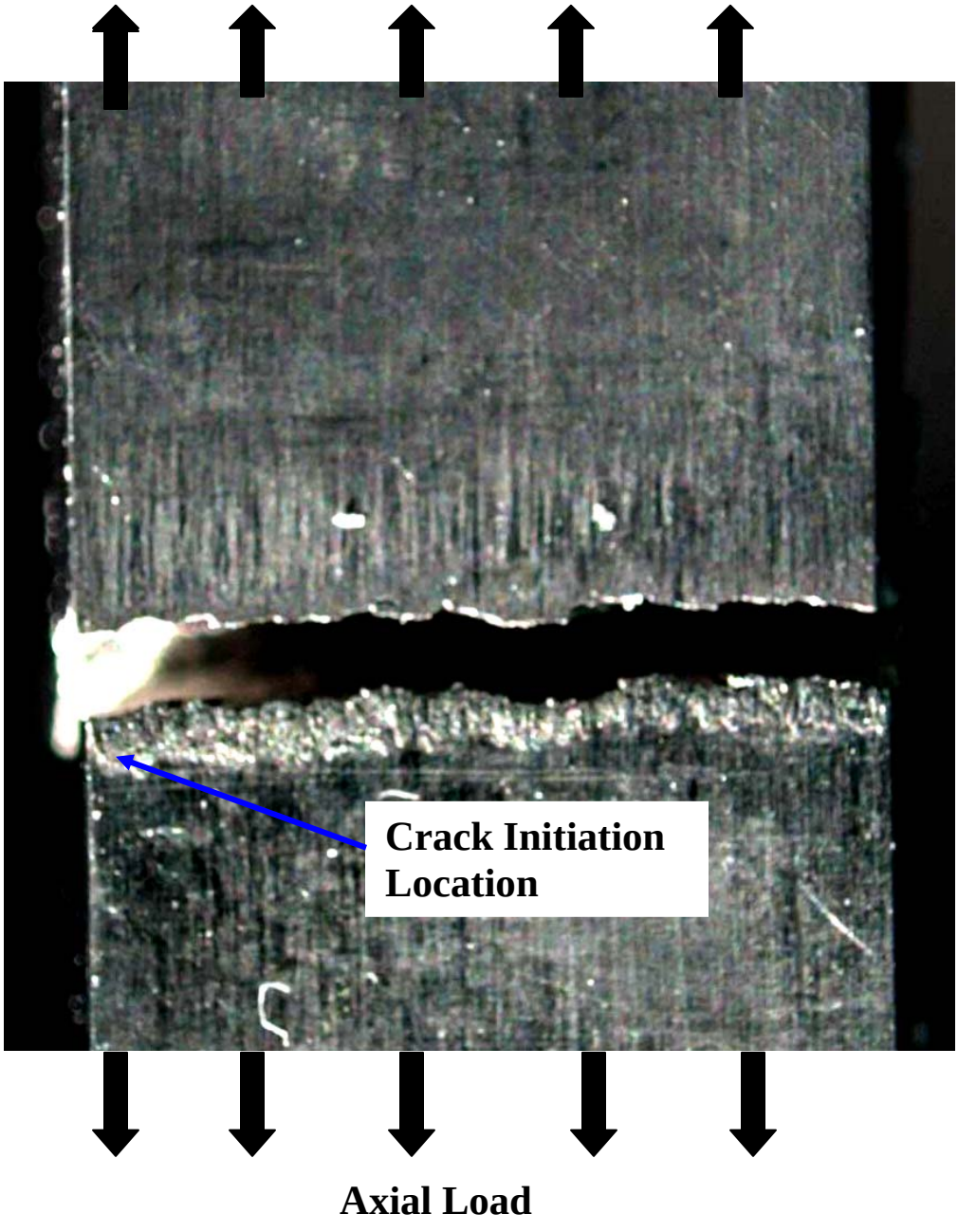

Figure 5.24 Crack initiation location for test # 2

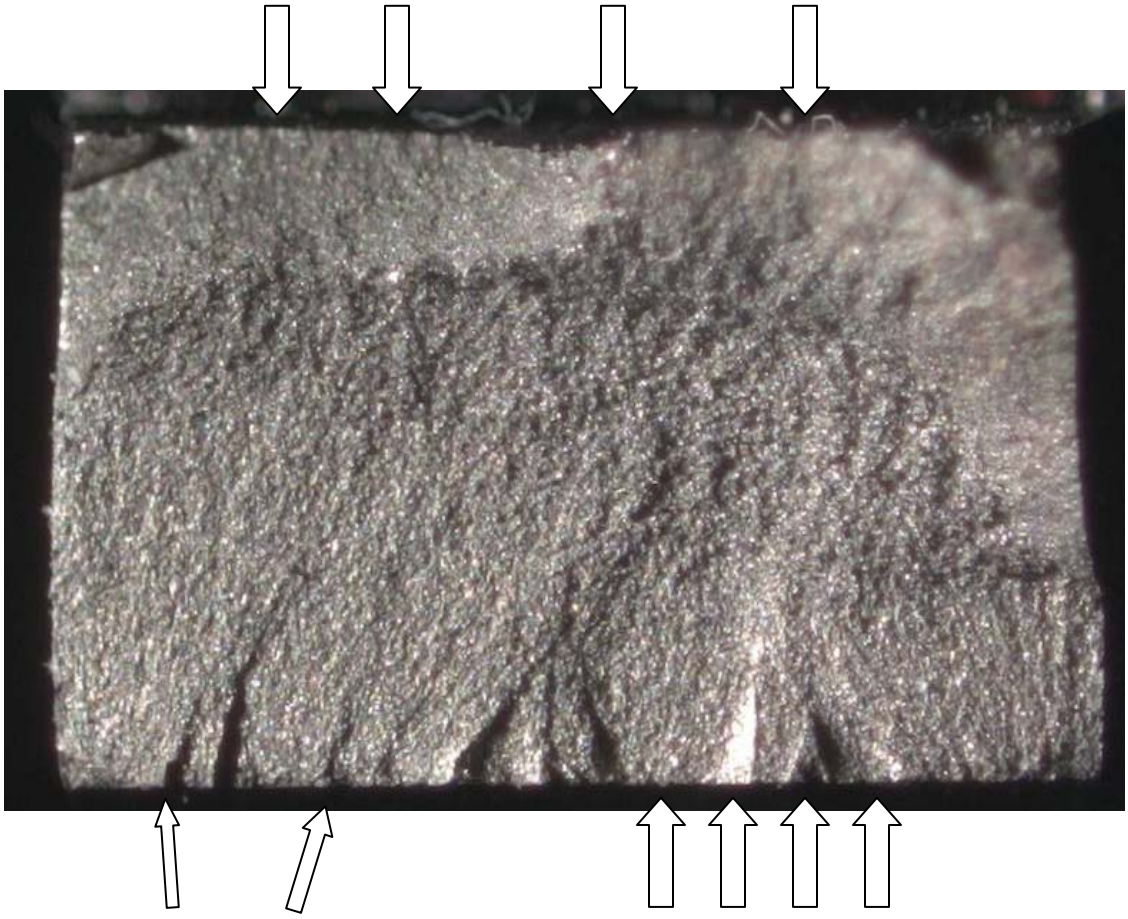

Figure 5.25 Crack initiation location and contact surface for test # 2

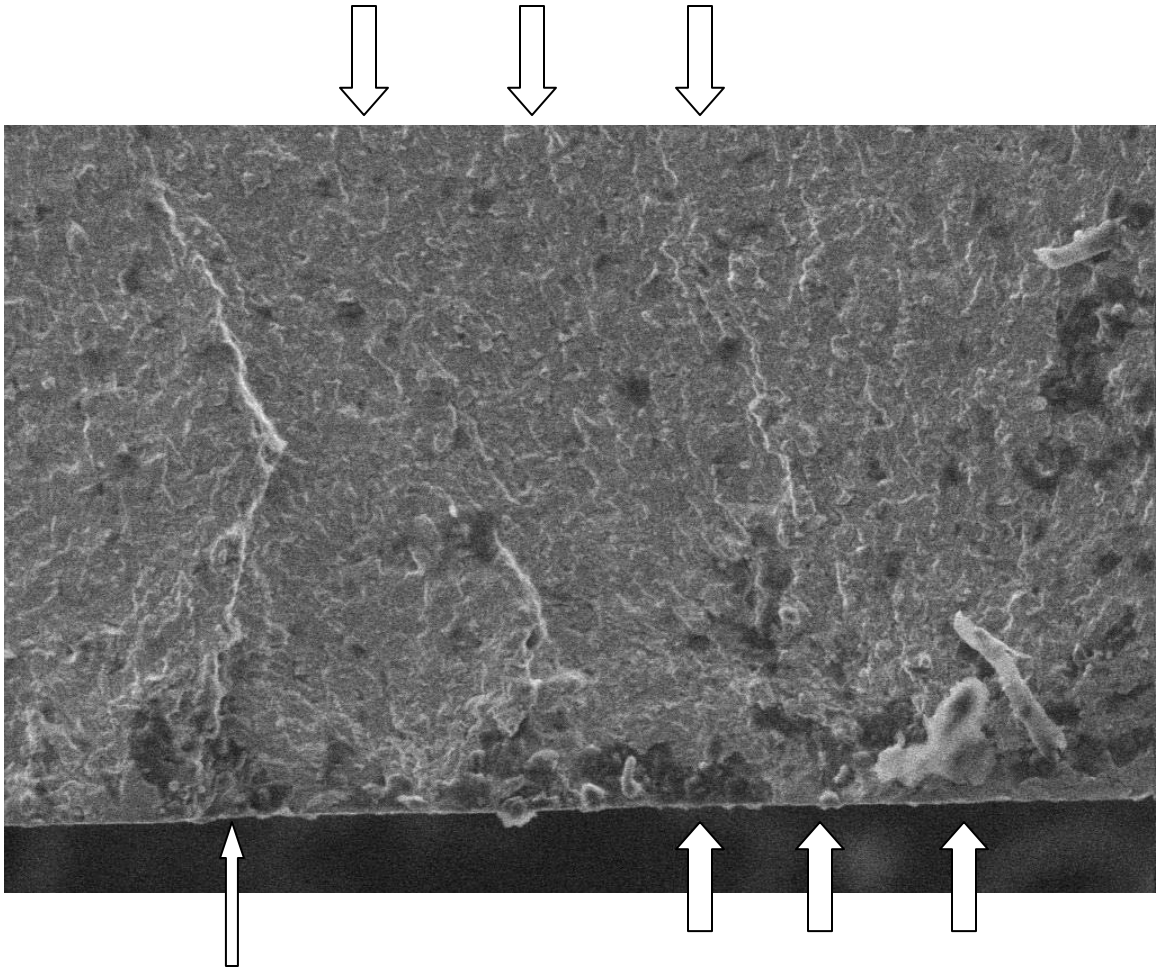

Figure 5.26 Crack initiation location and contact surface for test # 2 under high magnification

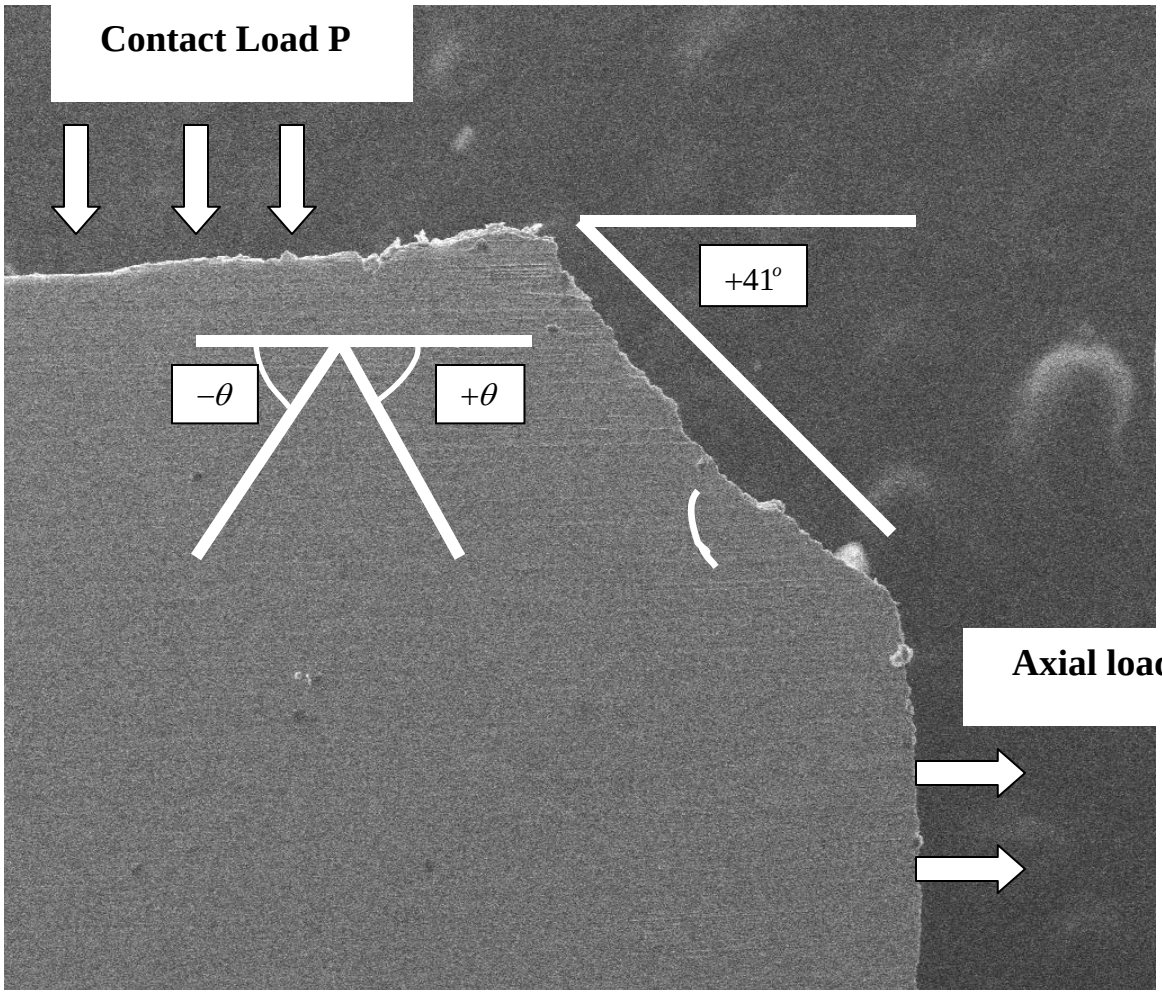

Figure 5.27 Crack initiation orientations for test # 2 (in-phase)

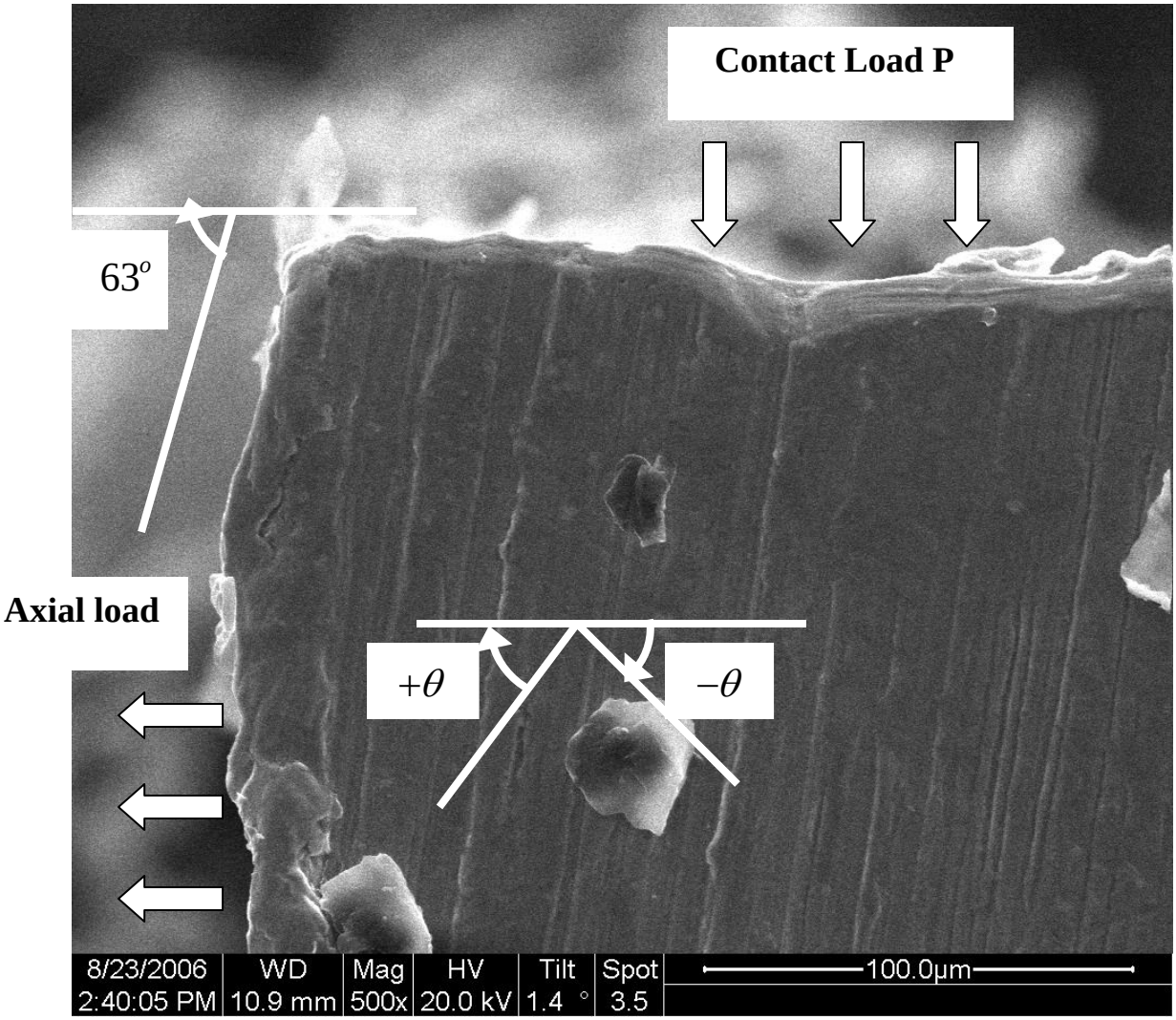

Figure 5.28 Crack initiation orientations for test # 3 (out of phase)

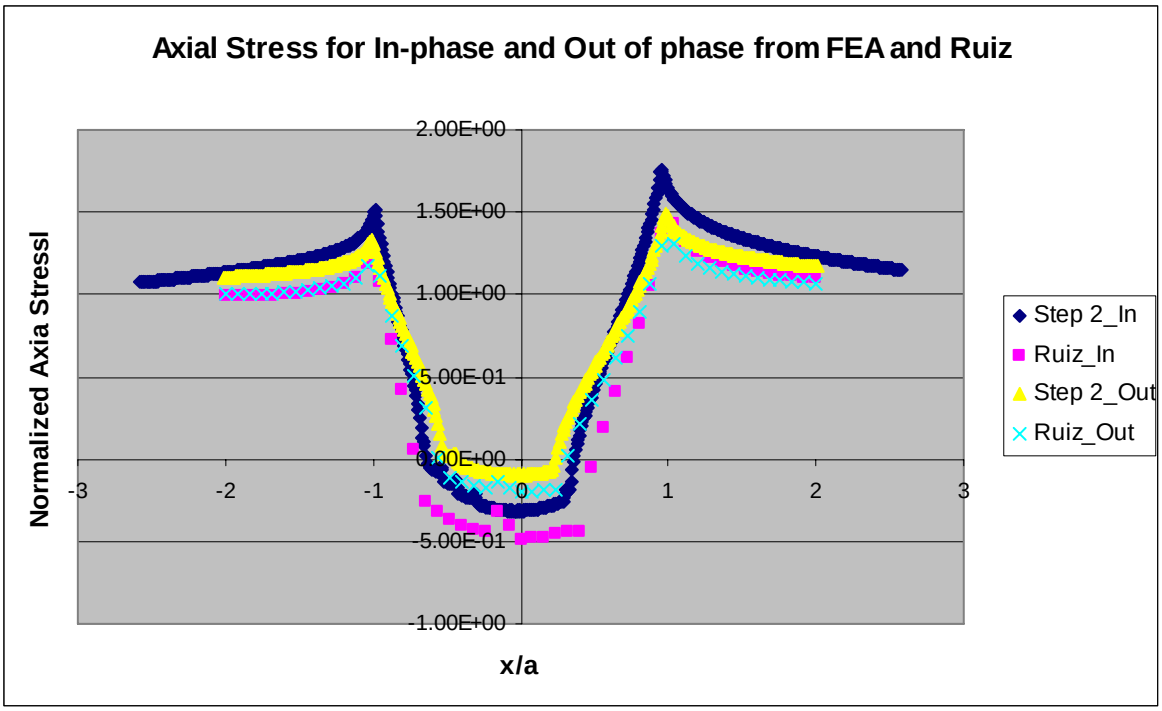

Figure 5.29 Stress distribution of axial stress for test # 2 and test # 3

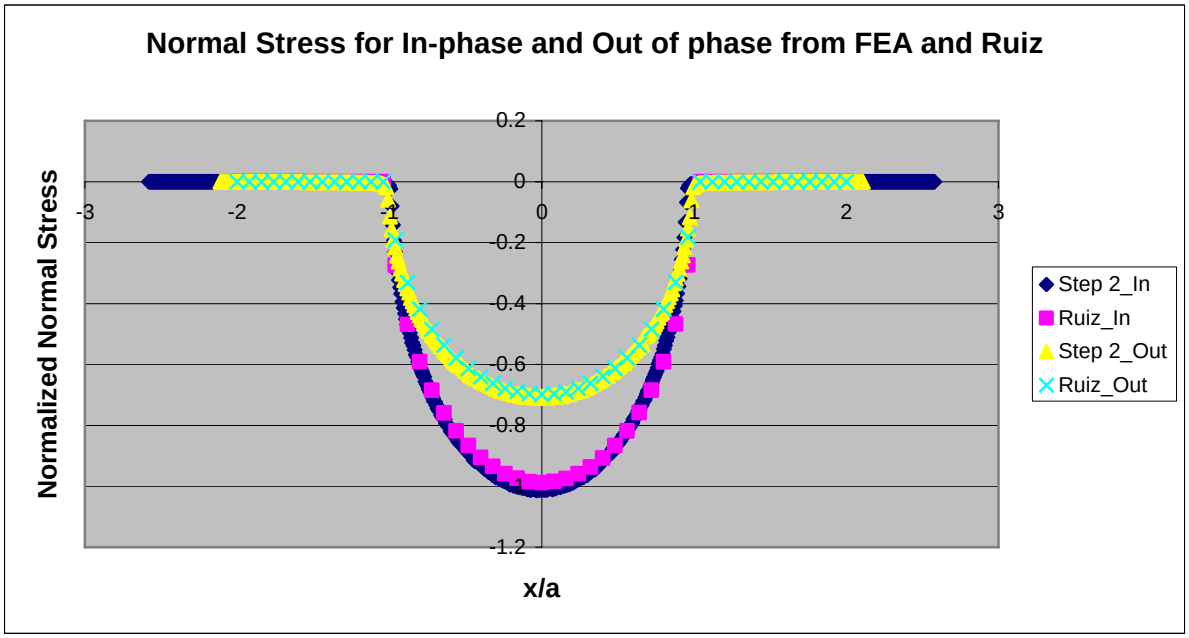

Figure 5.30 Stress distribution of normal stress for test # 2 and test # 3

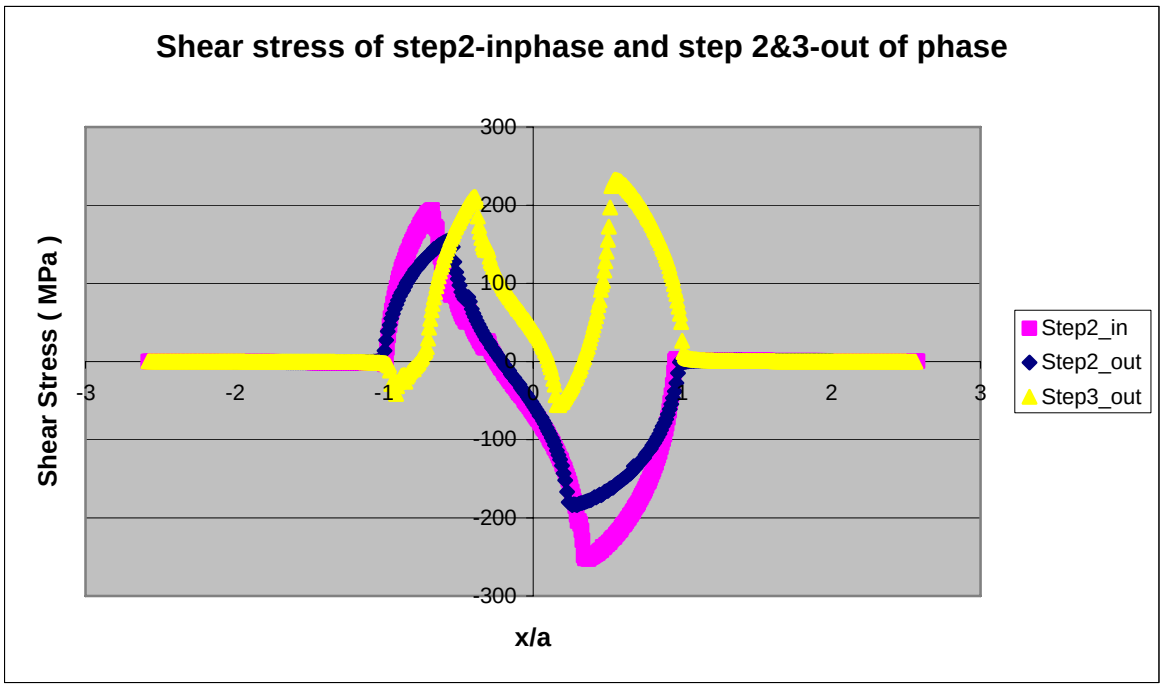

Figure 5.31 Shear stress distribution of step 2 (test # 2) and step 2&3 (test # 3)

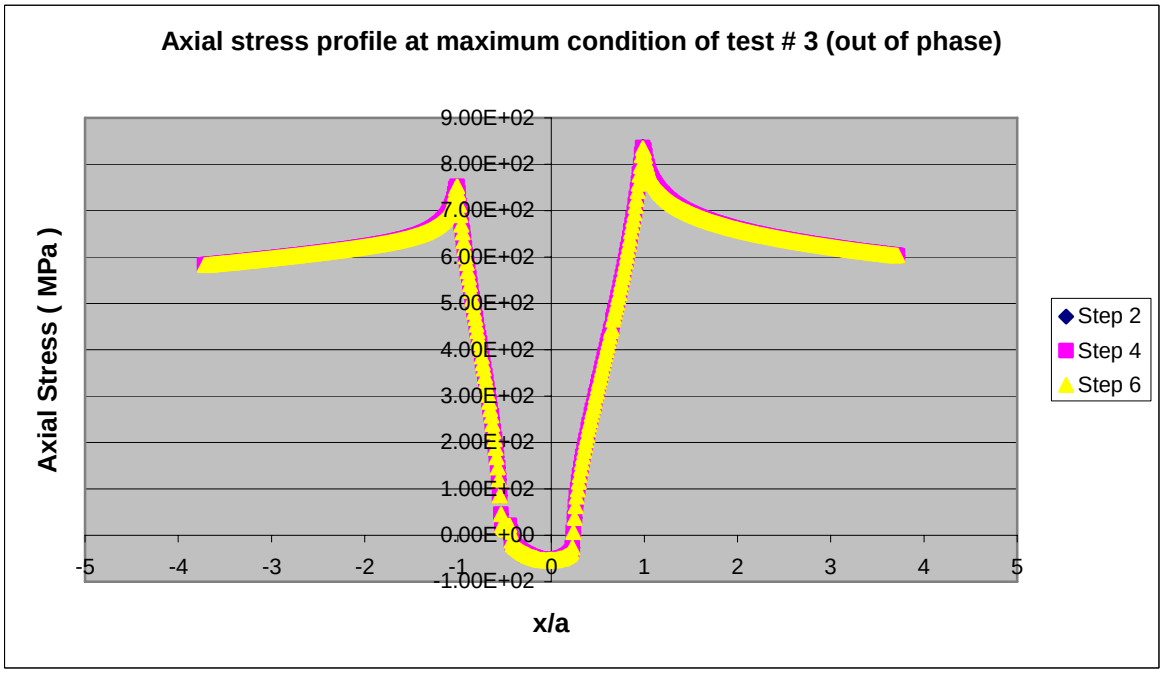

Figure 5.32 Axial stress profiles of steps 2, 4, and 6 for test # 3 (out of phase)

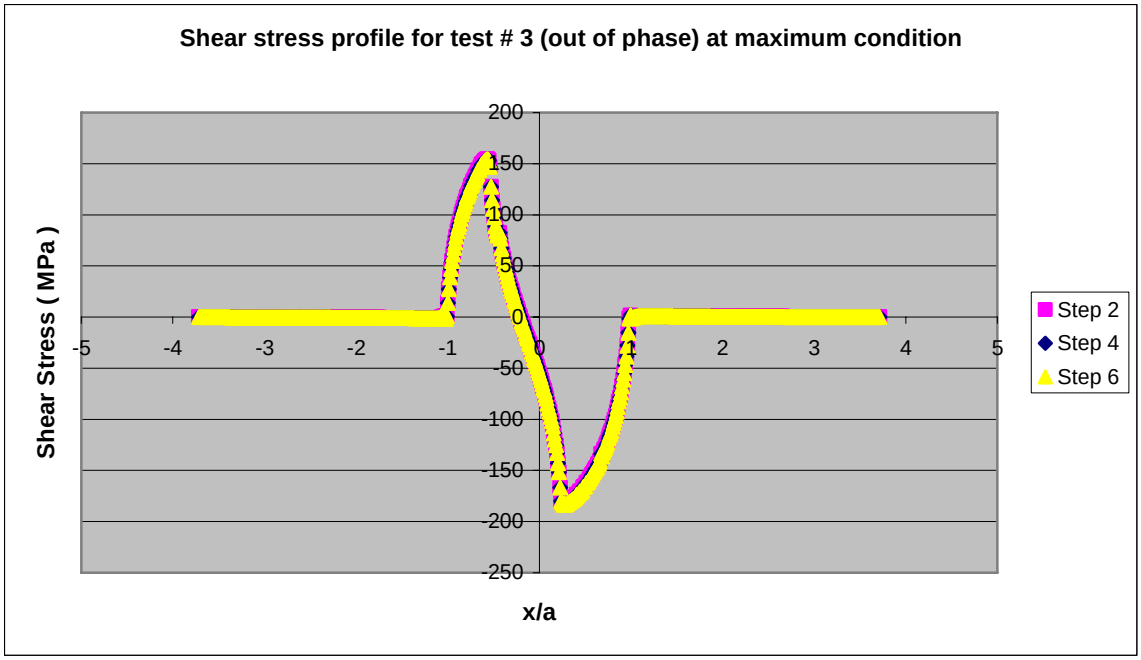

Figure 5.33 Shear stress profiles of steps 2, 4, and 6 for test # 3 (out of phase)

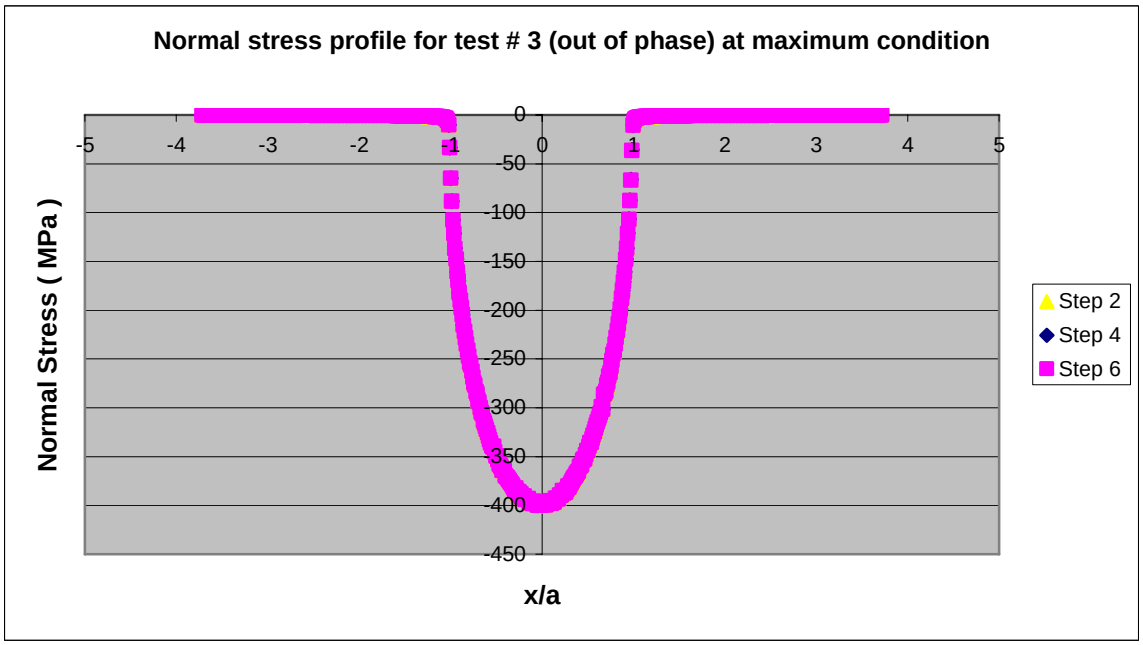

Figure 5.34 Normal stress profiles of steps 2, 4, and 6 for test # 3 (out of phase)

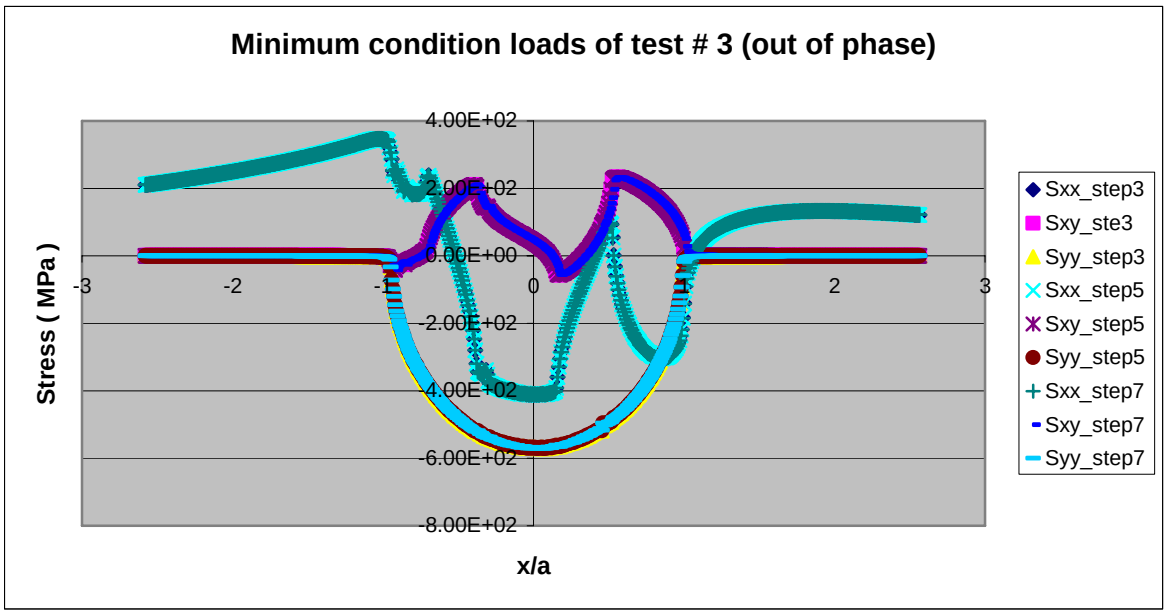

Figure 5.35 Stress profiles at minimum condition of test # 3 (out of phase)

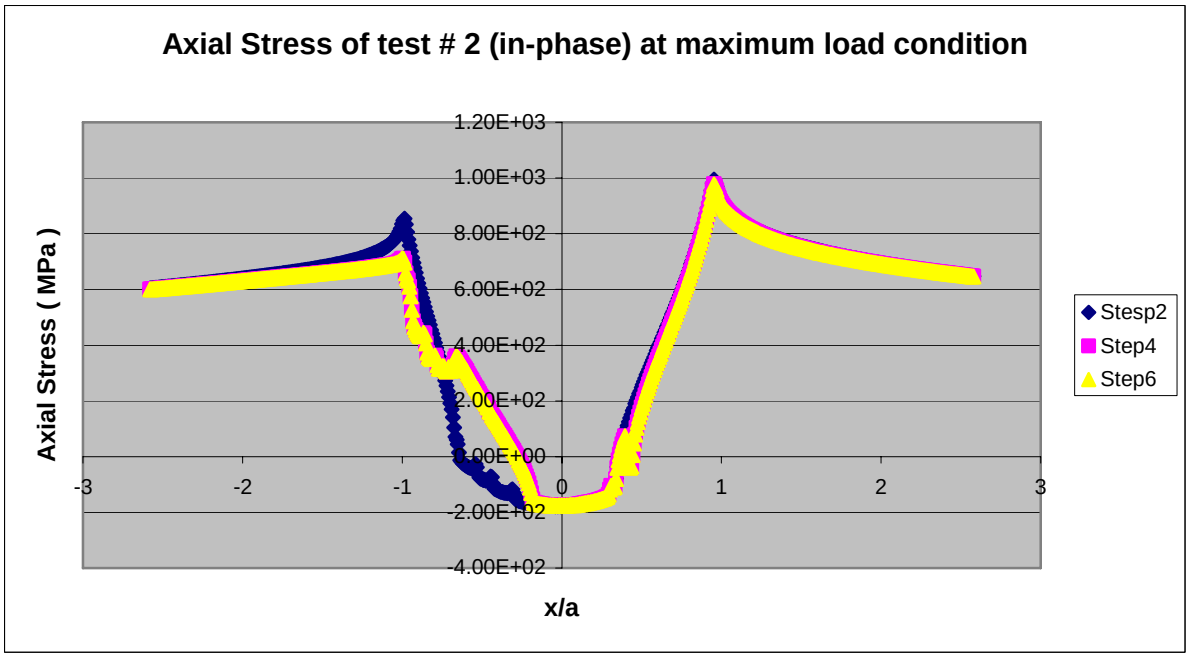

Figure 5.36 Axial stress profiles of maximum condition of test # 2 (in-phase)

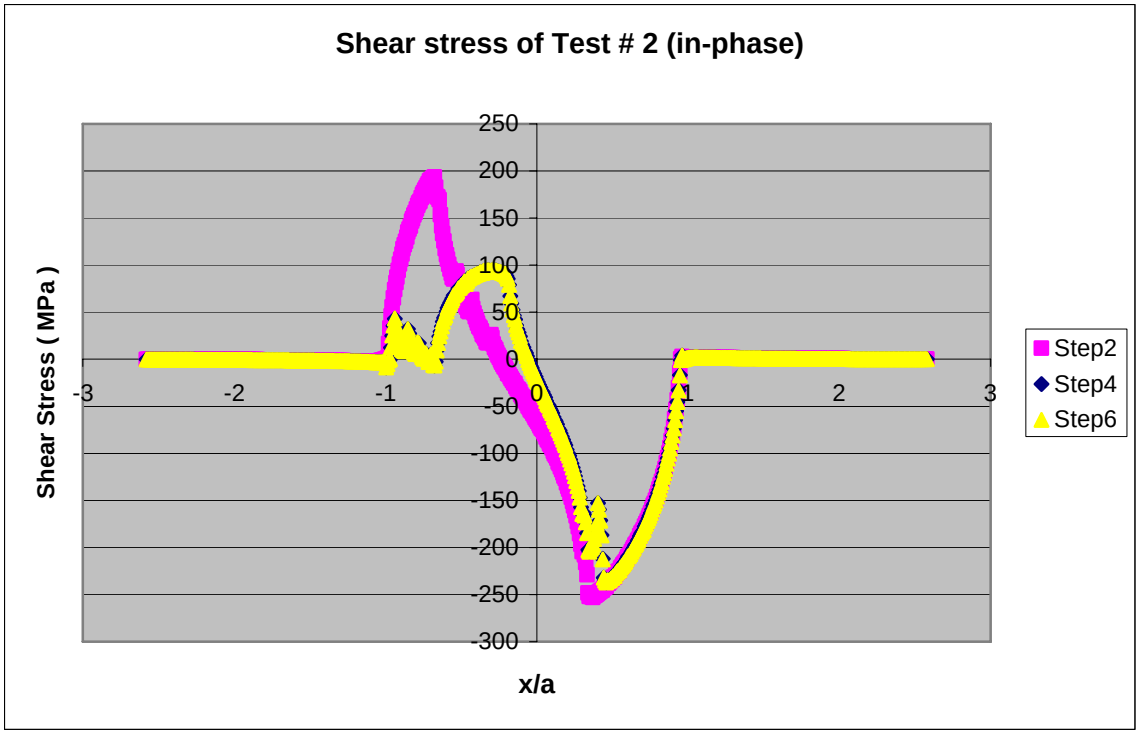

Figure 5.37 Shear stress profiles of maximum condition of test # 2 (in-phase)

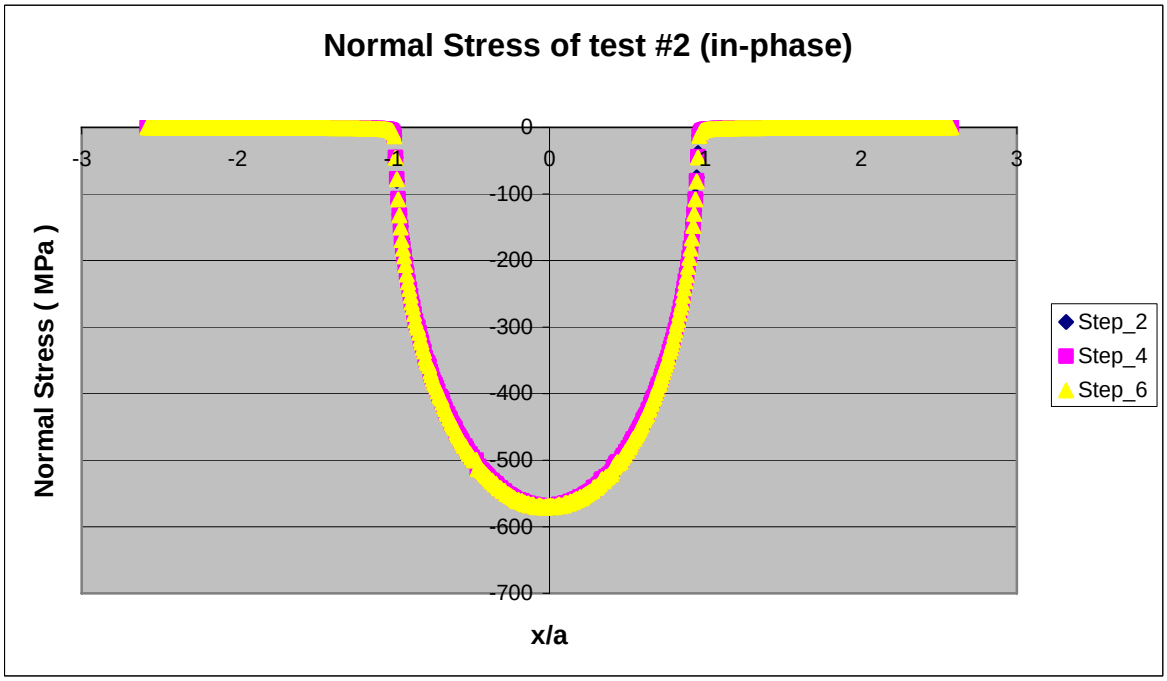

Figure 5.38 Normal stress profiles of maximum condition of test # 2 (in-phase)

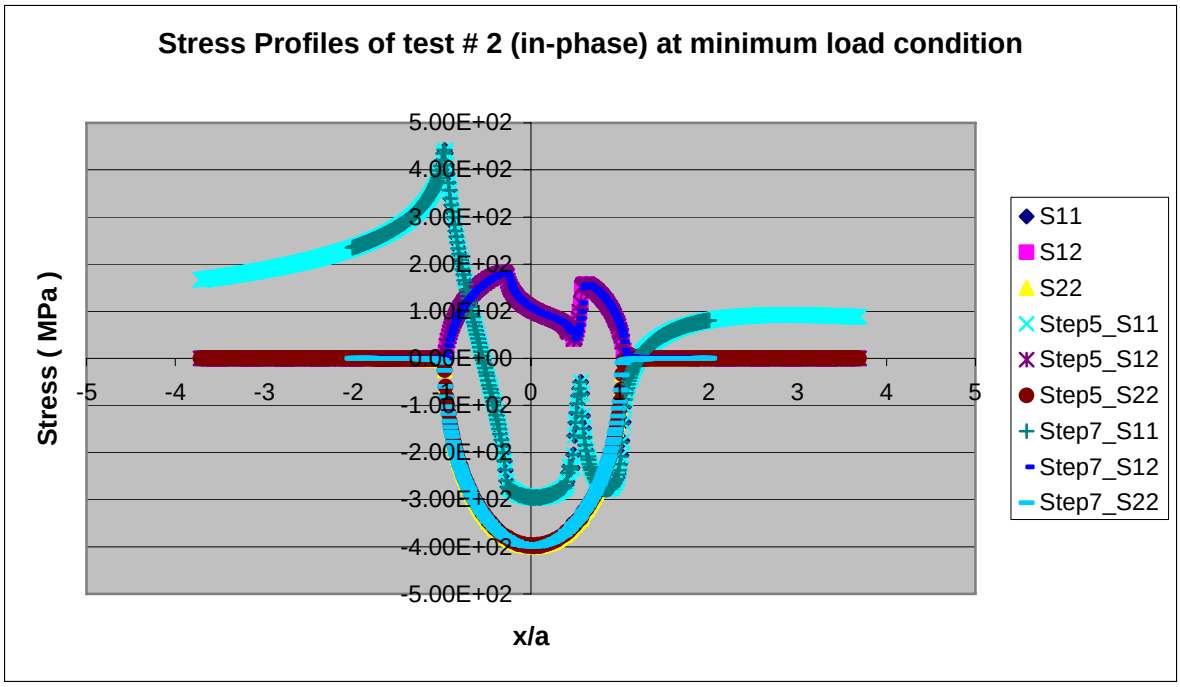

Figure 5.39 Stress profiles of minimum condition of test # 2 (in-phase)

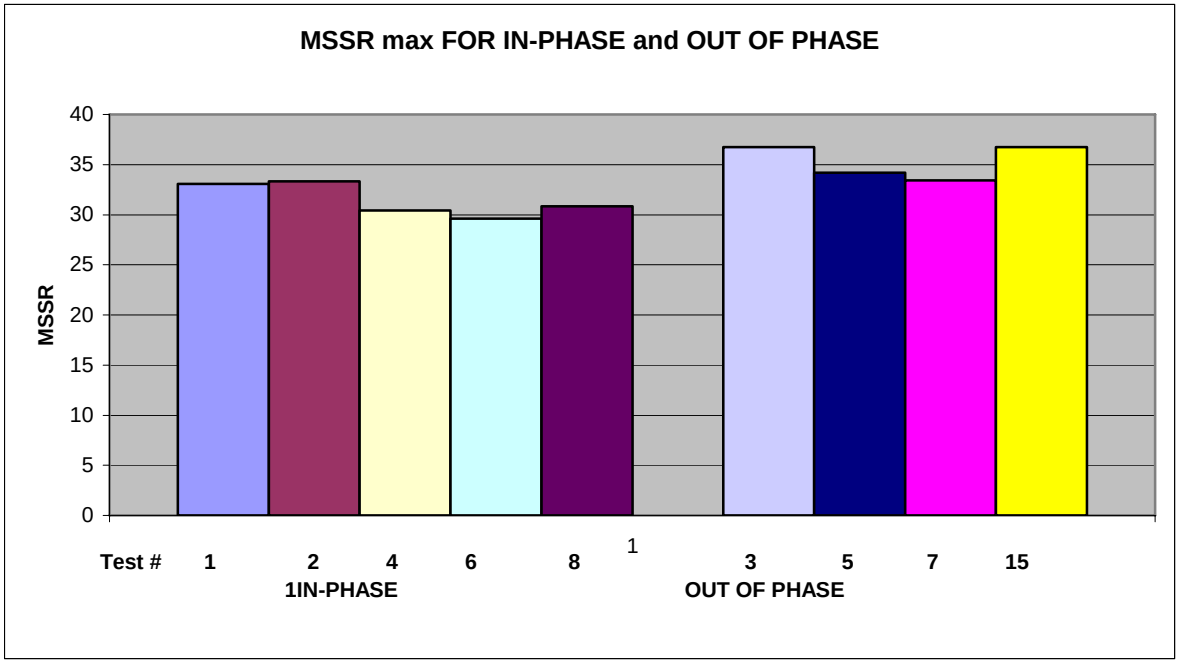

Figure 5.40 Max MSSR for in-phase and out of phase tests

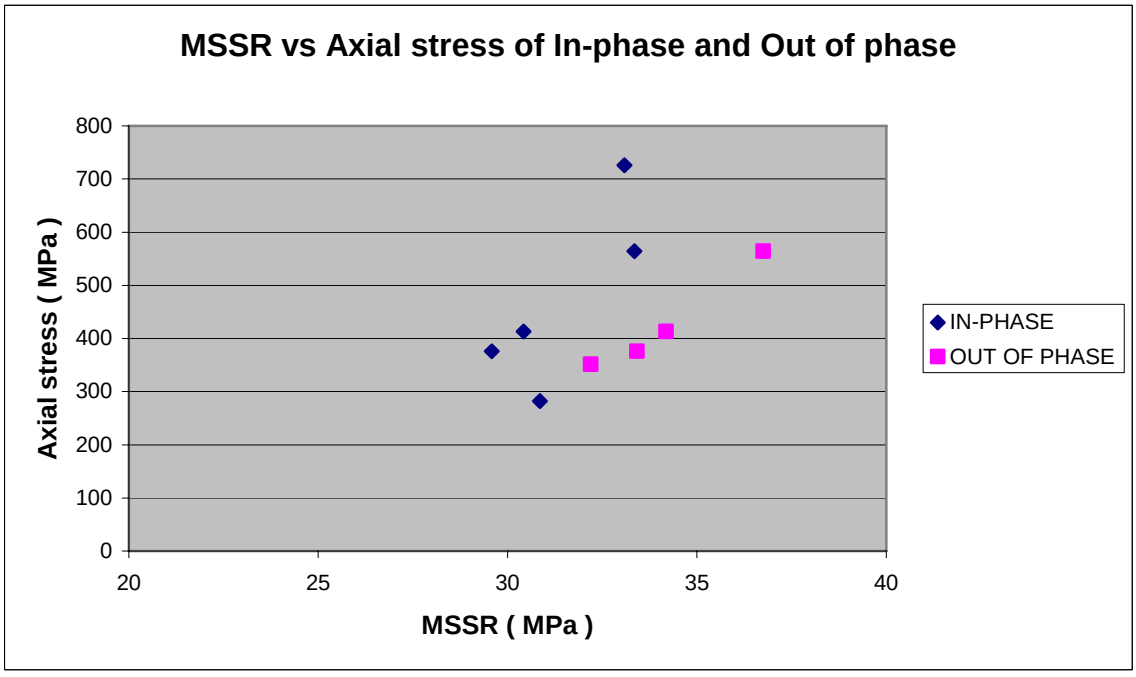

Figure 5.41 Max MSSR vs Axial Stress for in-phase and out-phase tests

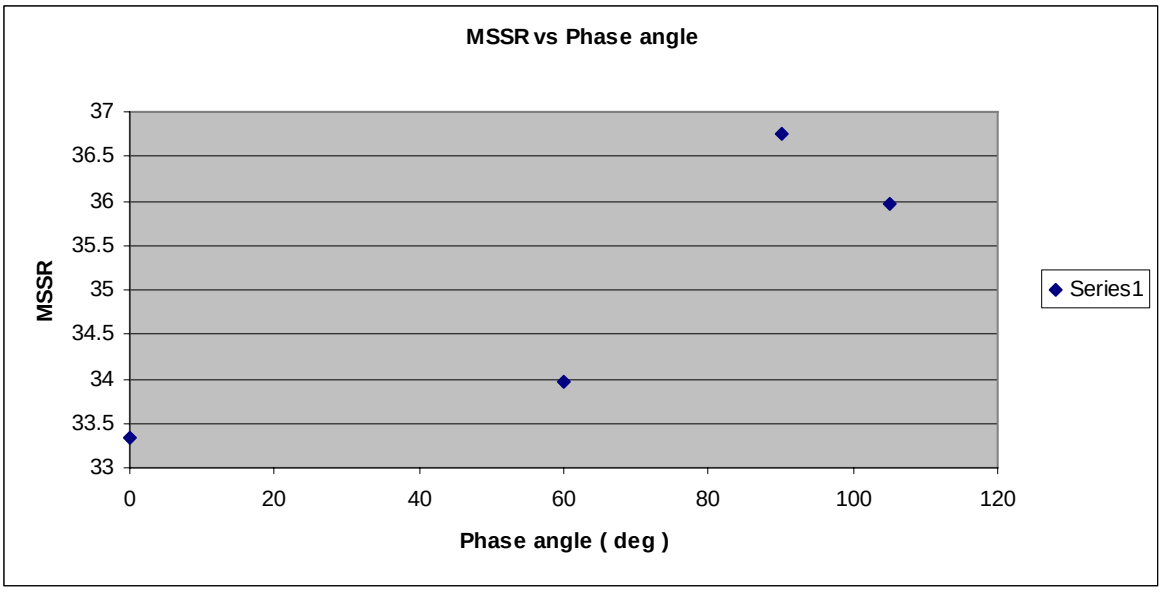

Figure 5.42 Max MSSR vs phase angle

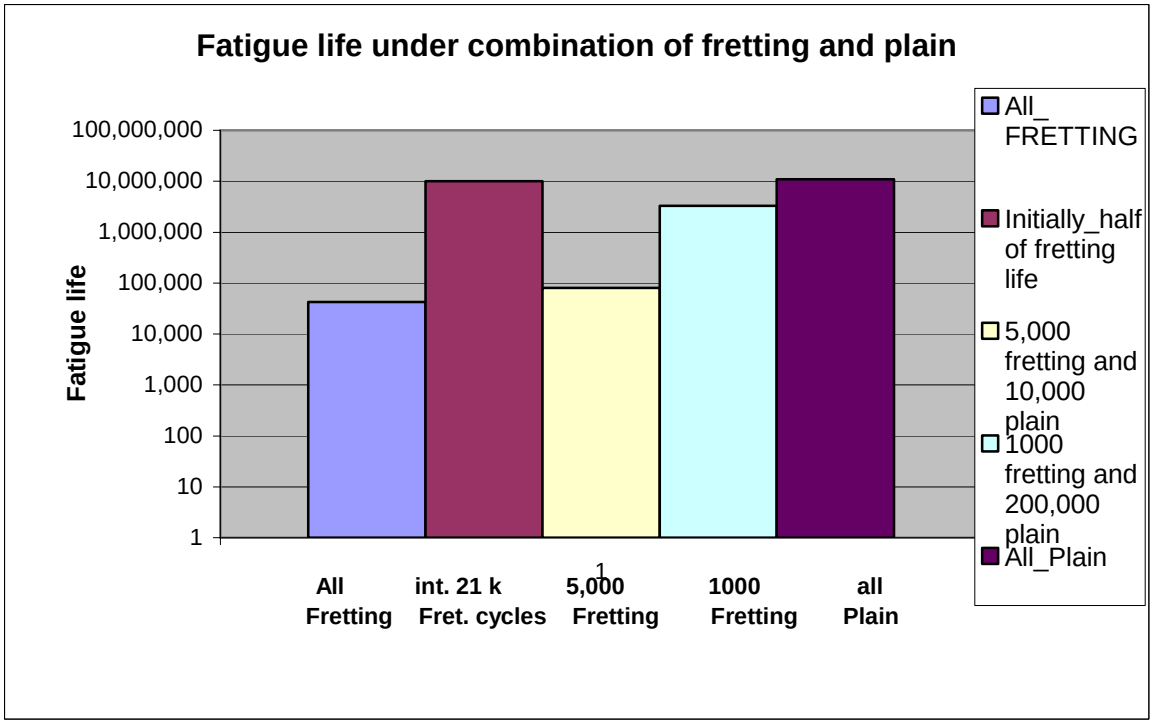

Figure 5.43 Fatigue Lives for the Combination Tests

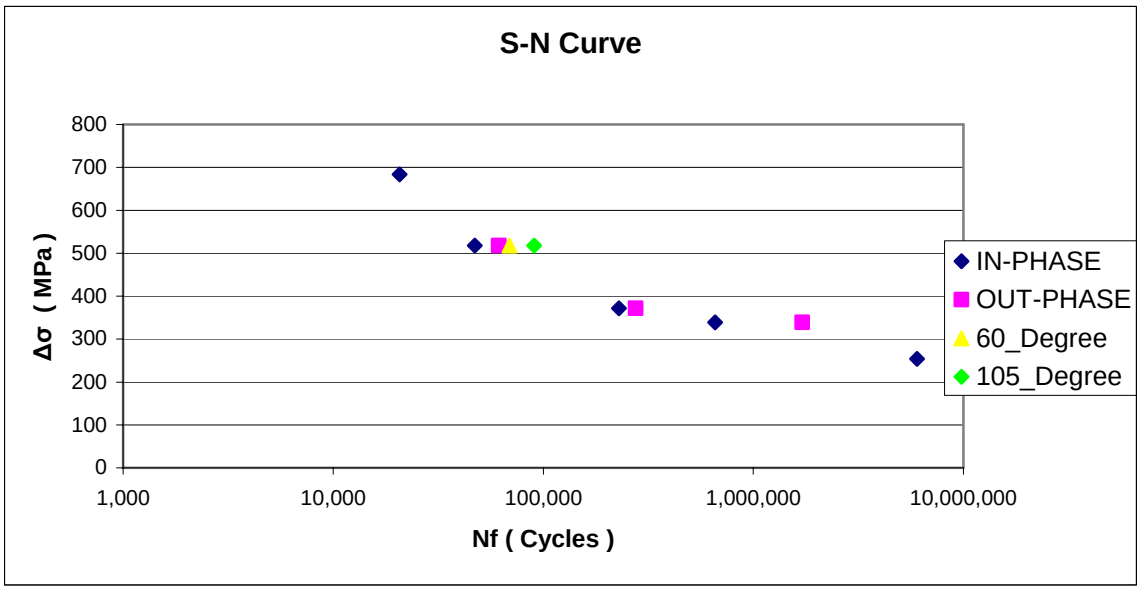

Figure 5.44 S_N Curve of the stress range from this study

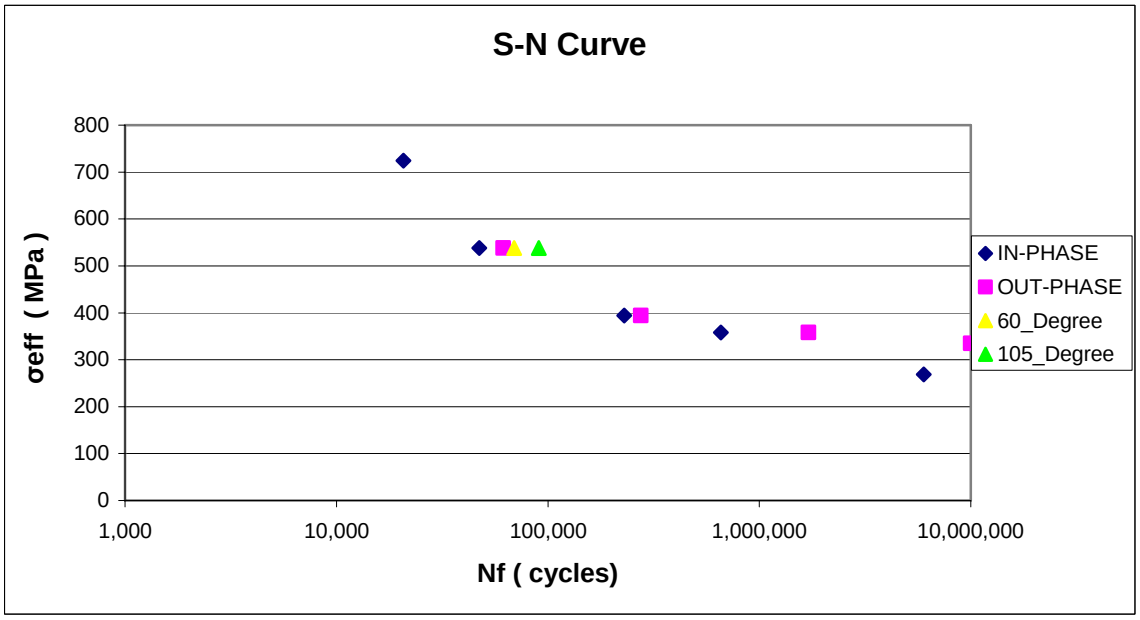

Figure 5.45 S_N Curve of the effective stress from this study

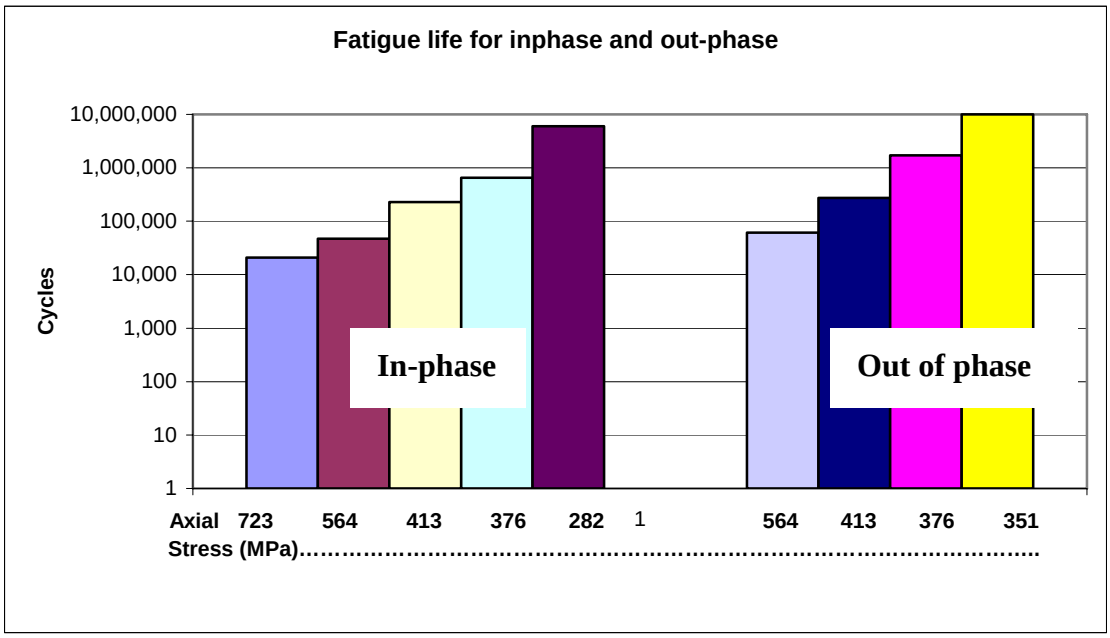

Figure 5.46 Cycles of the test for in-phase and out of phase

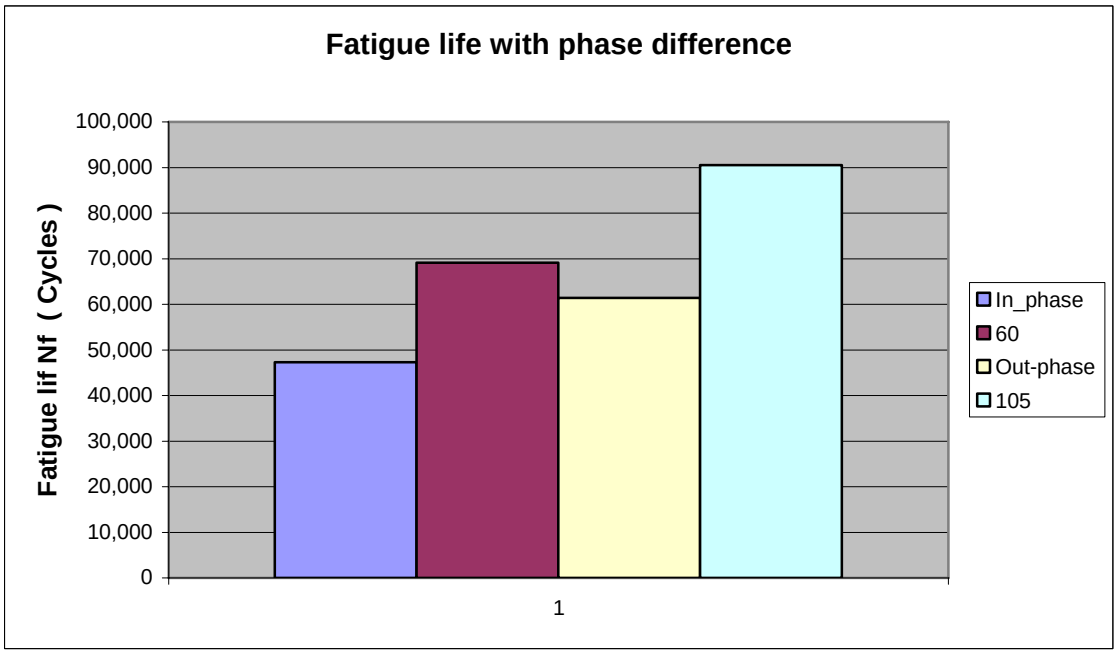

Figure 5.47 Cycles of the test at same axial load with different phase angles

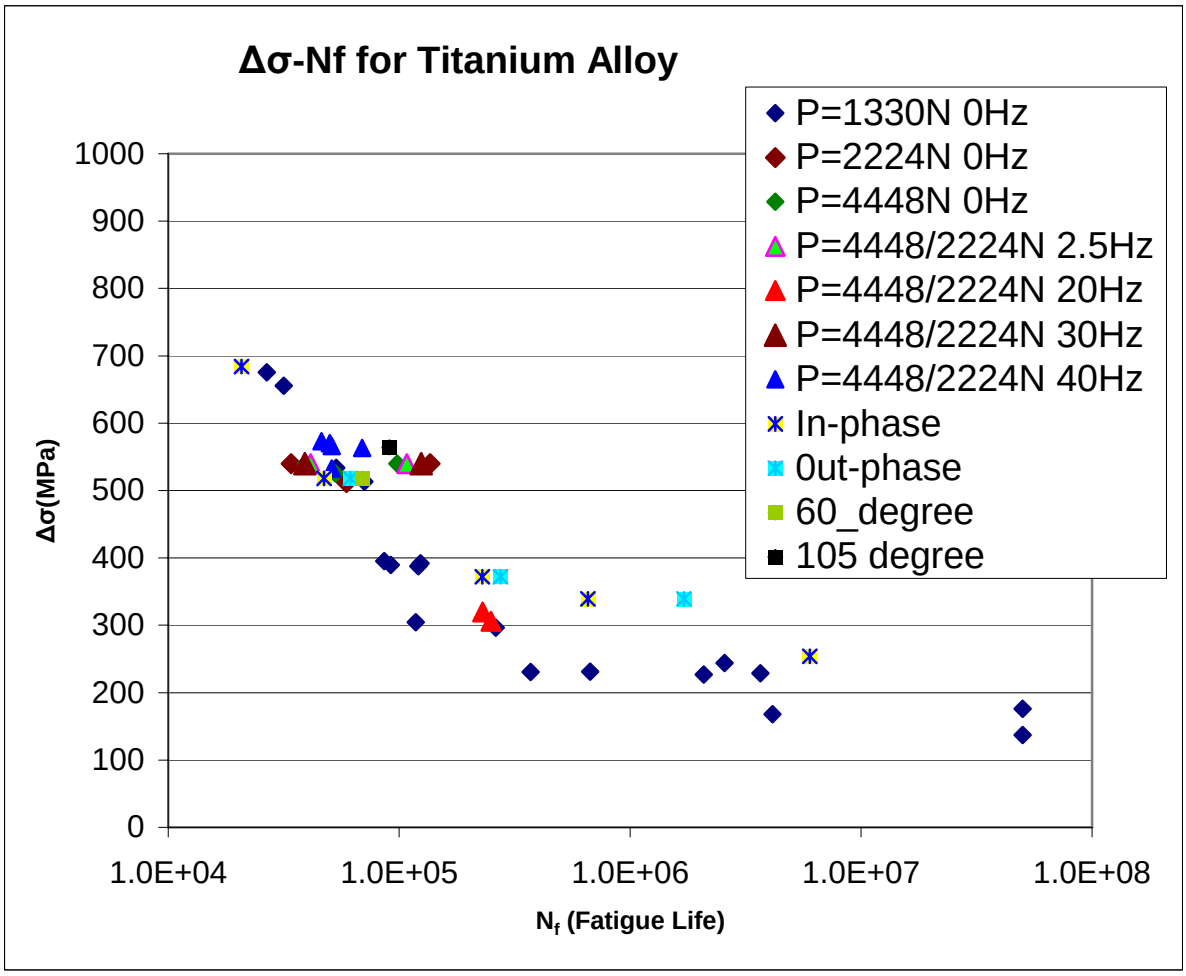

Figure 5.48 S_N Curve of the stress range from this study and the previous studies

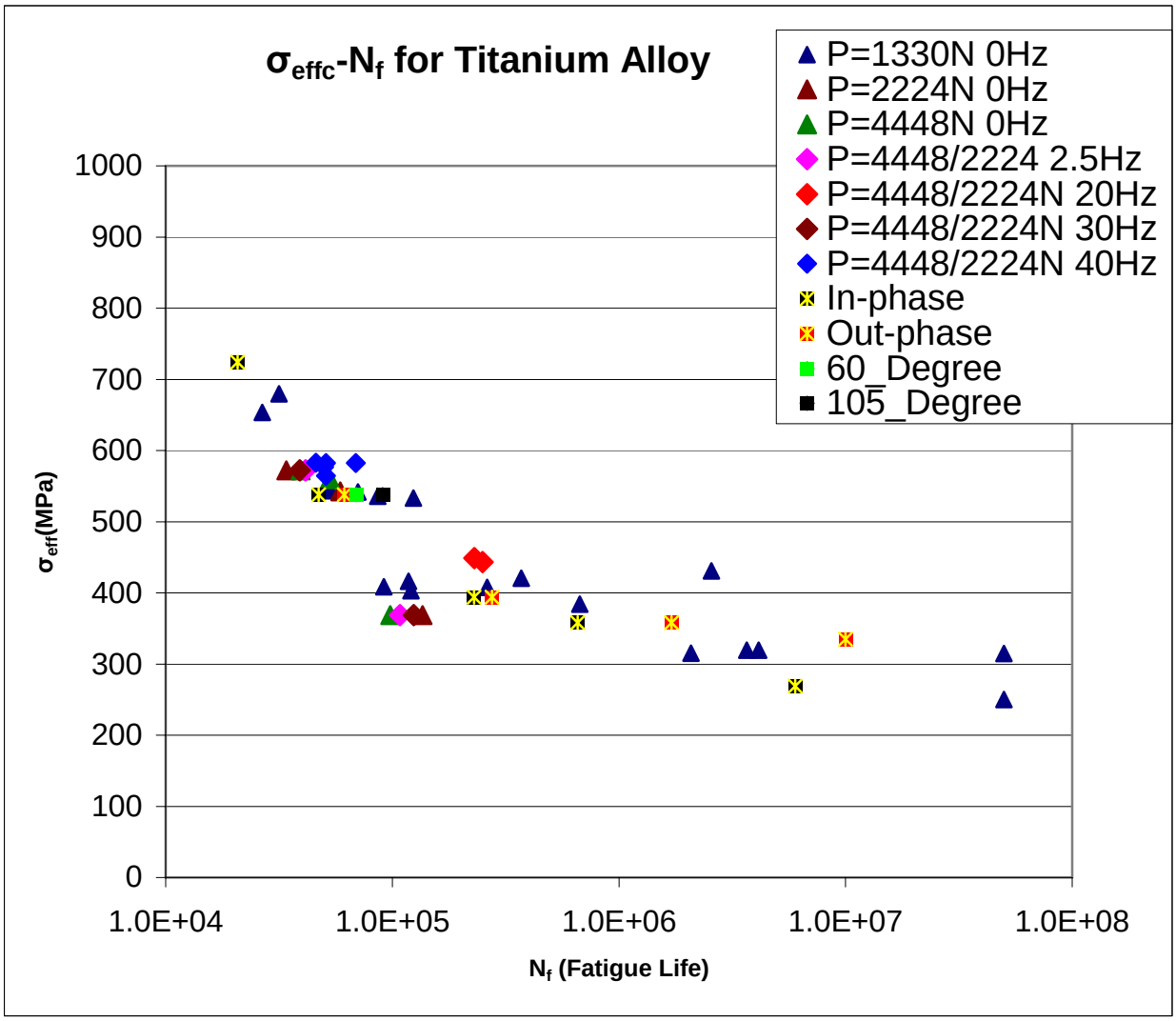

Figure 5.49 S_N Curve of the effective stress from this study and the previous studies

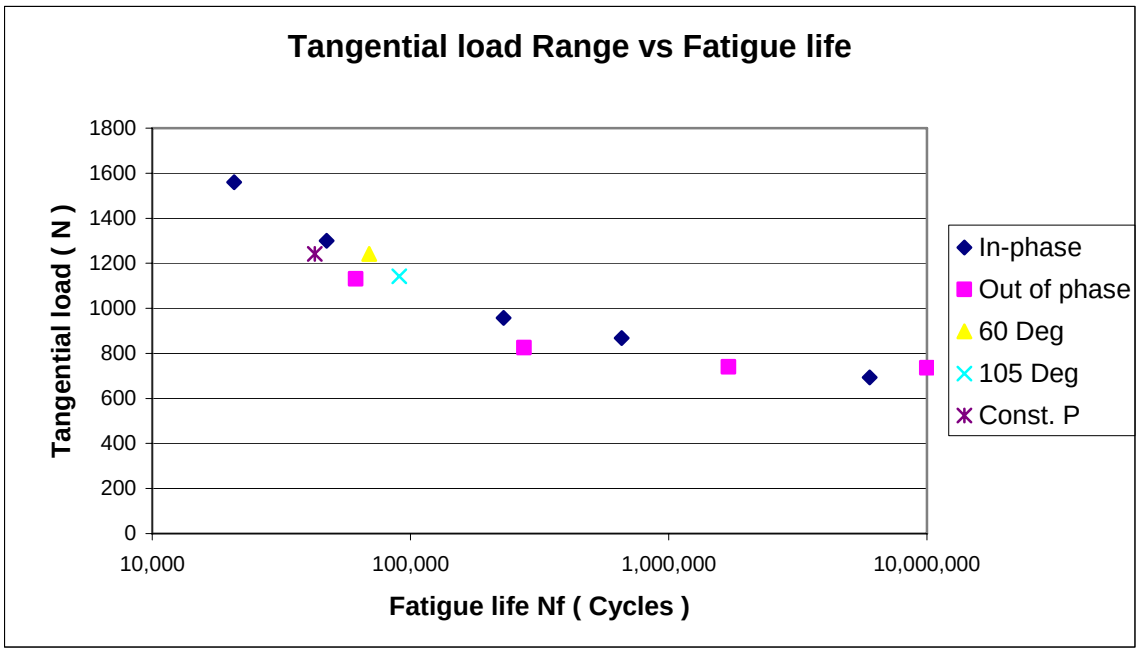

Figure 5.50 S_N Curve of the tangential load range from this study

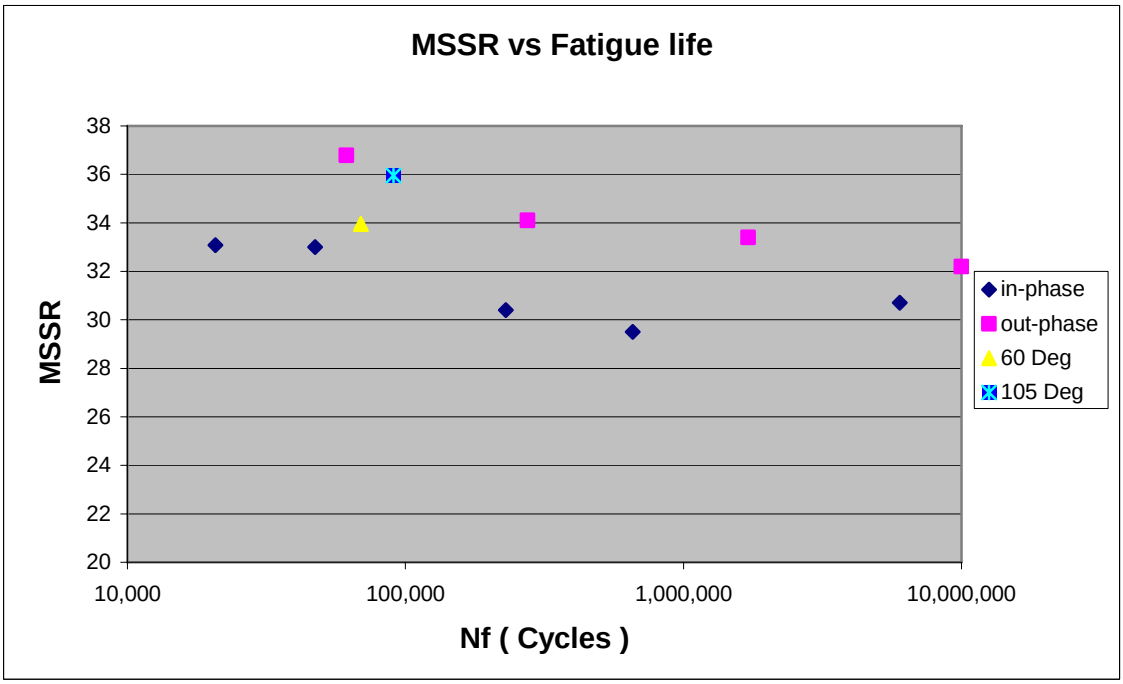

Figure 5.51 S_N Curve of MSSR from this study

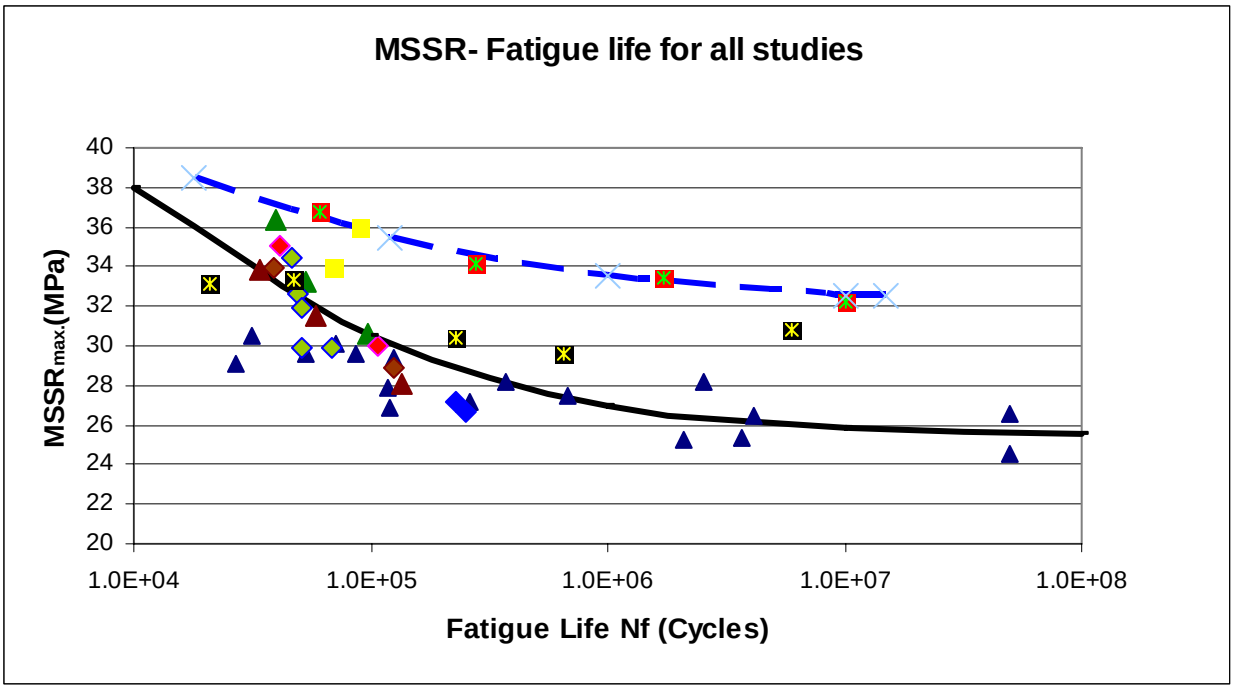

Figure 5.52 S_N Curve of MSSR from this study and previous studies

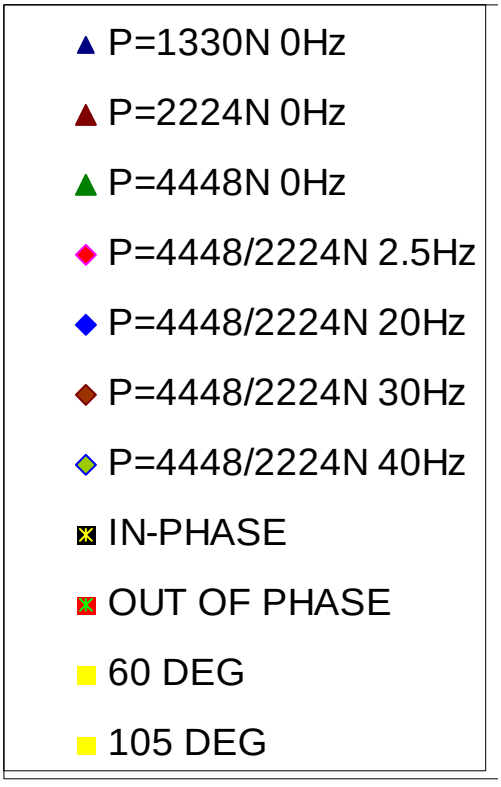

Table 5.1 Test inputs and results

Test #	σ_{max} MPa	σ_{min} MPa	$\Delta\sigma_{axial}$ MPa	P_{max} N	P_{min} N	Q_{max} N	Q_{min} N	N_f Cycles	Q/P max	ϕ Deg.
1	**760**	**76**	**684**	**4448**	**2224**	**369**	**-1191**	**20,734**	**0.5032**	**0**
2	**564**	**56**	**518**	**4448**	**2224**	**475.7**	**-824.3**	**47,298**	**0.3534**	**0**
3	**564**	**56**	**518**	**4448**	**2224**	**218.4**	**-912.8**	**61,428**	**0.2144**	**90**
4	**413**	**41**	**372**	**4448**	**2224**	**403**	**-555**	**229,477**	**0.2397**	**0**
5	**413**	**41**	**372**	**4448**	**2224**	**110**	**-715**	**275,172**	**0.1624**	**90**
6	**376**	**37**	**339**	**4448**	**2224**	**219.5**	**-648.5**	**657,432**	**0.2748**	**0**
7	**376**	**37**	**339**	**4448**	**2224**	**58.3**	**-682.3**	**1,706,847**	**0.1568**	**90**
8	**282**	**28**	**254**	**4448**	**2224**	**-398**	**-1092.5**	**> 6 million**	**0.4766**	**0**
9	**564**	**56**	**518**	**3336**	**3336**	**754**	**-486.95**	**42,640**	**0.2378**	**-**
10*	**564**	**56**	**518**	**3336**	**3336**	**-**	**-**	**10,049,531**	**-**	**-**
11**	**564**	**56**	**518**	**3336**	**3336**	**-**	**-**	**79,695**	**-**	**-**
12	**564**	**56**	**518**	**4448**	**2224**	**844**	**-397**	**69,149**	**0.3099**	**60**
13	**564**	**56**	**518**	**4448**	**2224**	**729**	**-413**	**90,528**	**0.3475**	**105**
14***	**564**	**56**	**518**	**3336**	**3336**	**-**	**-**	**3,301,122**	**-**	**-**
15	**351**	**35**	**316**	**4448**	**2224**	**499.2**	**-236.1**	**10,000,000**	**0.242**	**90**

* Test done first with 21,320 fretting fatigue cycles and then under plain fatigue
** Test done with 5,000 fretting cycles followed by 10,000 plain cycles, then repeated
*** Test done with 1,000 fretting cycles followed by 200,000 plain cycles, then repeated

Table 5.2 Q/P values from the tests at same axial stress and different phase angle (Load condition: σ_{max} = 564 MPa, σ_{min} = 56 MPa, P_{max} = 4448 N, and P_{min} =2224 N)

Test #	Phase Angle Degree	Q/P
2	0	0.3534
12	60	0.3099
3	90	0.2144
13	105	0.3475

Table 5.3 Contact half-width values from Ruiz and experiments

Test #	$\Delta\sigma_{axial}$ MPa	P_{max} N	P_{min} N	$a_{Experemnt}$ mm	$a_{Ruiz/max}$ mm
1	684	4448	2224	0.775	0.801
2	518	4448	2224	0.81	0.801
3	518	4448	2224	0.77	0.801
4	372	4448	2224	0.775	0.801
5	372	4448	2224	0.77	0.801
6	339	4448	2224	0.76	0.801
7	339	4448	2224	0.76	0.801
8	254	4448	2224	0.818	0.801
9	518	3336	3336	0.725	0.693
10	518	3336	3336	0.69	0.693
11	518	3336	3336	0.67	0.693
12	518	4448	2224	0.775	0.801
13	518	4448	2224	0.775	0.801
14	518	3336	3336	0.67	0.693
15	316	4448	2224	0.775	0.801

Table 5.4 MSSR calculation for test # 2 (in-phase) and test # 3 (out of phase)

Steps	MSSR	$\Delta\tau$ MPa	$\Delta\tau_{crit}$ MPa	θ Deg	$R_{\Delta\tau}$	σ_{max} MPa	σ_{min} MPa	x mm	x/a_{max}	x/a_{min}
Test 2										
2_3	**33.347**	482.776	491.19	42.8	0.0309	497.27	16.508	0.1114	1.3736	0.9535
3_4	**33.088**	475.961	484.37	42.4	0.0313	488.79	16.723	0.1114	1.3739	0.9537
4_5	**33.09**	476.298	484.53	42.4	0.0307	488.79	16.358	0.1114	1.3739	0.9537
5_6	**33.108**	476.471	484.7	42.3	0.0306	489.63	16.411	0.1114	1.3739	0.9537
Test 3										
2_3	**36.63**	737.022	529.68	149.7	-1.2147	666.92	254.09	0.1026	0.9731	0.6754
3_4	**36.741**	751.889	539.62	150.5	-1.208	663.5	231.58	0.1029	0.9845	0.6834
4_5	**36.748**	752.294	540.04	150.5	-1.2091	663.5	230.8	0.1029	0.9845	0.6834
5_6	**35.622**	671.992	494.34	148.1	-1.3377	638.17	319.26	0.1014	0.9156	0.6356
6_7	**36.384**	757.309	544.32	151.3	-1.2152	634.09	202.51	0.1034	1.0075	0.6994

Table 5.5 Max MSSR calculation for all tests

Test	MSSR	$\Delta\tau$ MPa	$\Delta\tau_{crit}$ MPa	Θ Deg	$R_{\Delta\tau}$	σ_{max} MPa	σ_{min} MPa	Depth mm	x/a_{max}	x/a_{min}
1-	***33.09***	476.3	484.53	42.4	0.0307	488.78	16.358	0.1114	1.3739	0.9537
2-	***33.347***	482.776	491.19	42.8	0.0309	497.27	16.508	0.1114	1.3736	0.9535
3-	***36.748***	752.294	540.04	60.5	-1.2091	663.5	230.8	0.1029	0.9845	0.6834
4-	***30.42***	394.482	408.39	40.8	0.061	414.18	29.313	0.1113	1.3443	0.9499
5-	***34.19***	640.985	488.67	63.1	-1.5681	551.33	250.2	0.103	0.9914	0.6881
6-	***29.131***	366.203	376.428	40.5	0.04884	377.927	21.6266	0.11152	1.37937	0.95746
7-	***33.418***	597.968	465.53	64.9	-1.7347	528.14	271.22	0.103	0.9903	0.6874
8-	***30.857***	474.735	409.45	16.7	-0.3086	373.49	437.13	0.0605	-0.9534	-0.6618
9-	***35.923***	644.565	535.77	40.1	-0.3995	612.62	82.708	0.1069	0.9359	0.9359
12-	***33.96***	504.578	357.85	67.8	-0.8677	541.22	695	0.1022	0.9514	0.6604
13-	***35.956***	652.894	455	62.7	-1.0774	375.8	708.13	0.1021	0.947	0.6574
15-	***32.2***	752.293	540.04	60.5	-1.20914	663.50	230.798	0.102880	0.9845	0.6834

Table 5.6 Axial stress range and effective stress from Lee Study [8].

Test	σ_{max}	σ_{min}	$\Delta\sigma$	σ_{eff} (Mpa)	P_{max}	P_{min}	P_{Freq}	N_f
#	(MPa)	(MPa)	(MPa)	MPa	(N)	(N)	(Hz)	Cycles
1	600	60	540	572	2224	2224	0	**34,072**
2	600	60	540	572	4448	4448	0	**39,434**
3	600	60	540	572	4448	2224	2.5	**41,400**
4	600	60	540	572	4448	2224	30	**39,004**
5	270	-270	540	369	2224	2224	0	**136,092**
6	270	-270	540	369	4448	4448	0	**98,072**
7	270	-270	540	369	4448	2224	2.5	**108,056**
8	270	-270	540	369	4448	2224	30	**124,417**

Table 5.7 Axial stress range and effective stress from Lykins [29]

Test #	σ_{max} MPa	σ_{min} MPa	$\Delta\sigma$ MPa	$\sigma_{eff\ (Mpa)}$ MPa	P_{max} N	P_{min} N	P_{Freq} Hz	N_f Cycles
1	636	-40	675	653	1330	1330	0	**26,700**
2	700	44	656	679	1330	1330	0	**31,600**
3	552	18	534	544	1330	1330	0	**53,400**
4	566	53	513	542	1330	1330	0	**70,600**
5	687	291	396	536	1330	1330	0	**86,200**
6	425	35	389	408	1330	1330	0	**91,900**
7	538	233	305	416	1330	1330	0	**118,000**
8	416	29	388	403	1330	1330	0	**121,000**
9	686	294	392	533	1330	1330	0	**124,000**
10	529	232	297	408	1330	1330	0	**262,000**
11	687	456	231	420	1330	1330	0	**371,000**
12	582	351	231	384	1330	1330	0	**672,000**
13	413	186	227	315	1330	1330	0	**2,080,000**
14	686	442	244	431	1330	1330	0	**2,560,000**
15	420	191	229	320	1330	1330	0	**3,660,000**
16	540	372	168	319	1330	1330	0	**4,140,000**
17	507	331	176	315	1330	1330	0	**50,000,000**
18	410	273	137	250	1330	1330	0	**50,000,000**

Table 5.8 Axial stress range and effective stress from Jutte's [12]

Test	σ_{max}	σ_{min}	$\Delta\sigma$	σ_{eff}	P_{max}	P_{min}	P_{Freq}	N_f
#	MPa	MPa	MPa	MPa	N	N	Hz	Cycles
11	600	294	306	443	4448	2224	20	**250,000**
12	592	272	320	449	4448	2224	20	**230,000**
15	569	57	512	543	2224	2224	0	**59,000**
17	590	65	525	560	4448	4448	0	**53,000**
18	599	36	563	583	4448	2224	36	**69,000**
19	582	12	570	577	4448	2224	36	**50,000**
20	596	30	566	582	4448	2224	36	**51,000**
21	591	18	573	583	4448	2224	40	**46,000**
22	592	59	533	565	4448	2224	40	**51,000**

Table 5.9 Axial stress range and effective stress from this study

Test	σ_{max}	$\Delta\sigma$	σ_{eff}	P_{max}	P_{min}	P_{Freq}	Phase Angle	N_f
#	MPa	MPa	MPa	N	N	Hz	Degree	cycle
1	760	684	724	4448	2224	10	0	20,734
2	564	518	538	4448	2224	10	0	47,298
3	564	518	538	4448	2224	10	90	61,428
4	413	372	394	4448	2224	10	0	229,477
5	413	372	394	4448	2224	10	90	275,172
6	376	339	358	4448	2224	10	0	657,432
7	376	339	358	4448	2224	10	90	1,706,847
8	282	254	269	4448	2224	10	0	> 6 million
12	564	518	538	4448	2224	10	60	69,149
13	564	518	538	4448	2224	10	105	90,528
15	351	316	335	4448	2224	10	90	10,000,000

Table 5.10 Shear stress range and fatigue life from this study

Test	σ_{max}	σ_{min}	**Δσaxial**	Q_{max}	Q_{min}	**ΔQ**	N_f	ϕ
#	**MPa**	**MPa**	**MPa**	**N**	**N**	**N**	**Cycles**	**Deg**
1	760	76	684	369	-1191	**`1560**	**20,734**	0
2	564	56	518	475.7	-824.3	**1300**	**47,298**	0
3	564	56	518	218.4	-912.8	**1131**	**61,428**	90
4	413	41	372	403	-555	**958**	**229,477**	0
5	413	41	372	110	-715	**825**	**275,172**	90
6	376	37	339	219.5	-648.5	**868**	**657,432**	0
7	376	37	339	58.3	-682.3	**740.6**	**1,706,847**	90
8	282	28	254	-398	-1092.5	**694**	**> 6 million**	0
9	564	56	518	754	-486.95	**1241**	**42,640**	-
12	564	56	518	844	-397	**1241**	**69,149**	60
13	564	56	518	729	-413	**1142**	**90,528**	105
15	351	35	316	499.2	-236.1	**735.3**	**10,000,000**	90

Table 5.11 MSSR calculation from Lykin's study

Test #	σ_{max} (MPa)	σ_{min} (MPa)	P_{max} (N)	P_{min} (N)	P_{Freq} (Hz)	N_f Cycles	$MSSR_{max}$
1	636	-40	1330	1330	0	26,700	**29.1**
2	700	44	1330	1330	0	31,600	**30.5**
3	552	18	1330	1330	0	53,400	**29.6**
4	566	53	1330	1330	0	70,600	**30.1**
5	687	291	1330	1330	0	86,200	**29.6**
7	538	233	1330	1330	0	118,000	**27.8**
8	416	29	1330	1330	0	121,000	**26.9**
9	686	294	1330	1330	0	124,000	**29.4**
10	529	232	1330	1330	0	262,000	**27.2**
11	687	456	1330	1330	0	371,000	**28.2**
12	582	351	1330	1330	0	672,000	**27.5**
13	413	186	1330	1330	0	2,080,000	**25.3**
14	686	442	1330	1330	0	2,560,000	**28.2**
15	420	191	1330	1330	0	3,660,000	**25.4**
16	540	372	1330	1330	0	4,140,000	**26.5**
17	507	331	1330	1330	0	50,000,000	**26.6**
18	410	273	1330	1330	0	50,000,000	**24.5**

Table 5.12 MSSR calculation from Jutte's study

Test #	σ_{max} (MPa)	σ_{min} (MPa)	P_{max} (N)	P_{min} (N)	P_{Freq} (Hz)	N_f Cycles	$MSSR_{max}$
11	600	294	4448	2224	20	250,000	**26.7**
12	592	272	4448	2224	20	230,000	**27.1**
15	569	57	2224	2224	0	58,600	**31.5**
17	590	65	4448	4448	0	53,000	**33.3**
18	599	36	4448	2224	36	69,000	**29.9**
19	582	12	4448	2224	36	49,500	**32.6**
20	596	30	4448	2224	36	50,700	**29.9**
21	591	18	4448	2224	40	46,000	**34.5**
22	592	59	4448	2224	40	51,000	**32.0**

Table 5.13 MSSR calculation from Lee's study

Test	σ_{max}	σ_{min}	P_{max}	P_{min}	P_{Freq}	N_f	$MSSR_{max}$
#	(MPa)	(MPa)	(N)	(N)	(Hz)	Cycles	
1	600	60	2224	2224	0	34,072	**33.88**
2	600	60	4448	4448	0	39,434	**36.32**
3	600	60	4448	2224	2.5	41,400	**35.07**
4	600	60	4448	2224	30	39,004	**33.97**
5	270	-270	2224	2224	0	136,092	**28.12**
6	270	-270	4448	4448	0	98,072	**30.64**
7	270	-270	4448	2224	2.5	108,056	**30.03**
8	270	-270	4448	2224	30	124,417	**28.84**

Table 5.14 MSSR calculation from this study

Test #	σ_{max} (MPa)	σ_{min} (MPa)	P_{max} (N)	P_{min} (N)	P_{Freq} (Hz)	N_f Cycles	$MSSR_{max}$
1	760	76	4448	2224	10	**20,734**	***33.09***
2	564	56	4448	2224	10	**47,298**	***33.347***
3	564	56	4448	2224	10	**61,428**	***36.748***
4	413	41	4448	2224	10	**229,477**	***30.42***
5	413	41	4448	2224	10	**275,172**	***34.19***
6	376	37	4448	2224	10	**657,432**	***29.131***
7	376	37	4448	2224	10	**1,706,847**	***33.418***
8	282	28	4448	2224	10	**> 6 million**	***30.857***
9	564	56	3336	3336	0	**42,640**	***35.923***
12	564	56	4448	2224	10	**69,149**	***33.96***
13	564	56	4448	2224	10	**90,528**	***35.956***
15	351	35	4448	2224	10	**10,000,000**	***32.2***

6. Conclusion and Recommendation

This chapter represents the summary of this study; including the requirement of this work and how it was done, the conclusion of the analyzed and discussed results from this work, and a recommendation for the future work which can be accomplished based on the results those achieved in this study.

6.1. Summary

Since the titanium alloy Ti-6Al-4V is used in high technology applications, there was a lot of work that has been accomplished to get a better understanding of the behavior of this material under fretting fatigue condition. Most of these studies assumed that the applied contact load is constant, while a little effort has been conducted under variable contact load. Fretting fatigue phenomenon, as in the components of the turbine engine, is a very difficult area to study due to the complicated oscillatory movements at the contact region. These movements are resulted from the application of both the axial and the contact loads. The application of these loads can be in any condition; variable contact load, in-phase, phase lag between the axial and the contact load, or even an alternate between plain fatigue and fretting fatigue. Therefore, investigating the fretting fatigue under phase difference and combinations between fretting fatigue and plain fatigue was the main objective of this work in order to give a better understanding of the behavior of fretting fatigue.

Four experiments were conducted under combinations between fretting fatigue and plain fatigue. In these experiments; the contact load was kept constant at 3336 N, while the axial stress range was kept in between 564 MPa and 56 MPa, and the ratio between the plain fatigue cycles and fretting fatigue cycles was chosen to be: 0, 1, 2, and 200. On the other hand; eleven tests were conducted under phase difference between the applied axial load and the applied contact load. In these experiments; the maximum axial load was varied between 726 MPa and 282 MPa at a constant stress ratio of 0.1, the applied contact load was kept constant between 4448 N and 2224 N, and the selected phase angles were: 0^o, 60^o, 90^o, and 105^o. The frequency for both the axial and contact loads was the same i.e.10 Hz.

All of the experiments were accomplished by using Ti-6Al-4V alloy specimens, which has a modulus of elasticity of 126 GPa and Poison's ratio of 0.33, and a dimension of 3.81 mm thickness and 6.35 mm width, and a 50.8 mm pad configuration. The applied load condition and their frequencies and phase angles were controlled by a computer controlled bi-axial servo-hydraulic machine by using a peak valley compensator to reduce the variation between control and feedback signals. The applied loads outputs were monitored and recorded continuously until failure of the specimen occurred. The resulting tangential loads were found as the half difference between the lower axial loads and the upper grip loads. After the specimen failed, it was taken to the Scanning Electron Microscope (SEM) in order to examine the fracture surface area, measure the crack initiation orientation, and locate the crack initiation location. And prior to SEM the contact half width of the failed specimen was determined by using the lower magnification microscope.

The recorded and resulting loads were used as an input to the Finite Element Analysis (FEA) model. The infinite half-space assumption was invalid in this study and this was the requirement of the FEA which doesn't require a finite half-space assumption, hence the commercial available software ABAQUAS was used to conduct the FEA in this study. The maximum contact load was always applied initially at the first step to prevent the gross slip condition, and in step 2 the maximum axial load with the corresponding tangential load were applied. Since the frequency was the same for the applied axial and the applied contact loads only seven steps were needed. The coefficient of friction was selected for all tests to be 0.5 which was the maximum calculated Q/P from this study. The results from FEA were compared with the analytical Ruiz solution to validate the FEA model. The maximum load condition was used here at the maximum axial load condition for in-phase or phase difference. The effect of the different variables such as; out of phase condition, axial stress concentration, stress distribution, and all loads condition, were conducted in details in FEA model.

The FEA outputs were obtained to be used an input into the MSSR calculation, which was adopted in this study as the effective parameter in predicting the fretting fatigue life, and the crack initiation location and orientation. In addition to MSSR parameter; the axial stress range and the effective stress as well as the tangential load range were investigated to determine their effect on the fatigue life and the crack initiation mechanism. Both the tangential load range and the axial stress range were formulated on the global axial and tangential load and didn't take the local load range into consideration, while the MSSR was analyzed in details to get how much did it affect in predicting the fatigue life, and the crack initiation location and orientation.

6.2. Conclusions

The conclusion of both the effect of phase difference between the axial and the contact loads and effect of the combination of the fretting fatigue and the plain fatigue on the fretting fatigue behavior will be discussed in this section.

6.2.1 Combination of Fretting and Plain Fatigue

1. A steady state condition was met after a few hundreds of fretting fatigue cycles each time the fretting fatigue condition alternated the plain fatigue condition. And also the resulting tangential load converged to the same magnitude when the contact load reapplied after the plain fatigue condition.
2. There was no effect on the plain fatigue life if half of the whole fretting fatigue life was applied initially and then followed by the plain fatigue cycles until a failure of the specimen occurred. This shows that most of the fretting fatigue life is expended in the crack initiation.
3. The only effect on fatigue life during a combination of fretting fatigue condition and plain fatigue condition is from the ratio between them. As the ratio between the plain fatigue cycles to the fretting fatigue cycles decreases the effect of the fretting fatigue increases that results in reduction of the fatigue life. This is well known information that the fretting fatigue decreases the fatigue life compared to the plain fatigue.

6.2.2. Phase Difference

1. For all experiments that have been conducted under in-phase condition or with phase difference condition in this study, the crack initiation location always occurred at or very near the trailing edge of the contact region, i.e. $x/a \approx +1$.
2. A steady state condition of the fretting fatigue variables; including the applied axial and contact loads, the tangential load, and the coefficient of friction, was observed after a few hundreds of fretting fatigue cycles.
3. The Q/P ratio under fretting fatigue condition varied during a cycle and the maximum magnitude was barely reached 0.5. However the greatest value of the Q/P ratio was found under in-phase condition, while the least one was under out of phase condition.
4. The tangential load varied in the same manner as the axial load. In other words; the frequency, phase angle, and wave of the tangential load were the same as the axial load and there was no effect from the applied contact load on the tangential load except on the magnitude.
5. At the same axial stress the global tangential load range of the out of phase condition is less than that of the in-phase condition.
6. Four distinguishable regions were found in the fracture surface area under out of phase or in-phase condition, and they were debris in region 1, striation in region 2, large dimples in region 3, and catastrophic fracture in region 4.
7. The crack initiation orientation angle for the in-phase condition was 48^{o} which is close to the previous studies. The angle for the out of phase condition was

found to be 63^o and this value differed from the previous studies with a deviation of 10^o. This deviation due to the change in the contact stress and the shear stress for the out of phase condition from the in-phase condition.

8. The analytical solution for determining the contact half-width was very accurate compared to the measured contact half-width from the experiments.
9. From FEA outputs, as they validated with the Ruiz program, the maximum local axial stress magnitude for the out of phase condition is less than the in-phase condition that results in less stress concentration factor in axial stress.
10. At the same axial stress the calculated MSSR for the out of phase condition was found to be more than the one of the in-phase condition with a deviation between 10 % and 12 %.
11. MSSR parameter was very effective in predicting the crack initiation location and the crack initiation orientation; under in-phase condition the orientation angle was ranged between $40.8^o \sim 42.8^o$, while under out of phase condition this angle was $60.5^o \sim 67.5^o$.
12. The crack initiation location, as a result from the MSSR, was at x/a = 0.9499 ~ 0.9537 for the in-phase condition and at x/a = 0.9845 ~ 0.9914 for the out of phase condition.
13. In general the phase difference improved the fatigue life and this improvement depended on the magnitude of the axial stress range. At high axial stress range, 508 MPa the fatigue life increased 30 %, while at low axial stress range, 339 MPa, the fatigue life increased by 150 %.

14. As the effective stress or the axial stress range decreases the fatigue life will increase and this is true for both out of phase and in-phase conditions.
15. The global tangential load range was very effective in predicting the fatigue life even though for any phase. At the same axial stress, the shear stress range for the in-phase condition is greater than the one for the out of phase condition; hence the life of the out of phase condition is greater.

6.3. Recommendations for Future Work

As seen in the summary section; the work in this study was focused on the investigation of the effect of phase difference between the axial and the contact load and the combination between the fretting fatigue and the plain fatigue on the behavior of fretting fatigue on titanium alloy. This work was done with a 50.8 mm radius cylindrical-end pads in a laboratory environment at about 25˚ C and the axial and contact load frequency was constant at 10 Hz. Since the operating temperature inside the engine is very high comparing to the room temperature and in addition to that the investigation of titanium alloy under elevated temperature didn't improve the fatigue life, investigating the fretting fatigue behavior under phase difference between the axial and contact load, which increased the fatigue life, under elevated temperature will be a very interesting subject to study.

The dovetail joint shape between disk slot and blade in real engine is more complicated that the simplified model and also the fretting pad geometry play a crucial role in fatigue life determination. Further efforts should be devoted to investigate the

significance of different pad geometry under phase difference between the axial and the contact load. Due to the limitation on the test machine capacity, the axial and contact load frequency was 10 Hz, however in the real engine this frequency is much greater than that. So the investigation of different phase under high frequency is also an interesting work to study.

Surface treatment such as shot-peening procedure is one of the most methods that is used to improve the material performance and the fatigue life of the material and hence a combination between the phase difference and shot-peening, both of them improve the fatigue life, should be included in the future work. In addition to environmental corrosion, where the real engines operate, the dissimilar materials are used in turbine engine components. So investigating the fretting fatigue under phase difference inside environmental corrosion or with dissimilar materials is another work that can be accounted for future work.

In this study the MSSR parameter was adopted as the most effective parameter in predicting the crack initiation location and orientation, and the fatigue life. This parameter was very effective in determining the cracks details, however in predicting the fatigue life MSSR worked very well for the in-phase conditions, but for the out phase condition and at the same axial stress the MSSR was higher than the in-phase condition and at the same time the fatigue life was higher also. This comes from three different things that the MSSR depends on' the maximum axial stress, the critical shear stress range, and the arbitrary constants. So if fretting fatigue will be investigated under phase difference, the MSSR should be evaluated with different methods such as; changing the arbitrary constants to be higher with the axial stress than the shear stress, taking the

maximum axial stress with its corresponding shear stress and not taking the magnitudes of them which gives the maximum MSSR.

Bibliography

1. D. Hills and D. Nowell. *Mechanics of Fretting Fatigue*, Kluwer Academic Publishers, Netherlands, 1994.
2. K. Chan and Y. Lee. *Ruiz Program*, South West Research Institute, Personal Communication, 1998.
3. K. Iyer and S. Mall. "Effects of Cyclic Frequency and Contact Pressure on Fretting Fatigue under Two-level Block Loading," *Fatigue Fract. Engng. Mater. Struct*., 23: 335-346 (2000).
4. D. Hills, D. Nowell, and A. Sackelfield. "Surface Fatigue Considerations in Fretting Interface Dynamic, Proceedings of the 14th Leeds-Lyon Symposium on Tribiology, D. Dawson, C. M. Taylor, M. Godet, D. Berthe Eds. Elsevier, Amsterdam, 1988.
5. C.D Lykins, S. Mall, and V.K Jain. "A Shear Stress Based Parameter for Fretting Fatigue Crack Initiation," *Fatigue and Fracture of Engineering Materials and Structures*, 24: 461-473 (2001).
6. K. Iyer and S. Mall. "Analysis of Contact Pressure and Stress Amplitude Effects on Fretting Fatigue Life," *Journal of Engineering Materials and Technology*, 123:85-93 (January 2001).
7. S.A. Namjoshi, S. Mall, V.K. Jain, and O. Jain. "Effects of Process Variables on Fretting Fatigue Crack Initiation in Ti-6Al-4V," *Journal of Strain Analysis*, 37, No.6: 535-542 (2002).
8. Chia-hwa Lee. "Effect of variable contact load on fretting fatigue behavior of shot-peened and un-peened titanium alloy", Thesis AFIT/GAE/ENY/04-D01, Dec 2004M.H.
9. C.D Lykins, S. Mall, and V.K Jain. "A Shear Stress Based Parameter for Fretting Fatigue Crack Initiation," *Fatigue and Fracture of Engineering Materials and Structures*, 24: 461-473 (2001).
10. S. A. Namjoshi, S. Mall, V. K. Jain, and O. Jin. "Fretting Fatigue Crack Initiation Mechanism in Ti-6Al-4V," *Fatigue Fract Engng Master Struct*, 25: 955-964 (2002).
11. MADHI. " Fretting fatigue behavior of Nickel alloy IN-100," Thesis AFIT/GAE/ENY/06-M22, March 2006.

12. A.J. Jutte. ”Effect of a Variable Contact Load on Fretting Fatigue Behavior of Ti-6Al-4V,” Thesis, Air Force Institute of Technology, Wright-Patterson Air Force Base, Ohio, 2004.
13. H. Lee, O. Jin, and S. Mall. “Fretting Fatigue Behavior of Shot-peened Ti-6Al-4V at Room and Elevated Temperature,” *Fatigue Fract Engng Master Struct*, 26: 1-12 (2003).
14. H. Lee, S. Mall. “Stress Relaxation Behavior of Shot-peened Ti-6Al-4V under Fretting Fatigue at Elevated Temperature,” *Materials Science and Engineering* A366: 412-420 (2004).
15. R.B. Waterhouse and M.K. Dutta. “The Fretting Fatigue of Titanium and Some Titanium Alloys in a Corrosive Environment,” *Wear*, 25: 171-175 (1973).
16. M.H. Wharton and R.B. Waterhouse. “Environmental Effects in the Fretting Fatigue of Ti-6Al-4V,” *Wear*, 62:287-297 (1980).
17. D.W. Hoeppner, A.M. Taylor, and V. Chandrasekaran. “Fretting Fatigue Behavior of Titanium Alloys,” In: Fretting Fatigue: Advances in Basic Understanding and Applications. Eds. Y. Mutoh, S.E. Kinyon, and D.W. Hoeppner. West Conshohocken PA: ASTM International (2003).
18. L.C. Lietch. ”Fretting Fatigue Behavior of the Titanium Alloy Ti-6Al-4V under Seawater Conditions,” Master’s thesis, AFIT/GMS/ENY/04-M02, Air Force Institute of Technology, Wright-Patterson Air Force Base, Ohio, 2004.
19. H.I. Yuksel. “Effects of Shot-peening on High Cycle Fretting Fatigue Behavior of Ti-6Al-4V,” MS Thesis AFIT/GAE/ENY/02-12. Air Force Institute of Technology (AU), Wright-Patterson AFB OH, December 2002.
20. L. Coffin, Jr. “A Study of the Effects of Cyclic Thermal Stresses on a Ductile Metal,” Trans. ASME, 76: 931-950 (1954).
21. S. Manson. “Behavior of Materials under Conditions of Thermal Stress,” *NACA Technical Report* TN 2933 (1953).
22. O. Basquin. “The Exponential Law of Endurance Tests,” *Am. Soc. Test. Mater Proc.*, 10: 625-630 (1910).
23. K. Walker. “The Effect of Stress Relation during Crack Propagation and Fatigue for 2024-T3 and 7075-T6 Aluminum,” Presented to subcommittee E-9V Winter Meeting (Feb 1969).

.

24. S. Mall, V.K. Jain, S. Namjoshi, and C.D. Lykins. ”Fretting Fatigue Crack Initiation Behavior of Ti-6Al-4V,” *Standard Technical publication 1425*, ASTM International (2003).
25. M. Szolwinski, and T. Farris. “Mechanics of Fretting Fatigue Crack Formation”, *Wear*, 93-107 (1996).
26. R. Neu, J. Pape, and D. Swalla-Michaud. “Methodologies for Linking Nucleation and Propagation Approaches for Predicting Life under Fretting Fatigue”, Fretting Fatigue: Current Technology and Practices, ASTM 1367, D. Hoeppner, V. Chandrasekaran and C. Elliot, Eds. American Society for Testing and Materials.
27. W.N. Findley. ”Fatigue of Metals under Combination of Stresses,” *Trans ASME*, 79: 1337-48 (1975).
28. Maganizer, R. S. examination of Contact Width on Fretting Fatigue. Ph.D. dissertation, Graduate School of Engineering, Air Force Institute of Technology (AFIT), WPAFB, March 2002. AFIT/GAE/ENY/02-8.
29. C.D Lykins, S. Mall, and Douglas. “An Investigation of Fretting Fatigue Crack Initiation Behavior of the Titanium Alloy Ti-9Al-4V,” PhD.dissertation, University of Dayton, December 1999

Vita

Ltc. Mohammad Almajali holds a Bachelor of Science in Mechanical Engineering since 1989 and he graduated from Jordanian University of Science and Technology in Irbid city, Jordan. After that he enrolled in Royal Jordanian Air Force on Feb 3, 1990 as a maintenance officer with 2nd Lt. Rank. In Air Force he started his work in Air Lift Wing (ALW) where he gained the experience by maintaining the following Aircrafts: C-130, Casa 121, Super puma, and finally the old Aircraft Dove Havilland. He headed the first line, engine shop, and electrical shop during his service in ALW.

On 1993 he was selected to serve in the Royal Squadron where the best engineers in Air Force are going. He was sent, on the same year, to Kirtland AFB, NM in United States to get the basic training course on Black Hawk Helicopter which he worked on untill 2004. During this period he had the following training courses: Basic Black Hawk maintenance on 1993, Refresher course on S-70 at Sikorsky Company on 1999, Auto Flight Control System at Flight Safety on 2001, Infra Red Counter Measurement course in Jordan, and a safety course at Queen Noor Center.

Afterwards, on 2004, Royal Jordanian Air Force chose him for getting a Master of Science in Aeronautical Engineering and hence they sent him to Air Force Institute of Technology WPAFB, Dayton OH, in United States where he accomplished this project.

REPORT DOCUMENTATION PAGE

Form Approved
OMB No. 074-0188

1. REPORT DATE *(DD-MM-YYYY)*	**2. REPORT TYPE**	**3. DATES COVERED** *(From – To)*
14-09-2006	**Master's Thesis**	Aug 2004 – Sep 2006

4. TITLE AND SUBTITLE

Effects of Phase Difference Between Axial and Contact loads on Fretting Fatigue Behavior of Titanium Alloy.

5a. CONTRACT NUMBER

5b. GRANT NUMBER

5c. PROGRAM ELEMENT NUMBER

6. AUTHOR(S)

Almajali, Mohammad, Ltc, Royal Jordanian Air Force

5d. PROJECT NUMBER

5e. TASK NUMBER

5f. WORK UNIT NUMBER

7. PERFORMING ORGANIZATION NAMES(S) AND ADDRESS(S)
Air Force Institute of Technology
Graduate School of Engineering and Management (AFIT/EN)
2950 Hobson Way, Building 640
WPAFB OH 45433-7765

8. PERFORMING ORGANIZATION REPORT NUMBER

AFIT/GAE/ENY/06-S02

9. SPONSORING/MONITORING AGENCY NAME(S) AND ADDRESS(ES)
AFRL/MLLP
Attn: Dr. Mark Blodgett
Metals, Ceramics and NDE Division
Materials and Manufacturing Directorate
2230 Tenth St. Suite 1 Bldg 655
Wright Patterson Air Force Base, OH DSN: 785-9799

10. SPONSOR/MONITOR'S ACRONYM(S)

11. SPONSOR/MONITOR'S REPORT NUMBER(S)

12. DISTRIBUTION/AVAILABILITY STATEMENT
APPROVED FOR PUBLIC RELEASE; DISTRIBUTION UNLIMITED.

13. SUPPLEMENTARY NOTES

14. ABSTRACT

Fretting fatigue is the surface damage that occurs at the interface between two components that are under going a small amplitude oscillatory movement. It results in a reduction of the material life as compared to the plain fatigue. Most of the previous works were accomplished under a constant applied normal load and a little effort was done under a variable contact load, while none of these studies have considered the phase difference between the axial and the contact load. The primary goal of this study is to investigate the effect of phase difference between axial and contact loads on fretting fatigue behavior of Ti-6Al-4V. The frequency of both axial and contact loads was the same .i.e. 10 Hz. Under variable contact load condition; only the axial stress range and the phase angle were varied. Cracks were always found to initiate on the contact surface and near the trailing edge for all tests. The software program, ABAQUAS, was used in finite element analysis to determine the contact region state variables such as stress, strain, and displacement. The fatigue parameters; such as the stress range, effective stress, and modified shear stress range (MSSR) were analyzed to predict the fatigue life. The fatigue life with in-phase variable contact load was almost same as that of constant contact load. The out of phase condition was found to increase the fatigue life from 20 % to 30% in the low cycle regime and up to 150 % in the high cycle regime relative to its counterpart from in-phase loading. The MSSR parameter was effective in predicting the fatigue life, crack initiation location, and crack initiation orientation.

15. SUBJECT TERMS
Fatigue, Fretting, Titanium Alloys, Out of phase, Combination.

16. SECURITY CLASSIFICATION OF:			**17. LIMITATION OF ABSTRACT**	**18. NUMBER OF PAGES**	**19a. NAME OF RESPONSIBLE PERSON**
REPORT	**ABSTRACT**	**c. THIS PAGE**			Dr. Shankar Mall, AFIT/ENY
U	**U**	**U**	**UU**	164	**19b. TELEPHONE NUMBER** *(Include area code)* (937) 255-3636X4587; e-mail: shankar.mall @afit.edu